CHAPTER

12

Turbulence

OUTLINE

CHAPTER OBJECTIVES

- To introduce and describe turbulent flow
- To define the statistics and functions commonly used to quantify turbulent flow phenomena
- To derive the Reynolds-averaged equations
- To present assumptions and approximations leading to the classical scaling laws for turbulent flow
- To provide useful summaries of mean flow results for free and wall-bounded turbulent shear flows
- To introduce the basic elements of turbulence modeling
- To describe basic turbulence phenomena relevant in atmospheric turbulence

12.1. INTRODUCTION

Nearly all macroscopic flows encountered in the natural world and in engineering practice are turbulent. Winds and currents in the atmosphere and ocean; flows through residential, commercial, and municipal water (and air) delivery systems; flows past transportation devices (cars, trains, aircraft, ships, etc.); and flows through turbines, engines, and reactors used for power generation and conversion are all turbulent. Turbulence is an enigmatic state of fluid flow that may be simultaneously beneficial and problematic. For example, in air-breathing combustion systems, it is exploited for mixing reactants but, within the same device, it also leads to noise and efficiency losses. Within the earth's ocean and atmosphere, turbulence sets the mass, momentum, and heat transfer rates involved in pollutant dispersion and climate regulation.

Turbulence involves fluctuations that are unpredictable in detail, and it has not been conquered by deterministic or statistical analysis. However, useful predictions about it are still possible and these may arise from physical intuition, dimensional arguments, direct numerical simulations, or empirical models and computational schemes. In spite of our everyday experience with it, turbulence is not easy to define precisely and there is a tendency to confuse turbulence with randomness. A turbulent fluid velocity field conserves mass, momentum, and energy while a purely random time-dependent vector field need not. With some humor, Lesieur (1987) said:

> Turbulence is a dangerous topic which is at the origin of serious fights in scientific meetings since it represents extremely different points of view, all of which have in common their complexity, as well as an inability to solve the problem. It is even difficult to agree on what exactly is the problem to be solved. (p. 000)

This chapter presents basic features of turbulence beginning with this listing of generic characteristics.

(1) *Fluctuations*: Turbulent flows contain fluctuations in the dependent-field quantities (velocity, pressure, temperature, etc.) even when the flow's boundary conditions are steady. Turbulent fluctuations appear to be irregular, chaotic, and unpredictable.

(2) *Nonlinearity*: Turbulence is found to occur when the relevant nonlinearity parameter, say the Reynolds number Re, the Rayleigh number Ra, or the inverse Richardson number Ri^{-1}, exceeds a critical value. The nonlinearity of turbulence is evident since it is the final state of a nonlinear transition process. Once the critical parametric value is exceeded small perturbations can grow spontaneously and may equilibrate as finite amplitude disturbances. However, the new equilibrium state can become unstable to more complicated disturbances, and so on, until the flow eventually reaches a nonrepeating unpredictable state (turbulence). The nonlinearity of a turbulent flow is also evident in vortex stretching, a key process by which three-dimensional turbulent flows maintain their fluctuations.

(3) *Vorticity*: Turbulence is characterized by fluctuating vorticity. A cross-section view of a turbulent flow typically appears as a diverse collection of streaks, strain regions, and swirls of various sizes that deform, coalesce, divide, and spin. Identifiable structures in a turbulent flow, particularly those that spin, are called *eddies*. Turbulence always

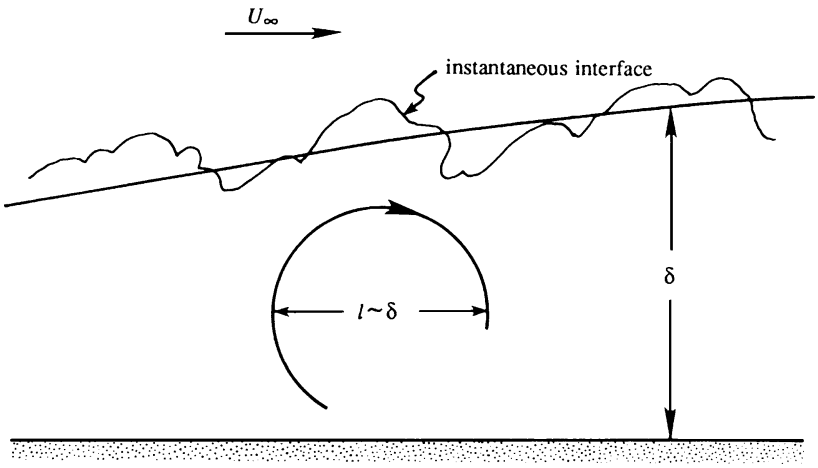

FIGURE 12.1 Turbulent boundary-layer flow showing a typical large eddy of size l, the average layer thickness δ, and the instantaneous interface between turbulent and nonturbulent (typically irrotational) fluid. Here, as in most turbulent flows, the size of the largest eddies is comparable to the overall layer thickness.

involves a range of eddy sizes and the size range increases with increasing Reynolds number. The characteristic size of the largest eddies is the width of the turbulent region; in a turbulent boundary layer this is the thickness of the layer (Figure 12.1). Such layer-spanning eddies commonly contain most of the fluctuation energy in a turbulent flow and may be several orders of magnitude larger than the smallest eddies.

(4) *Dissipation*: On average, the vortex stretching mechanism transfers fluctuation energy and vorticity to smaller and smaller scales via nonlinear interactions, until velocity gradients become so large that the energy is converted into heat (i.e., dissipated) by the action of viscosity and the motion of the smallest eddies. Persistent turbulence therefore requires a continuous supply of energy to make up for this energy loss.

(5) *Diffusivity*: Due to the prevalence of agitation and overturning motions (macroscopic mixing), turbulent flows are characterized by a rapid rate of mixing and diffusion of species, momentum, and heat compared to equivalent laminar flows that lack fluctuations.

These features of turbulence suggest that many flows that seem random, such as wind-driven ocean-surface waves or internal waves in the ocean or the atmosphere, are not turbulent because they are not simultaneously dissipative, vortical, and nonlinear.

Although imperfect, a simple definition of turbulence as *a dissipative flow state characterized by nonlinear fluctuating three-dimensional vorticity* is offered for the reader who may benefit from keeping a concise description in mind while gaining a greater appreciation of this subject. Incompressible turbulent mean flows in systems not large enough to be influenced by the Coriolis force are emphasized in this chapter. The fluctuations in such flows are three dimensional. In large-scale geophysical systems, on the other hand, the existence of stratification and the Coriolis force severely restricts vertical motion and leads to chaotic flow that may be nearly two dimensional or *geostropic*. *Geostrophic turbulence* is briefly mentioned in Chapter 13. More extensive treatments of turbulence are provided

in Monin and Yaglom (1971, 1975), Tennekes and Lumley (1972), Hinze (1975), and Pope (2000).

12.2. HISTORICAL NOTES

Turbulence is a leading topic in modern fluid dynamics research, and some of the best-known physicists have worked in this area during the last century. Among them are G. I. Taylor, Kolmogorov, Reynolds, Prandtl, von Karman, Heisenberg, Landau, Millikan, and Onsagar. A brief historical outline is given in what follows; further interesting details can be found in Monin and Yaglom (1971). The reader is expected to fully appreciate these historical remarks only after reading the chapter.

The first systematic work on turbulence was carried out by Osborne Reynolds in 1883. His experiments in pipe flows showed that the flow becomes turbulent or irregular when the dimensionless ratio $\mathrm{Re} = UL/\nu$, later named the *Reynolds number* by Sommerfeld, exceeds a certain critical value. (Here ν is the kinematic viscosity, U is the velocity scale, and L is the length scale.) This dimensionless number subsequently proved to be the parameter that determines the dynamic similarity of viscous flows. Reynolds also separated turbulent flow-dependent variables into mean and fluctuating components, and arrived at the concept of turbulent stress. The meaning of the Reynolds number and the existence of turbulent stresses are foundational elements in our present understanding of turbulence.

In 1921 the British physicist G. I. Taylor, in a simple and elegant study of turbulent diffusion, introduced the idea of a correlation function. He showed that the root-mean-square distance of a particle from its source point initially increases with time as t, and subsequently as $t^{1/2}$, as in a random walk. Taylor continued his outstanding work in a series of papers during 1935–1936 in which he laid down the foundation of the statistical theory of turbulence. Among the concepts he introduced were those of homogeneous and isotropic turbulence and of a turbulence spectrum. Although real turbulent flows are not isotropic (turbulent shear stresses, in fact, vanish for isotropic flows), the mathematical techniques involved have proved valuable for describing the *small scales* of turbulence, which are isotropic or nearly so. In 1915 Taylor also introduced the mixing length concept, although it is generally credited to Prandtl for making full use of the idea.

During the 1920s Prandtl and his student von Karman, working in Göttingen, Germany, developed semi-empirical theories of turbulence. The most successful of these was the mixing length theory, which is based on an analogy with the concept of mean free path in the kinetic theory of gases. By guessing at the correct form for the mixing length, Prandtl was able to deduce that the average turbulent velocity profile near a solid wall is logarithmic, one of the most reliable results for turbulent flows. It is for this reason that subsequent textbooks on fluid mechanics have for a long time glorified the mixing length theory. Recently, however, it has become clear that the mixing length theory is not helpful since there is really no rational way of predicting the form of the mixing length. In fact, the logarithmic law can be justified from dimensional considerations alone.

Some very important work was done by the British meteorologist Lewis Richardson. In 1922 he wrote the very first book on numerical weather prediction. In this book he proposed that the turbulent kinetic energy is transferred from large to small eddies, until it is

destroyed by viscous dissipation. This idea of a spectral energy cascade is at the heart of our present understanding of turbulence. However, Richardson's work was largely ignored at the time, and it was not until some 20 years later that the idea of a spectral cascade took a quantitative shape in the hands of Kolmogorov and Obukhov in Russia. Richardson also did another important piece of work that displayed his amazing physical intuition. On the basis of experimental data for the movement of balloons in the atmosphere, he proposed that the effective diffusion coefficient of a patch of turbulence is proportional to $l^{4/3}$, where l is the scale of the patch. This is called *Richardson's four-third law*, which has been subsequently found to be in agreement with Kolmogorov's famous five-third law for the energy spectrum.

The Russian mathematician Kolmogorov, generally regarded as the greatest probabilist of the twentieth century, followed up on Richardson's idea of a spectral energy cascade. He hypothesized that the statistics of small scales are isotropic and depend on only two parameters, namely ν, the kinematic viscosity, and $\overline{\varepsilon}$, the average rate of kinetic energy dissipation per unit mass of fluid. On dimensional grounds, he derived that the smallest scales must be of size $\eta = (\nu^3/\overline{\varepsilon})^{1/4}$. His second hypothesis was that, at scales much smaller than l (see Figure 12.1) and much larger than η, there must exist an inertial subrange of turbulent eddy sizes for which ν plays no role; in this range the statistics depend only on a single parameter $\overline{\varepsilon}$. Using this idea, in 1941 Kolmogorov and Obukhov independently derived that the spectrum in the inertial subrange must be proportional to $\varepsilon^{2/3}k^{-5/3}$, where k is the wave number. The five-thirds law is one of the most important results of turbulence theory and is in agreement with high Reynolds number observations.

Recent decades have seen much progress in theory, calculations, and measurements. Among these may be mentioned the work on the modeling, coherent structures, direct numerical simulations, and multidimensional diagnostics. Observations in the ocean and the atmosphere (which von Karman called "a giant laboratory for turbulence research"), in which the Reynolds numbers are very large, are shedding new light on the structure of stratified turbulence.

12.3. NOMENCLATURE AND STATISTICS FOR TURBULENT FLOW

The dependent-field variables in a turbulent flow (velocity components, pressure, temperature, etc.) are commonly analyzed and described using definitions and nomenclature borrowed from the theory of *stochastic processes* and *random variables* even though fluid-dynamic turbulence is not entirely random. Thus, the characteristics of turbulent-flow field variables are commonly specified in terms of their *statistics* or *moments*. In particular, a turbulent field quantity, $\tilde{\vartheta}$, is commonly separated into is first moment, $\overline{\vartheta}$, and its fluctuations, $\vartheta \equiv \tilde{\vartheta} - \overline{\vartheta}$, which have zero mean. This separation is known as the *Reynolds decomposition* and is further described and utilized in Section 12.5.

To define moments precisely, specific terminology is needed. A *collection* of independent realizations of a random variable, obtained under identical conditions, is called an *ensemble*. The ordinary arithmetic average over the collection is called an *ensemble average* and is denoted herein by an over bar. When the number N of realizations in the ensemble is large, $N \to \infty$, the ensemble average is called an *expected value* and is denoted with angle brackets.

With this terminology and notation, the mth-*moment*, $\overline{u^m}$, of the random variable u at location $\mathbf{x}$ and time t is defined as the ensemble average of u^m:

$$\langle u^m(\mathbf{x},t)\rangle = \lim_{N\to\infty} \overline{u^m(\mathbf{x},t)} \equiv \lim_{N\to\infty} \frac{1}{N}\sum_{n=1}^{N}(u(\mathbf{x},t{:}n))^m, \tag{12.1}$$

where $u(\mathbf{x},t{:}n)$ is nth the realization in the ensemble. The limit $N\to\infty$ can only be taken formally in theoretical analysis, so when dealing with measurements, $\overline{u^m}$ is commonly used in place of $\langle u^m\rangle$ and good experimental design ensures that N is large enough for reliable determination of the first few moments of u. Thus, the over-bar notation for ensemble average is favored in the remainder of this chapter. Collectively, the moments for integer values of m are known as the *statistics* of $u(\mathbf{x},t)$.

Under certain circumstances, ensemble averaging is not necessary for moment estimation. When u is *stationary in time*, its statistics do not depend on time, and $\overline{u^m}$ at $\mathbf{x}$ can be reliably estimated from time averaging:

$$\overline{u^m(\mathbf{x})} = \frac{1}{\Delta t}\int_{t-\Delta t/2}^{t+\Delta t/2} u^m(\mathbf{x},t)dt, \tag{12.2}$$

when Δt is large enough. Time averages are relevant for turbulent flows that persist with the same boundary conditions for long periods of time, an example being the turbulent boundary-layer flow on the hull of a long-range ship that traverses a calm sea at a constant speed. Example time histories of temporally stationary and nonstationary processes are shown in Figure 12.2. When u is *homogeneous* or *stationary in space*, its statistics do not depend on location, and $\overline{u^m}$ at time t can be reliably estimated from spatial averaging in a volume V,

$$\overline{u^m(t)} = \frac{1}{V}\int_V u^m(\mathbf{x},t)dV, \tag{12.3}$$

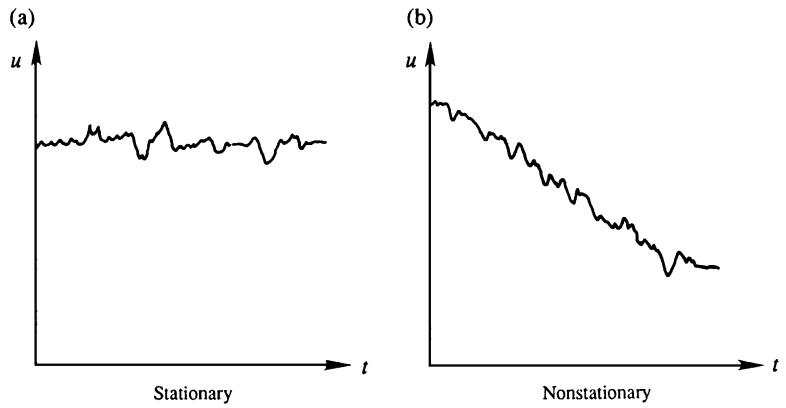

FIGURE 12.2 Sample time series indicating temporally stationary (a) and nonstationary processes (b). The time series in (b) clearly shows that the average value of u decreases with time compared to the time series in (a).

when V is large enough and defined appropriately. This type of average is often relevant in confined turbulent flows subject to externally imposed temporal variations, an example being the in-cylinder swirling and tumbling gas flow driven by piston motion and valve flows in an internal combustion piston engine.

For the discussions in this chapter, all moments denoted by over bars are ensemble averages determined from (12.1), unless otherwise specified. Equations (12.2) and (12.3) are provided here because they are commonly used to convert turbulent flow measurements into moment values. In particular, (12.2) or (12.3) are used in atmospheric and oceanic field measurements because ongoing natural phenomena like weather or the slow meandering of ocean currents make it is practically impossible to precisely repeat field observations under identical circumstances. For such measurements, a judicious selection of Δt or V is necessary; they should be long or large enough for reliable moment estimation but small enough so that the resulting statistics are only weakly influenced by ongoing natural variations.

Before defining and describing specific moments, several important properties of the process of ensemble averaging defined by (12.1) must be mentioned. First, ensemble averaging *commutes* with differentiation, that is, the application order of these two operators can be interchanged:

$$\overline{\frac{\partial u^m}{\partial t}} = \frac{1}{N}\sum_{n=1}^{N}\frac{\partial}{\partial t}(u(\mathbf{x},t{:}n))^m = \frac{\partial}{\partial t}\left(\frac{1}{N}\sum_{n=1}^{N}(u(\mathbf{x},t{:}n))^m\right) = \frac{\partial}{\partial t}\overline{u^m}.$$

Similarly, ensemble averaging commutes with addition, multiplication by a constant, time integration, spatial differentiation, and spatial integration. Thus the following are all true:

$$\overline{u^m + v^m} = \overline{u^m} + \overline{v^m},\ \overline{Au^m} = A\overline{u^m},\ \overline{\frac{\partial u^m}{\partial t}} = \frac{\partial}{\partial t}\overline{u^m}, \qquad (12.4,\ 12.5,\ 12.6)$$

$$\overline{\int_a^b u^m dt} = \int_a^b \overline{u^m} dt\ ,\ \overline{\frac{\partial u^m}{\partial x_j}} = \frac{\partial}{\partial x_j}\overline{u^m},\ \overline{\int u^m d\mathbf{x}} = \int \overline{u^m} d\mathbf{x}, \qquad (12.7,\ 12.8,\ 12.9)$$

where v is another random variable; a, b, m, and A are all constants; and $d\mathbf{x}$ represents a general spatial increment. In particular, (12.5) with $m = 0$ implies $\overline{A} = A$, so if $A = \overline{u}$ then $\overline{\overline{u}} = \overline{u}$; the ensemble average of an average is just the average. However, the ensemble average of a product of random variables is not necessarily the product of the ensemble averages. In general,

$$\overline{u^m} \neq \overline{u}^m \quad \text{and} \quad \overline{uv} \neq \overline{u}\,\overline{v},$$

when $m \neq 1$, and u and v are different random variables.

The simplest statistic of a random variable u is its *first moment*, *mean*, or *average*, $\overline{u}$. From (12.1) with $m = 1$, $\overline{u}$ is:

$$\overline{u(\mathbf{x},t)} \equiv \frac{1}{N}\sum_{n=1}^{N} u(\mathbf{x},t{:}n). \qquad (12.10)$$

In general, $\overline{u}$ may depend on both space and time, and is obtained by summing the N separate realizations of the ensemble, $u(\mathbf{x},t{:}n)$ for $1 \leq n \leq N$, at time t and location $\mathbf{x}$, and then dividing the sum by N. A graphical depiction of ensemble averaging, as specified by (12.10), is shown in

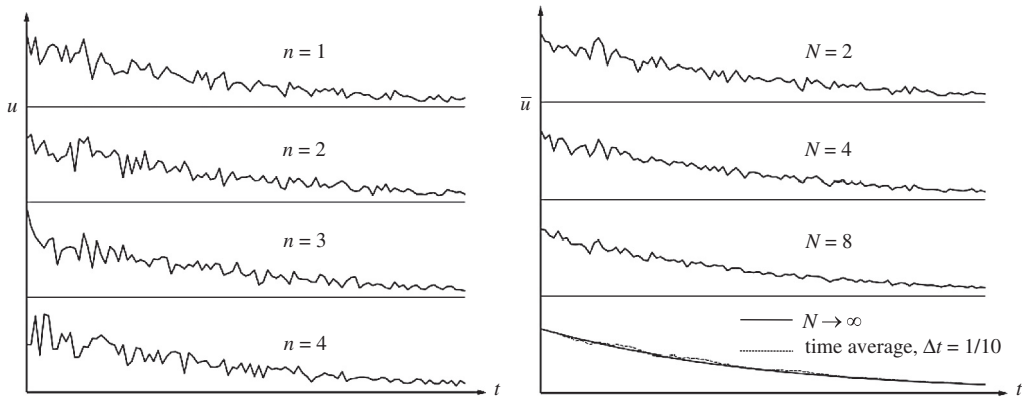

FIGURE 12.3 Illustration of ensemble and temporal averaging. The left panel shows four members of an ensemble of time series for the decaying random variable u. In all four cases, the fluctuations are different but the decreasing trend with increasing N is clearly apparent in each. The right panel shows averages of two, four, and eight members of the ensemble in the upper three plots. As the sample number N increases, fluctuations in the ensemble average decreases. The lowest plot on the right shows the $N \to \infty$ curve—this is the expected value of $u(t)$—and a simple sliding time average of the $n = 4$ curve where the duration of the time average is one-tenth of the time period shown. In this case, time and ensemble averaging produce nearly the same curve.

Figure 12.3 for time-series measurements recorded at the same point $\mathbf{x}$ in space. The left panel of the figure shows four members, $u(\mathbf{x},t{:}n)$ for $1 \leq n \leq 4$, of the ensemble. Here the average value of u decreases with increasing time. Time records such as these might represent atmospheric temperature measurements during the first few hours after sunset on different days, or they might represent a component of the flow velocity from an engine cylinder in the first 10 or 20 milliseconds after an exhaust valve opens. The right panel of Figure 12.3 shows the ensemble average $\overline{u(\mathbf{x},t)}$ obtained from the first two, four, and eight members of the ensemble. The solid smooth curve in the lower right panel of Figure 12.3 is the expected value that would be obtained from ensemble averaging in the limit $N \to \infty$. The dashed curve is a time average computed from only the fourth member of the ensemble using (12.2) with $m = 1$ and Δt equal to one-tenth of the total time displayed for each time history. Figure 12.3 clearly shows the primary effect of averaging is to suppress fluctuations since they become less prominent as N increases and are absent from the expected value. In addition, it shows that differences between an ensemble average of many realizations and a finite-duration temporal average of a single realization may be small, even when the flow is not stationary in time.

Although useful and important in many situations, the average or *first moment* alone does not directly provide information about turbulent fluctuations. Such information is commonly reported in terms of one or more *higher order central moments* defined by:

$$\overline{(u - \langle u \rangle)^m} \equiv \frac{1}{N} \sum_{n=1}^{N} (u(\mathbf{x},t{:}n) - \langle u(\mathbf{x},t) \rangle)^m, \tag{12.11}$$

where in practice $\overline{u(\mathbf{x},t)}$ often replaces $\langle u \rangle$. The central moments primarily carry information about the fluctuations since (12.11) explicitly shows that the mean is removed from each ensemble member. The first central moment is zero by definition. The next three have special

names: $\overline{(u-\overline{u})^2}$ is the *variance* of u, $\overline{(u-\overline{u})^3}$ is the *skewness* of u, and $\overline{(u-\overline{u})^4}$ is the *kurtosis* of u. In addition, the square root of the variance, $\sqrt{\overline{(u-\overline{u})^2}}$, is known as the *standard deviation*, the square root of the second moment, $\sqrt{\overline{u^2}} = u_{rms}$, is known as the *root mean square*, and these are equal when $\overline{u} = 0$. In the study of turbulence, a field variable's first moment and variance are most important.

EXAMPLE 12.1

Compute the time average of the function $u(t) = Ae^{-t/\tau} + B\cos(\omega t)$ using (12.2). Presuming this function is meant to represent a turbulent field variable with zero-mean fluctuations, $B\cos(\omega t)$, superimposed on a decaying time-dependent average, $Ae^{-t/\tau}$, what condition on Δt leads to an accurate recovery of the decaying average? And, what condition on Δt leads to suppression of the fluctuations?

Solution

Start by directly substituting the given function into (12.2):

$$\overline{u(t)} = \frac{1}{\Delta t}\int_{t-\Delta t/2}^{t+\Delta t/2}\left(Ae^{-t/\tau} + B\cos(\omega t)\right)dt,$$

and evaluating the integral:

$$\overline{u(t)} = \frac{1}{\Delta t}\left(-A\tau\exp\left(-\frac{t+\Delta t/2}{\tau}\right) + A\tau\exp\left(-\frac{t-\Delta t/2}{\tau}\right) + \frac{B}{\omega}\sin\left[\omega(t+\Delta t/2)\right] - \frac{B}{\omega}\sin\left[\omega(t-\Delta t/2)\right]\right).$$

This can be simplified to find:

$$\overline{u(t)} = \left[\frac{\sinh(\Delta t/2\tau)}{\Delta t/2\tau}\right]Ae^{-t/\tau} + \left[\frac{\sin(\omega\Delta t/2)}{\omega\Delta t/2}\right]B\cos(\omega t).$$

In the limit $\Delta t \to 0$, both factors in [,]-braces go to unity and the original function is recovered. Thus, the condition for properly determining the decaying average is $\Delta t \ll \tau$; the averaging interval Δt must be short compared to the time scale for decay, τ. However, to suppress the contribution of the fluctuations represented by the second term, its coefficient must be small. This occurs when $\omega\Delta t \gg 1$ which implies the averaging interval must be many fluctuation time periods long. Therefore, a proper averaging interval should satisfy: $1 \ll \omega\Delta t \ll \omega\tau$, but such a choice for Δt is not possible unless $\omega\tau \gg 1$.

12.4. CORRELATIONS AND SPECTRA

While moments of a random variable are important and interesting, they do not convey information about the temporal duration or spatial extent of fluctuations, nor do they indicate

anything about relationships between one or more dependent-field variables at different places and times. In the study of turbulence, correlations and spectra are commonly used to further characterize fluctuations and are described in this section. Furthermore, since we seek to describe fluctuations, all the random variables in this section are assumed to have zero mean, an assumption that is consistent with the Reynolds decomposition. The material presented here starts with general definitions that are simplified for a temporally stationary random variable sampled at the same point in space, or a spatially stationary random variable sampled at different points at the same time. Other approaches to specifying the temporal and spatial character of fluctuations, such as structure functions, fractal dimensions, multi-fractal spectra, and multiplier distributions, etc., are beyond the scope of this text.

In three spatial dimensions, the *correlation function* of the random variable u_i at location $\mathbf{x}_1$ and time t_1 with the random variable u_j at location $\mathbf{x}_2$ and time t_2 is defined as

$$R_{ij}(\mathbf{x}_1, t_1, \mathbf{x}_2, t_2) \equiv \overline{u_i(\mathbf{x}_1, t_1) u_j(\mathbf{x}_2, t_2)}, \tag{12.12}$$

where we will soon interpret u_i and u_j as turbulent-flow velocity-component fluctuations. Note that this R_{ij} is not the rotation tensor defined in Chapter 3. The correlation function R_{ij} can be computed via (12.1) when each realization of the ensemble contains time history pairs: $u_i(\mathbf{x},t{:}n)$ and $u_j(\mathbf{x},t;n)$. First, the N pairs $u_i(\mathbf{x}_1,t_1{:}n)$ and $u_j(\mathbf{x}_2,t_2{:}n)$ are selected from the realizations and multiplied together. Then the N pair-products are summed and divided by N to complete the calculation of R_{ij}.

The correlation R_{ij} specifies how similar $u_i(\mathbf{x}_1,t_1)$ and $u_j(\mathbf{x}_2,t_2)$ are to each other. The magnitude of R_{ij} is zero when positive values of $u_i(\mathbf{x}_1,t_1{:}n)$ are associated with equal likelihood with both positive and negative values of $u_j(\mathbf{x}_2,t_2{:}n)$. In this case, $u_i(\mathbf{x}_1,t_1)$ and $u_j(\mathbf{x}_2,t_2)$ are said to be *uncorrelated* when $R_{ij} = 0$, or *weakly correlated* if R_{ij} is small and positive. If, a positive value of $u_i(\mathbf{x}_1,t_1{:}n)$ is mostly associated with a positive value of $u_j(\mathbf{x}_2,t_2{:}n)$, and a negative value of $u_i(\mathbf{x}_1,t_1{:}n)$ is mostly associated with a negative value of $u_j(\mathbf{x}_2,t_2{:}n)$, then the magnitude of R_{ij} is large and positive. In this case, $u_i(\mathbf{x}_1,t_1)$ and $u_j(\mathbf{x}_2,t_2)$ are said to be *strongly correlated*. It is also possible for $u_i(\mathbf{x}_1,t_1{:}n)$ to be mostly associated with values of $u_j(\mathbf{x}_2,t_2{:}n)$ having the opposite sign so that R_{ij} is negative. In this case, $u_i(\mathbf{x}_1,t_1)$ and $u_i(\mathbf{x}_2,t_2)$ are said to be *anticorrelated*.

When $i \neq j$ in (12.12) the resulting function is called a *cross-correlation* function. When $i = j$ in (12.12) and $u_j(\mathbf{x}_2,t_2)$ is replaced by $u_i(\mathbf{x}_2,t_2)$, the resulting function is called an *autocorrelation* function; for example, $i = 1$ implies

$$R_{11}(\mathbf{x}_1, t_1, \mathbf{x}_2, t_2) \equiv \overline{u_1(\mathbf{x}_1, t_1) u_1(\mathbf{x}_2, t_2)}. \tag{12.13}$$

The two definitions, (12.12) and (12.13), may be normalized to define the *correlation coefficients*. For example when $i = 1$ and $j = 2$:

$$r_{12}(\mathbf{x}_1, t_1, \mathbf{x}_2, t_2) \equiv \frac{R_{12}(\mathbf{x}_1, t_1, \mathbf{x}_2, t_2)}{\sqrt{R_{11}(\mathbf{x}_1, t_1, \mathbf{x}_1, t_1) R_{22}(\mathbf{x}_2, t_2, \mathbf{x}_2, t_2)}} = \frac{\overline{u_1(\mathbf{x}_1, t_1) u_2(\mathbf{x}_2, t_2)}}{\sqrt{\overline{u_1^2(\mathbf{x}_1, t_1)}} \sqrt{\overline{u_2^2(\mathbf{x}_2, t_2)}}} \text{ and} \tag{12.14}$$

$$r_{11}(\mathbf{x}_1, t_1, \mathbf{x}_2, t_2) \equiv \frac{R_{11}(\mathbf{x}_1, t_1, \mathbf{x}_2, t_2)}{\sqrt{R_{11}(\mathbf{x}_1, t_1, \mathbf{x}_1, t_1) R_{11}(\mathbf{x}_2, t_2, \mathbf{x}_2, t_2)}} = \frac{\overline{u_1(\mathbf{x}_1, t_1) u_1(\mathbf{x}_2, t_2)}}{\sqrt{\overline{u_1^2(\mathbf{x}_1, t_1)}} \sqrt{\overline{u_1^2(\mathbf{x}_2, t_2)}}}, \tag{12.15}$$

which are restricted to lie between -1 (perfect anticorrelation) and $+1$ (perfect correlation). For any two functions u and v, it can be proved that

$$\overline{u(\mathbf{x}_1,t_1)v(\mathbf{x}_2,t_2)} \leq \sqrt{\overline{u^2(\mathbf{x}_1,t_1)}}\sqrt{\overline{v^2(\mathbf{x}_2,t_2)}}, \tag{12.16}$$

which is called the *Schwartz inequality*. It is analogous to the rule that the inner product of two vectors cannot be larger than the product of their magnitudes. Obviously, from (12.15), $r_{11}(\mathbf{x}_1,t_1,\mathbf{x}_1,t_1)$ is unity.

For temporally stationary processes that are sampled at the same point in space, $\mathbf{x} = \mathbf{x}_1 = \mathbf{x}_2$, the above formulas simplify, and the listing of $\mathbf{x}$ as an argument may be dropped to streamline the notation. The statistics of temporally stationary random processes are independent of the time origin, so we can shift the time origin to t_1 when computing a correlation so that $\overline{u_i(t_1)u_j(t_2)} = \overline{u_i(0)u_j(t_2-t_1)} = \overline{u_i(0)u_j(\tau)}$, where $\tau = t_2 - t_1$ is the *time lag*, without changing the correlation. Or, we can change t_1 in (12.13) into t, $\overline{u_i(t)u_j(t_2)} = \overline{u_i(t)u_j(t+\tau)}$, without changing the correlation. Thus, the correlation and autocorrelation functions can be written:

$$R_{ij}(\tau) = \overline{u_i(t)u_j(t+\tau)} \text{ and } R_{11}(\tau) = \overline{u_1(t)u_1(t+\tau)}, \tag{12.17}$$

where the over bar can be regarded as either an ensemble or time average in this case. Furthermore, under these conditions, the autocorrelation is symmetric:

$$R_{11}(\tau) = \overline{u_1(t)u_1(t+\tau)} = \overline{u_1(t-\tau)u_1(t)} = \overline{u_1(t)u_1(t-\tau)} = R_{11}(-\tau).$$

However, this is not the case for cross correlations, $R_{ij}(\tau) \neq R_{ij}(-\tau)$ when $i \neq j$. The value of a cross-correlation function at $\tau = 0$, $\overline{u_i(t)u_j(t)}$, is simply written as $\overline{u_iu_j}$ and called the *correlation* of u_i and u_j.

Figure 12.4 illustrates several of these concepts for two temporally stationary random variables $u(t)$ and $v(t)$. The left panel shows $u(t)$, $u(t+t_o)$, $v(t)$, and the time shift t_o is indicated near the top. The right panel shows the autocorrelation of u, the cross correlation of u and u with an imposed time shift of t_o, and the cross correlation of u and v. The tic-mark spacing represents the same amount of time in both panels. The time shift necessary for $\overline{u(t)u(t+\tau)}$ to reach zero is comparable to the width of peaks or valleys of $u(t)$. As expected, the autocorrelation is maximum when the two time arguments of u under the ensemble average are equal, and this correlation peak is symmetric about this time shift. Correlation is a mathematical shape-comparison indicator that is sensitive to time alignment. Consider $u(t)$, $u(t+t_o)$, and $\overline{u(t+t_o)u(t+\tau)}$. When $\tau = 0$ the peaks and valleys of $u(t)$ and $u(t+t_o)$—which are of course are identical—are not temporally aligned so $\overline{u(t+t_o)u(t+\tau)}$ in Figure 12.4 is nearly zero when $\tau = 0$. However, as τ increases—this corresponds to moving the time history of $u(t)$ to the left—the peaks and valleys of $u(t)$ and $u(t+t_o)$ come closer into temporal alignment. Perfect alignment is reached when $\tau = t_o$ and this produces the correlation maximum in $\overline{u(t+t_o)u(t+\tau)}$ at $\tau = t_o$. The cross-correlation function results in Figure 12.4 can be understood in a similar manner by looking for temporal alignment in u and v as v slides to the left with increasing τ. As shown in the left panel, the largest peak of u is temporally aligned with the largest peak of v when $\tau = t_+$ and this leads to the positive correlation maximum in $\overline{u(t)v(t+\tau)}$ at $\tau = t_+$. However, as τ increases further, the largest peak of u becomes

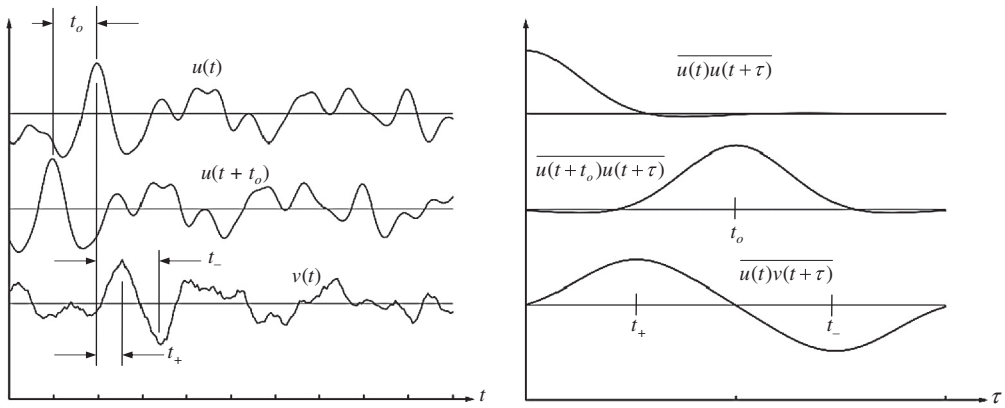

FIGURE 12.4 Sample results for auto- and cross-correlation functions of $u(t)$, $u(t+t_o)$, and $v(t)$. These three time series are shown on the left. The upper curve on the right is the autocorrelation function, $\overline{u(t)u(t+\tau)}$, of the upper time series on the left. The tic marks on the axes represent the same time interval so the width of a peak of $u(t)$ is about equal to the correlation time determined from $\overline{u(t)u(t+\tau)}$. The correlation of $u(t+t_o)$ and $u(t)$ is shown as the middle curve on the right, and it is just a shifted replica of $\overline{u(t)u(t+\tau)}$. The cross correlation of $u(t)$ and $v(t)$ is the lower curve on the right. Here the maximum cross correlation occurs when $\tau = t_+$ and the peaks of u and v coincide. Similarly, u and v are most anti-correlated when peaks in u align with valleys in v at $\tau = t_-$.

temporally aligned with the deepest valley of v, and this leads to the cross-correlation minimum at $\tau = t_-$. Thus, the zeros and extrema of correlation functions indicate the time shifts necessary to temporally misalign, align, or anti-align field-variable fluctuations. Such timing information cannot be obtained from moments.

Several time scales can be determined from the autocorrelation function. For turbulence, the most important of these is the *integral time scale* Λ_t. Under normal conditions R_{11} goes to 0 as $\tau \to \infty$ because the turbulent fluctuation u_1 becomes uncorrelated with itself after a long time. The integral time scale is found by equating the area under the autocorrelation coefficient curve to a rectangle of unity height and duration Λ_t:

$$\Lambda_t \equiv \int_0^\infty r_{11}(\tau)d\tau = (1/R_{11}(0)) \int_0^\infty R_{11}(\tau)d\tau, \tag{12.18}$$

where $r_{11}(\tau) = R_{11}(\tau)/R_{11}(0)$ is the autocorrelation coefficient for the stream-wise velocity fluctuation u_1. Of course, (12.18) can be written in terms of r_{22} or r_{33}, but for the purposes at hand this is not necessary. The calculation in (12.18) is shown graphically in Figure 12.5. The integral time scale is a generic specification of the time over which a turbulent fluctuation is correlated with itself. In other words, Λ_t is a measure of the *memory* of the turbulence. The correlation time t_c is also shown in Figure 12.5 as the time when $r_{11}(\tau)$ first reaches zero. When temporally averaging a single random-variable time history of length Δt to mimic an ensemble average, the equivalent number of ensemble members can be estimated from $N \approx \Delta t/t_c$. A third time scale, the Taylor microscale λ_t, can also be extracted from $r_{11}(\tau)$. It is obtained from the curvature of the autocorrelation peak at $\tau = 0$ and is given by:

$$\lambda_t^2 \equiv -2 \Big/ \left[d^2 r_{11}/d\tau^2\right]_{\tau=0} \tag{12.19}$$

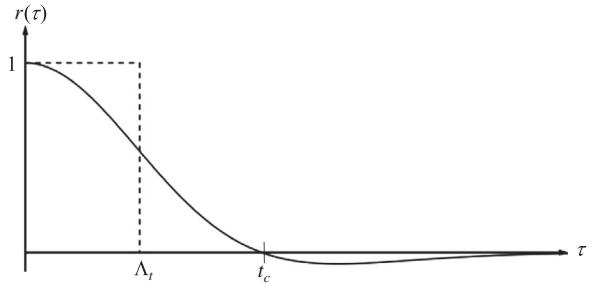

FIGURE 12.5 Sample plot of an autocorrelation coefficient showing the integral time scale Λ_t, and the correlation time t_c. The normalization requires $r(0) = 1$. In the limit $\tau \to \infty$, $r(\tau) \to 0$ and thereby indicates that the random process used to construct r becomes uncorrelated with itself when the time shift τ is large enough.

(see Exercise 12.9). The Taylor microscale λ_t is much less than Λ_t in high Reynolds number turbulence, and it indicates where a turbulent fluctuation, $u_1(t)$ in (12.19), is well correlated with itself.

A second (and equivalent) means of describing the characteristics of turbulent fluctuations, which also complements the information provided by moments, is the *energy spectrum* $S_e(\omega)$ defined as the Fourier transform of the autocorrelation function $R_{11}(\tau)$:

$$S_e(\omega) \equiv \frac{1}{2\pi} \int_{-\infty}^{+\infty} R_{11}(\tau) \exp\{-i\omega\tau\}\, d\tau. \tag{12.20}$$

Thus, $S_e(\omega)$ and $R_{11}(\tau)$ are a Fourier transform pair:

$$R_{11}(\tau) \equiv \int_{-\infty}^{+\infty} S_e(\omega) \exp\{+i\omega\tau\}\, d\omega. \tag{12.21}$$

The relationships (12.20) and (12.21) are not special for $S_e(\omega)$ and $R_{11}(\tau)$ alone, but hold for many function pairs for which a Fourier transform exists. Roughly speaking, a Fourier transform can be defined if the function decays to zero fast enough as its argument goes to infinity. Since $R_{11}(\tau)$ is real and symmetric, then $S_e(\omega)$ is real and symmetric (see Exercise 12.6). Substitution of $\tau = 0$ in (12.21) gives

$$\overline{u_1^2} \equiv \int_{-\infty}^{+\infty} S_e(\omega) d\omega. \tag{12.22}$$

This shows that the integrand increment $S_e(\omega)d\omega$ is the contribution to the variance (or fluctuation energy) of u_1 from the frequency band $d\omega$ centered at ω. Therefore, the function $S_e(\omega)$ represents the way fluctuation energy is distributed across frequency ω. From (12.20) it also follows that

$$S_e(0) = \frac{1}{2\pi} \int_{-\infty}^{\infty} R_{11}(\tau) d\tau = \frac{\overline{u_1^2}}{\pi} \int_{0}^{\infty} r_{11}(\tau) d\tau = \frac{\overline{u_1^2}}{\pi} \Lambda_t,$$

which shows that the spectral value at zero frequency is proportional to the variance of u_1 and the integral time scale.

From (12.16) to this point, u_i and u_j have been considered stationary functions of time measured at the same point in space. In a similar manner, we now consider u_i and u_j to be stationary functions in space measured at the same instant in time t. For simplicity we drop the listing of t as an independent variable. In this case, the correlation tensor only depends on the vector separation between $\mathbf{x}_1$ and $\mathbf{x}_2$, $\mathbf{r} = \mathbf{x}_2 - \mathbf{x}_1$,

$$R_{ij}(\mathbf{r}) \equiv \overline{u_i(\mathbf{x})u_j(\mathbf{x}+\mathbf{r})}. \tag{12.23}$$

An instantaneous field measurement of $u_i(\mathbf{x})$ is needed to calculate the spatial autocorrelation $R_{ij}(\mathbf{x})$. This is a difficult task in three dimensions, although planar particle imaging velocimetry (PIV) makes it possible in two. However, single-point measurements of a time series $u_1(t)$ in turbulent flows are still quite common and spatial results may be obtained approximately by rapidly moving a probe in a desired direction. If the speed U_0 of the probe is high enough, we can assume that the field of turbulence is *frozen* and does not change while the probe moves through it during the measurement. Although the probe actually records a time series $u_1(t)$, it can be transformed into a spatial series $u_1(x)$ by replacing t by x/U_0. The assumption that the turbulent fluctuations at a point are caused by the advection of a frozen field past the point is called *Taylor's hypothesis*, and the accuracy of this approximation increases as the ratio u_{rms}/U_0 decreases.

12.5. AVERAGED EQUATIONS OF MOTION

In this section, the equations of motion for the mean state in a turbulent flow are derived. The contribution of turbulent fluctuations appears in these equations as a correlation of velocity-component fluctuations. A turbulent flow instantaneously satisfies the Navier-Stokes equations. However, it is virtually impossible to predict the flow in detail at high Reynolds numbers, as there is an enormous range of length and time scales to be resolved. Perhaps more importantly, we seldom want to know all the details. If a commercial aircraft must fly from Los Angeles, California, to Sydney, Australia, and turbulent skin-friction fluctuations occur in a frequency range from a few Hz to more than 10^4 Hz, the economically important parameter is the average skin friction because the time of the flight (many hours) is much longer than even the longest fluctuation time scale. Here, the integrated effect of the fluctuations approaches zero when compared to the integral of the average. This situation where the overall duration of the flow far exceeds turbulent-fluctuation time scales is very common in engineering and geophysical science.

The following development of the mean flow equations is for incompressible turbulent flow with constant viscosity where density fluctuations are caused by temperature fluctuations alone. The first step is to separate the dependent-field quantities into components representing the mean (capital letters and those with over bars) and those representing the deviation from the mean (lowercase letters and those with primes):

$$\tilde{u}_i = U_i + u_i,\ \tilde{p} = P + p,\ \tilde{\rho} = \overline{\rho} + \rho',\ \text{and}\ \tilde{T} = \overline{T} + T' \tag{12.24}$$

where—as in the preceding chapter—the complete field quantities are denoted by a tilde (~). As mentioned in Section 12.3, this separation into mean and fluctuating components is called the *Reynolds decomposition*. Although it doubles the number of dependent-field variables, this decomposition remains useful and relevant more than a century after it was first proposed. However, it leads to a closure problem in the resulting equation set that has still not been resolved. The mean quantities in (12.24) are regarded as expected values,

$$\overline{\tilde{u}}_i = U_i,\ \overline{\tilde{p}} = P,\ \overline{\tilde{\rho}} = \overline{\rho},\ \text{and}\ \overline{\tilde{T}} = \overline{T}, \tag{12.25}$$

and the fluctuations have zero mean,

$$\overline{u}_i = 0,\ \overline{p} = 0,\ \overline{\rho'} = 0,\ \text{and}\ \overline{T'} = 0. \tag{12.26}$$

The equations satisfied by the mean flow are obtained by substituting (12.24) into the governing equations and averaging. Here, the starting point is the Boussinesq set:

$$\frac{\partial \tilde{u}_i}{\partial t} + \tilde{u}_j \frac{\partial \tilde{u}_i}{\partial x_j} = \frac{\partial \tilde{u}_i}{\partial t} + \frac{\partial}{\partial x_j}(\tilde{u}_j \tilde{u}_i) = -\frac{1}{\rho_0}\frac{\partial \tilde{p}}{\partial x_i} - g\left[1 - \alpha(\tilde{T} - T_0)\right]\delta_{i3} + \nu \frac{\partial^2 \tilde{u}_i}{\partial x_j^2}, \tag{4.86}$$

$$\frac{\partial \tilde{u}_i}{\partial x_i} = 0,\ \text{and}\ \frac{\partial \tilde{T}}{\partial t} + \tilde{u}_j \frac{\partial \tilde{T}}{\partial x_j} = \frac{\partial \tilde{T}}{\partial t} + \frac{\partial}{\partial x_j}(\tilde{u}_j \tilde{T}) = \kappa \frac{\partial^2 \tilde{T}}{\partial x_j^2}, \tag{4.10, 4.89}$$

where the first equality in (4.86) and (4.89) follows from adding $\tilde{u}_i(\partial \tilde{u}_j/\partial x_j) = 0$ and $\tilde{T}(\partial \tilde{u}_j/\partial x_j) = 0$, respectively, to the leftmost sides of these equations. Simplifications for constant-density flow are easily obtained at the end of this effort.

The continuity equation for the mean flow is obtained by putting the velocity decomposition of (12.24) into (4.10) and averaging:

$$\overline{\frac{\partial \tilde{u}_i}{\partial x_i}} = \overline{\frac{\partial}{\partial x_i}(U_i + u_i)} = \frac{\partial}{\partial x_i}\overline{(U_i + u_i)} = \frac{\partial}{\partial x_i}(U_i + \overline{u}_i) = \frac{\partial U_i}{\partial x_i} = 0, \tag{12.27}$$

where (12.8), $\overline{U}_i = U_i$, and $\overline{u}_i = 0$ have been used. Subtracting (12.27) from (4.10) produces:

$$\partial u_i/\partial x_i = 0. \tag{12.28}$$

Thus, the mean and fluctuating velocity fields are each divergence free.

The procedure for the mean momentum equation is similar but requires slightly more effort. Substituting (12.24) into (4.86) produces:

$$\frac{\partial (U_i + u_i)}{\partial t} + \frac{\partial}{\partial x_j}\big((U_j + u_j)(U_i + u_i)\big) = -\frac{1}{\rho_0}\frac{\partial (P + p)}{\partial x_i} - g\left[1 - \alpha(\overline{T} + T' - T_0)\right]\delta_{i3} + \nu \frac{\partial^2 (U_i + u_i)}{\partial x_j^2}. \tag{12.29}$$

The averages of each term in this equation can be determined by using (12.26) and the properties of an ensemble average: (12.4) through (12.6) and (12.8). The term-by-term results are:

$$\overline{\frac{\partial(U_i+u_i)}{\partial t}} = \frac{\partial\left(\overline{U_i+u_i}\right)}{\partial t} = \frac{\partial(U_i+\overline{u}_i)}{\partial t} = \frac{\partial U_i}{\partial t},$$

$$\overline{\frac{\partial}{\partial x_j}\Big((U_j+u_j)(U_i+u_i)\Big)} = \frac{\partial}{\partial x_j}\overline{\Big(U_iU_j+U_iu_j+u_iU_j+u_iu_j\Big)} = \frac{\partial}{\partial x_j}\Big(U_iU_j+\overline{u}_iU_j+U_i\overline{u}_j+\overline{u_iu_j}\Big)$$

$$= \frac{\partial}{\partial x_j}\Big(U_iU_j+\overline{u_iu_j}\Big),$$

$$\overline{\frac{1}{\rho_0}\frac{\partial(P+p)}{\partial x_i}} = \frac{1}{\rho_0}\frac{\partial\left(\overline{P+p}\right)}{\partial x_i} = \frac{1}{\rho_0}\frac{\partial(P+\overline{p})}{\partial x_i} = \frac{1}{\rho_0}\frac{\partial P}{\partial x_i},$$

$$\overline{g[1-\alpha(\overline{T}+T'-T_0)]\delta_{i3}} = g\Big[1-\alpha(\overline{T}+\overline{T'}-T_0)\Big]\delta_{i3} = g\Big[1-\alpha(\overline{T}-T_0)\Big]\delta_{i3}, \text{ and}$$

$$\overline{\nu\frac{\partial^2\left(U_i+u_i\right)}{\partial x_j^2}} = \nu\frac{\partial^2\left(\overline{U_i+u_i}\right)}{\partial x_j^2} = \nu\frac{\partial^2\left(U_i+\overline{u}_i\right)}{\partial x_j^2} = \nu\frac{\partial^2 U}{\partial x_j^2}.$$

Collecting terms, the ensemble average of the momentum equation is:

$$\frac{\partial U_i}{\partial t}+\frac{\partial}{\partial x_j}(U_iU_j)+\frac{\partial}{\partial x_j}(\overline{u_iu_j}) = -\frac{1}{\rho_0}\frac{\partial P}{\partial x_i}-g\Big[1-\alpha(\overline{T}-T_0)\Big]\,\delta_{i3}+\nu\frac{\partial^2 U_i}{\partial x_j^2}.$$

This equation can be mildly rearranged by using the final result of (12.27) and combing the gradient terms together to form the mean stress tensor $\overline{\tau}_{ij}$:

$$\frac{\partial U_i}{\partial t}+U_j\frac{\partial U_i}{\partial x_j} = -g\Big[1-\alpha(\overline{T}-T_0)\Big]\,\delta_{i3}+\frac{1}{\rho_0}\frac{\partial\overline{\tau}_{ij}}{\partial x_j}$$

$$= -g\Big[1-\alpha(\overline{T}-T_0)\Big]\,\delta_{i3}+\frac{1}{\rho_0}\frac{\partial}{\partial x_j}\Big(-P\delta_{ij}+2\mu\overline{S}_{ij}-\rho_0\overline{u_iu_j}\Big), \tag{12.30}$$

where $\overline{S}_{ij} = 1/2(\partial U_i/\partial x_j+\partial U_j/\partial x_i)$ is the mean strain-rate tensor, and (4.40) has been used to put the mean viscous stress in the form shown in (12.30). The correlation tensor $\overline{u_iu_j}$ in (12.30) is generally nonzero even though $\overline{u}_i = 0$. Its presence in (12.30) is important because it has no counterpart in the instantaneous momentum equation (4.86) and it links the character of the fluctuations to the mean flow. Unfortunately, the process of reaching (12.30) does not provide any new equations for this correlation tensor. Thus, the final equality of (12.27), and (12.30) do not comprise a closed system of equations, even when the flow is isothermal.

The new tensor in (12.30), $-\rho_0\overline{u_iu_j}$, plays the role of a stress and is called the *Reynolds stress tensor*. When present, Reynolds stresses are often much larger than viscous stresses, $\mu(\partial U_i/\partial x_j+\partial U_i/\partial x_j)$, except very close to a solid surface where the fluctuations go to zero and mean flow gradients are large. The Reynolds stress tensor is symmetric since $\overline{u_iu_j} = \overline{u_ju_i}$, so it has six independent Cartesian components. Its diagonal components $\overline{u_1^2}$, $\overline{u_2^2}$, and $\overline{u_3^2}$ are normal stresses that augment the mean pressure, while its off-diagonal components $\overline{u_1u_2}$, $\overline{u_1u_3}$, and $\overline{u_2u_3}$ are shear stresses.

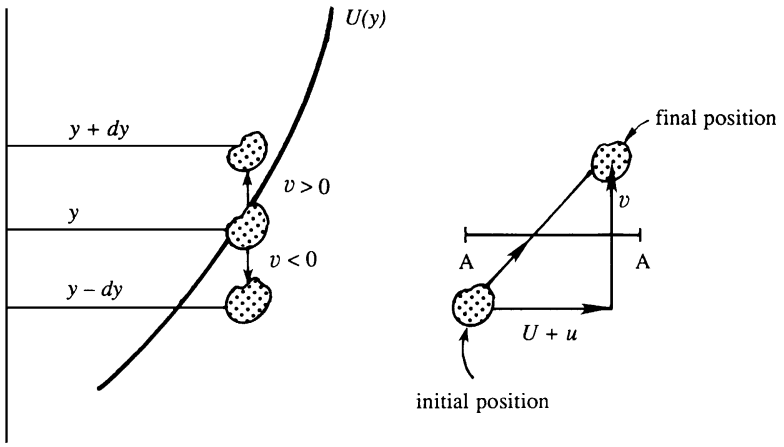

FIGURE 12.6 A schematic illustration of the development of nonzero Reynolds shear stress in a simple shear flow. A fluid particle that starts at y and is displaced upward to $y + dy$ by a positive vertical velocity fluctuation v brings an average horizontal fluid velocity of $U(y)$ that is lower than $U(y + dy)$. Thus, a positive vertical velocity fluctuation v is correlated with negative horizontal velocity fluctuation u, so $\overline{uv} < 0$. Similarly, a negative v displaces the fluid particle to $y - dy$ where it arrives on average with positive u, so again $\overline{uv} < 0$. Thus, turbulent fluctuations in shear flow are likely to produce negative nonzero Reynolds shear stress.

An explanation why the average product of the velocity fluctuations in a turbulent flow is not expected to be zero follows. Consider a shear flow where the mean shear dU/dy is positive (Figure 12.6). Assume that a fluid particle at level y travels upward because of a fluctuation ($v > 0$). On average this particle retains its original horizontal velocity during the migration, so when it arrives at level $y + dy$ it finds itself in a region where a larger horizontal velocity prevails. Thus the particle is on average slower ($u < 0$) than the neighboring fluid particles after it has reached the level $y + dy$. Conversely, fluid particles that travel downward ($v < 0$) tend to cause a positive u at their new level $y - dy$. Taken together, a positive v is associated with a negative u, and a negative v is associated with a positive u. Therefore, the correlation $\overline{uv}$ is negative for the velocity field shown in Figure 12.6, where $dU/dy > 0$. This makes sense, since in this case the x-momentum should tend to flow in the negative y-direction as the turbulence tends to diffuse the gradients and decrease dU/dy.

The Reynolds stresses arise from the nonlinear advection term $u_j(\partial u_i/\partial x_j)$ of the momentum equation, and are the average stress exerted by turbulent fluctuations on the mean flow. Another way to interpret the Reynolds stress is that it is the rate of mean momentum transfer by turbulent fluctuations. Consider again the shear flow $U(y)$ shown in Figure 12.6, where the instantaneous velocity is $(U + u, v, w)$. The fluctuating velocity components constantly transport fluid particles, and associated momentum, across a plane AA normal to the y-direction. The instantaneous rate of mass transfer across a unit area is $\rho_0 v$, and consequently the instantaneous rate of x-momentum transfer is $\rho_0(U + u)v$. Per unit area, the average rate of flow of x-momentum in the y-direction is therefore

$$\rho_0\overline{(U + u)v} = \rho_0 U\overline{u} + \rho_0\overline{uv} = \rho_0\overline{uv}.$$

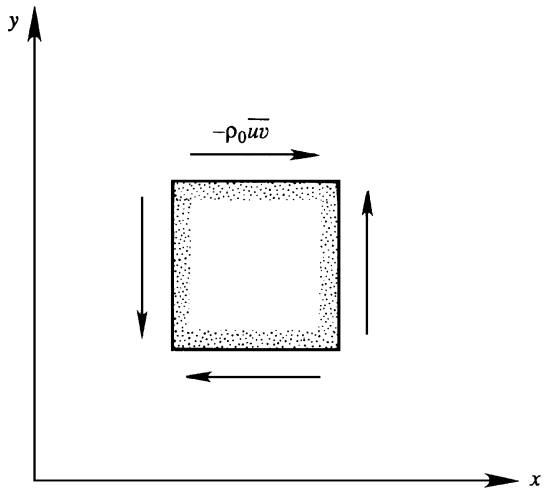

FIGURE 12.7 Positive directions of Reynolds stresses on a square element. These stress components are consistent with those drawn in Figure 2.4.

Generalizing, $\rho_0\overline{u_i u_j}$ *is the average flux of i-momentum along the j-direction, which also equals the average flux of j-momentum along the i-direction.*

The sign convention for the Reynolds stress is the same as that explained in Section 2.4. On a surface whose outward normal points in the positive i-direction, a positive τ_{ij} points along the j-direction. According to this convention, the Reynolds shear stresses $-\rho_0\overline{u_i u_j}$ $(i \neq j)$ on a rectangular element are directed as in Figure 12.7, if they are positive. Such a Reynolds stress causes mean transport of x-momentum along the negative y-direction.

The mean flow thermal energy equation comes from substituting the velocity and temperature decompositions of (12.24) into (4.89) and averaging. The substitution step produces:

$$\frac{\partial}{\partial t}(\overline{T}+T') + \frac{\partial}{\partial x_j}\Big((U_j+u_j)(\overline{T}+T')\Big) = \kappa\frac{\partial^2}{\partial x_j^2}(\overline{T}+T').$$

The averages of each term in this equation are:

$$\overline{\frac{\partial}{\partial t}(\overline{T}+T')} = \frac{\partial}{\partial t}(\overline{T}+\overline{T'}) = \frac{\partial \overline{T}}{\partial t},$$

$$\overline{\frac{\partial}{\partial x_j}\Big((U_j+u_j)(\overline{T}+T')\Big)} = \frac{\partial}{\partial x_j}\Big(U_j\overline{T}+\overline{u}_j\overline{T}+U_j\overline{T'}+\overline{u_jT'}\Big) = U_j\frac{\partial \overline{T}}{\partial x_j}+\frac{\partial}{\partial x_j}(\overline{u_jT'}), \text{ and}$$

$$\overline{\kappa\frac{\partial^2}{\partial x_j^2}(\overline{T}+T')} = \kappa\frac{\partial^2}{\partial x_j^2}(\overline{T}+\overline{T'}) = \kappa\frac{\partial^2 \overline{T}}{\partial x_j^2},$$

where the final equality of (12.27), (12.4) through (12.6), and (12.8) have been used. Collecting terms, the mean temperature equation takes the form:

$$\frac{\partial \overline{T}}{\partial t}+U_j\frac{\partial \overline{T}}{\partial x_j}+\frac{\partial}{\partial x_j}(\overline{u_jT'}) = \kappa\frac{\partial^2 \overline{T}}{\partial x_j^2}. \tag{12.31}$$

When multiplied by $\rho_o C_p$ and rearranged, (12.31) becomes the heat transfer equivalent of (12.30) and can be stated in terms of the mean heat flux Q_j:

$$\rho_0 C_p \left(\frac{\partial \overline{T}}{\partial t} + U_j \frac{\partial \overline{T}}{\partial x_j} \right) = -\frac{\partial Q_j}{\partial x_j} = -\frac{\partial}{\partial x_j} \left(-k \frac{\partial \overline{T}}{\partial x_j} + \rho_0 C_p \overline{u_j T'} \right), \tag{12.32}$$

where $k = \rho_o C_p \kappa$ is the thermal conductivity. Equation (12.32) shows that the fluctuations cause an additional mean *turbulent heat flux of* $\rho_0 C_p \overline{u_j T'}$ that has no equivalent in (4.89). The turbulent heat flux is the thermal equivalent of the Reynolds stress $-\rho_0 \overline{u_i u_j}$ found in (12.30). Unfortunately, the process of reaching (12.31) and (12.32) has not provided any new equations for the turbulent heat flux. However, some understanding of the turbulent heat flux can be gained by considering diurnal heating of the earth's surface. During daylight hours, the sun may heat the surface of the earth, resulting in a mean temperature that decreases with height and in the potential for turbulent convective air motion. When such motions occur, an upward velocity fluctuation is mostly associated with a positive temperature fluctuation, giving rise to an upward heat flux $\rho_0 C_p \overline{u_3 T'} > 0$.

The final mean-flow equation commonly considered for turbulent flows is that for transport of a dye or a nonreacting molecular species that is merely carried by the turbulent flow without altering the flow. Such passive contaminants are commonly called *passive scalars* or *conserved scalars* and the rate at which they are mixed with nonturbulent fluid is often of significant technological interest for pollutant dispersion and premixed combustion. Consider a simple binary mixture composed of a primary fluid with density ρ and a contaminant fluid (the passive scalar) with density ρ_s. The density ρ_m that results from mixing these two fluids is $\rho_m = \tilde{v}\rho_s + (1 - \tilde{v})\rho$, where $\tilde{v}$ is the volume fraction of the passive scalar. The relevant conservation equation for the passive scalar is:

$$\frac{\partial}{\partial t}(\rho_m \tilde{Y}) + \frac{\partial}{\partial x_j}(\rho_m \tilde{Y} \tilde{u}_j) = \frac{\partial}{\partial x_j} \left(\rho_m \kappa_m \frac{\partial}{\partial x_j} \tilde{Y} \right), \tag{12.33}$$

(see Kuo, 1986) where $\tilde{u}_j$ is the instantaneous mass-averaged velocity of the mixture, $\tilde{Y}$ is the mass fraction of the passive scalar, and κ_m is the mass-based molecular diffusivity of the passive scalar (see (1.1)). If the mean and fluctuating mass fraction of the conserved scalar are $\overline{Y}$ and Y', and the mixture density is constant, then the mean-flow passive scalar conservation equation is (see Exercise 12.12):

$$\frac{\partial \overline{Y}}{\partial t} + U_j \frac{\partial \overline{Y}}{\partial x_j} = \frac{\partial}{\partial x_j} \left(\kappa_m \frac{\partial \overline{Y}}{\partial x_j} - \overline{u_j Y'} \right), \tag{12.34}$$

where $\overline{u_j Y'}$ is the turbulent flux of the passive scalar. This equation is valid when the mixture density is constant, and this occurs when $\rho = \rho_s =$ constant and when the contaminant is dilute so that $\rho_m \approx \rho =$ constant. If the amount of a passive scalar is characterized by a concentration (mass per unit volume), molecular number density, or mole fraction—instead of a mass fraction—the forms of (12.33) and (12.34) are unchanged but the diffusivity may need to be adjusted and molecular number or mass density factors may appear (see Bird et al., 1960; Kuo, 1986). Equation (12.34) is of the same form as (12.32), and temperature may be considered a passive scalar in turbulent flows when it does not induce buoyancy, cause chemical reactions, or lead to significant density changes.

To summarize, (12.27), (12.30), (12.32), and (12.34) are the mean flow equations for incompressible turbulent flow (in the Boussinesq approximation). The process of reaching these equations is known as *Reynolds averaging*, and it may be applied to the full compressible-flow equations of fluid motion as well. The equations that result from **R**eynolds **a**veraging of any form of the **N**avier-**S**tokes equations are commonly known as *RANS equations*. The constant-density mean flow RANS equations commonly used in hydrodynamics are obtained from the results provided in this section by dropping the gravity term and the "0" from ρ_0 in (12.30), and reinterpreting the mean pressure as the deviation from hydrostatic (as explained in Section 4.9, "Neglect of Gravity in Constant Density Flows").

The primary problem with RANS equations is that there are more unknowns than equations. The system of equations for the first moments depends on correlations involving pairs of variables (second moments). And, RANS equations developed for these pair correlations involve triple correlations. For example, the conservation equation for the Reynolds stress correlation, $\overline{u_i u_j}$, is:

$$\begin{aligned}\frac{\partial \overline{u_i u_j}}{\partial t} + U_k \frac{\partial \overline{u_i u_j}}{\partial x_k} + \frac{\partial \overline{u_i u_j u_k}}{\partial x_k} = & -\overline{u_i u_k}\frac{\partial U_j}{\partial x_k} - \overline{u_j u_k}\frac{\partial U_i}{\partial x_k} - \frac{1}{\rho}\left(\overline{u_i \frac{\partial p}{\partial x_j}} + \overline{u_j \frac{\partial p}{\partial x_i}}\right) \\ & - 2\nu \overline{\frac{\partial u_i}{\partial x_k}\frac{\partial u_j}{\partial x_k}} + \nu \frac{\partial^2}{\partial x_k^2}\overline{u_i u_j} + g\alpha\left(\overline{u_j T'}\delta_{i3} + \overline{u_i T'}\delta_{j3}\right)\end{aligned} \tag{12.35}$$

(see Exercise 12.16), and triple correlations appear in the third term on the left. Similar conservation equations for the triple correlations involve quadruple correlations, and the equations for the quadruple correlations depend on fifth-order correlations, and so on. This problem persists at all correlation levels and is known as the *closure problem* in turbulence. At the present time there are three approaches to the closure problem. The first, known as *RANS closure modeling* (see Section 12.10), involves terminating the equation hierarchy at a given level and closing the resulting system of equations with models developed from dimensional analysis, intuition, symmetry requirements, and experimental results. The second, known as *direct numerical simulations* (DNS) involves numerically solving the time-dependent equations of motion and then Reynolds averaging the computational output to determine mean-flow quantities. The third, known as *large-eddy simulation* (LES), combines elements of the other two and involves some modeling and some numerical simulation of large-scale turbulent fluctuations.

A secondary problem associated with the RANS equations is that the presence of the Reynolds stresses in (12.30) excludes the possibility of converting it into a Bernoulli equation, even when the density is constant and the terms containing $\partial/\partial t$ and ν are zero.

12.6. HOMOGENEOUS ISOTROPIC TURBULENCE

It is clear from (12.27), (12.30), (12.32), and (12.34) that even with suitable boundary conditions the RANS equations for the mean flow are not directly solvable (even numerically) because of the closure problem. However, the idealization of turbulence as being homogeneous (or spatially stationary) and isotropic allows some significant simplifications. Turbulence behind a grid towed through a nominally quiescent fluid bath is approximately

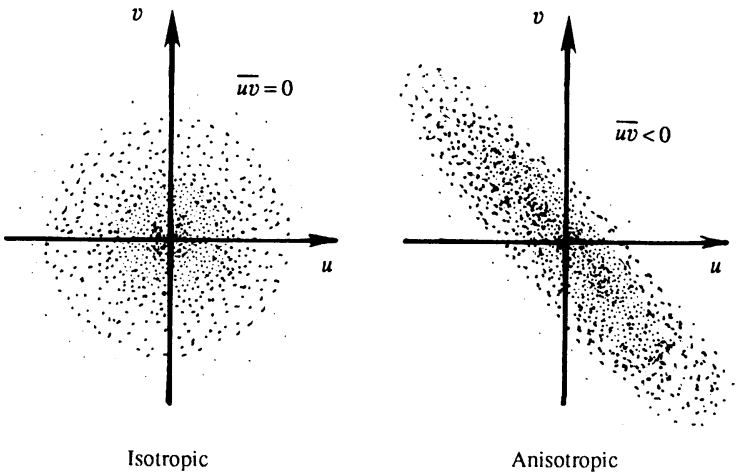

FIGURE 12.8 Scatter plots of velocity fluctuation samples in isotropic and anisotropic turbulent fields. Each dot represents a (u,v)-pair at a sample time and many sample times are represented in each panel. The isotropic case produces a symmetric cloud of points and indicates $\overline{uv} = 0$. The anisotropic case shows the data clustering around the line $v = -u$ and this indicates a negative correlation of u and v; $\overline{uv} < 0$.

homogeneous and isotropic, and turbulence in the interior of a real inhomogeneous turbulent flow is commonly assumed to be homogeneous and isotropic. Homogenous isotropic turbulence is discussed in greater detail in Batchelor (1953) and Hinze (1975).

If the turbulent fluctuations are completely isotropic, that is, if they do not have any directional preference, then the off-diagonal components of $\overline{u_i u_j}$ vanish, and the normal stresses are equal. This is illustrated in Figure 12.8, which shows a cloud of data points (sometimes called a *scatter plot*) on a uv-plane. The dots represent the instantaneous values of the (u,v)-velocity component pair at different times. In the isotropic case there is no directional preference, and the dots form a symmetric pattern. In this case positive u is equally likely to be associated with both positive and negative v. Consequently, *the average value of the product uv is zero when the turbulence is isotropic*. In contrast, the scatter plot in an anisotropic turbulent field has an orientation. The figure shows a case where a positive u is mostly associated with a negative v, giving $\overline{uv} < 0$.

If, in addition, the turbulence is homogeneous, then there are no spatial variations in the flow's statistics and all directions are equivalent:

$$\frac{\partial}{\partial x_i}\overline{u_j^n} = 0,\ \overline{u_1^2} = \overline{u_2^2} = \overline{u_3^2},\ \text{and}\ \overline{\left(\frac{\partial u_1}{\partial x_1}\right)^n} = \overline{\left(\frac{\partial u_2}{\partial x_2}\right)^n} = \overline{\left(\frac{\partial u_3}{\partial x_3}\right)^n}, \tag{12.36}$$

but relative directions must be respected,

$$\overline{\left(\frac{\partial u_1}{\partial x_2}\right)^n} = \overline{\left(\frac{\partial u_1}{\partial x_3}\right)^n} = \overline{\left(\frac{\partial u_2}{\partial x_1}\right)^n} = \overline{\left(\frac{\partial u_2}{\partial x_3}\right)^n} = \overline{\left(\frac{\partial u_3}{\partial x_1}\right)^n} = \overline{\left(\frac{\partial u_3}{\partial x_2}\right)^n}. \tag{12.37}$$

Note that the continuity equation requires derivatives in the third set of equalities of (12.36) to be zero when $n = 1$.

The spatial structure of the flow may be ascertained by considering the two-point correlation tensor, defined by (12.23), which reduces to the Reynolds stress correlation when $\mathbf{r} = 0$. In homogenous flow, R_{ij} does not depend on $\mathbf{x}$, and can only depend on $\mathbf{r}$. If the turbulence is also isotropic, the direction of $\mathbf{r}$ cannot matter. In this special situation, only two different

types of velocity-field correlations survive. These are described by the longitudinal (f) and transverse (g) correlation coefficients defined by:

$$f(r) \equiv \overline{u_{||}(\mathbf{x}+\mathbf{r})u_{||}(\mathbf{x})}/\overline{u_{||}^2} \text{ and } g(r) \equiv \overline{u_{\perp}(\mathbf{x}+\mathbf{r})u_{\perp}(\mathbf{x})}/\overline{u_{\perp}^2}, \tag{12.38}$$

where $u_{||}$ is parallel to $\mathbf{r}$, $u_{\perp}$ is perpendicular to $\mathbf{r}$, $\overline{u_{||}^2} = \overline{u_{\perp}^2} = \overline{u^2}$, and $f(0) = g(0) = 1$. The geometries for these two correlation functions are shown in Figure 12.9, where solid vectors indicate velocities and the dashed vector represents $\mathbf{r}$. Longitudinal and transverse integral scales and Taylor microscales are defined by:

$$\Lambda_f \equiv \int_0^\infty f(r)dr,\ \Lambda_g \equiv \int_0^\infty g(r)dr,\ \lambda_f^2 \equiv -2/\left[d^2f/dr^2\right]_{r=0}, \text{ and } \lambda_g^2 \equiv -2/\left[d^2g/dr^2\right]_{r=0}, \tag{12.39}$$

similar to the temporal integral scale and temporal Taylor microscale defined in (12.18) and (12.19), respectively. The most general possible form of $R_{ij}(r)$ that satisfies all the necessary symmetries is:

$$R_{ij} = F(r)r_ir_j + G(r)\delta_{ij}, \tag{12.40}$$

where the components of $\mathbf{r}$ are r_i, $|\mathbf{r}| = r$, and the functions $F(r) = \overline{u^2}(f(r) - g(r))r^{-2}$ and $G(r) = \overline{u^2}g(r)$ can be found by equating the diagonal components of R_{ij} (Exercise 12.17). For incompressible flow, $g(r)$ can be eliminated from (12.40) to find:

$$R_{ij} = \overline{u^2}\left\{f(r)\delta_{ij} + \frac{r}{2}\frac{df}{dr}\left(\delta_{ij} - \frac{r_ir_j}{r^2}\right)\right\} \tag{12.41}$$

(Exercise 12.18), and $\Lambda_g = \Lambda_f/2$ and $\lambda_g = \lambda_f/\sqrt{2}$.

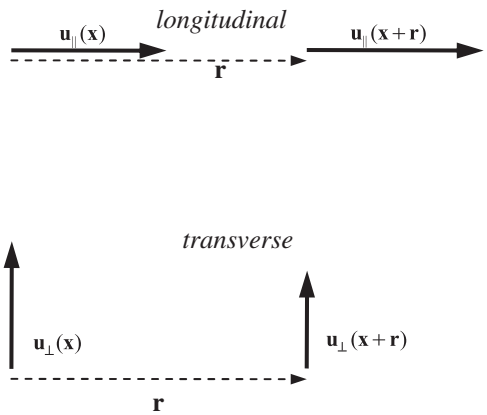

FIGURE 12.9 Longitudinal and transverse correlation geometries. In the longitudinal case, $\mathbf{u}_{||}$ is parallel to the displacement $\mathbf{r}$. In the transverse case, $\mathbf{u}_{\perp}$ is perpendicular to $\mathbf{r}$. Here $\mathbf{r}$ is shown horizontal but it may point in any direction.

Admittedly, the preceding formulae do not readily produce insights; however, the trace of R_{ij} evaluated at $r = 0$ is twice the average kinetic energy $\overline{e}$ (per unit mass) of the turbulent fluctuations

$$R_{ii}(0) \;=\; \overline{u_i u_i} \;=\; 2 \bullet \frac{1}{2}\left(\overline{u_1^2} + \overline{u_2^2} + \overline{u_3^2}\right) \;=\; 2\overline{e},$$

and $\overline{e}$ is an important element in understanding and modeling turbulence. We know from Section 4.8 that the kinetic energy of a flowing fluid may be converted into heat (dissipated) by the action of viscosity. Thus, the average kinetic energy dissipation rate $\overline{\varepsilon}$ (per unit mass) in an incompressible turbulent flow comprised entirely of fluctuations is the average of (4.58):

$$\overline{\varepsilon} \;=\; \frac{\nu}{2}\overline{\left(\partial u_i/\partial x_j + \partial u_j/\partial x_i\right)^2}. \tag{12.42}$$

When the flow is isotropic, the various directional symmetries, (12.36), and (12.37) imply:

$$\overline{\varepsilon} \;=\; 6\nu\left\{\overline{\left(\frac{\partial u_1}{\partial x_1}\right)^2} + \overline{\left(\frac{\partial u_1}{\partial x_2}\right)^2} + \overline{\left(\frac{\partial u_1}{\partial x_2}\right)\left(\frac{\partial u_2}{\partial x_1}\right)}\right\} \;=\; -15\nu\overline{u^2}\left[\frac{d^2 f}{dr^2}\right]_{r=0} \;=\; 30\nu\frac{\overline{u^2}}{\lambda_f^2} \;=\; 15\nu\frac{\overline{u^2}}{\lambda_g^2}, \tag{12.43}$$

where everything inside the {,}-braces has been put in terms of the first and second directions, and the second equality follows from the results of Exercise 12.19. Until the development of modern multidimensional measurement techniques, (12.43) was the primary means available for estimating $\overline{\varepsilon}$ from measurements in turbulent flows. Even today, fully resolved three-dimensional turbulent flow measurements are seldom possible, so reduced dimensionality relationships like (12.43), based on some assumed homogeneity and isotropy, commonly appear in the literature. In addition, Taylor-scale Reynolds numbers,

$$R_\lambda \equiv \lambda_{(g \text{ or } f)}\sqrt{\overline{u^2}}/\nu, \tag{12.44}$$

are occasionally quoted with $R_\lambda > 10^2$ being a nominal condition for fully turbulent flow (Dimotakis, 2000).

These concepts from homogeneous isotropic turbulence also allow the energy spectrum $S_{11}(k_1)$ of stream-wise velocity fluctuations along a stream-wise line through the turbulent field to be defined in terms of the autocorrelation function (12.23) when $i = j = 1$:

$$S_{11}(k_1) \;=\; \frac{1}{2\pi}\int_{-\infty}^{+\infty} R_{11}(r_1)\,\exp\{-ik_1 r_1\}dr_1 \;=\; \frac{\overline{u_1^2}}{2\pi}\int_{-\infty}^{+\infty} f(r_1)\,\exp\{-ik_1 r_1\}dr_1, \tag{12.45}$$

where "1" implies the stream-wise flow direction. Measured spectra reported in the turbulence literature are commonly produced using (12.45) or its alternative involving finite-window Fourier transformations (see Exercise 12.8). The basic procedure is to collect time-series measurements of u_1, convert them to spatial measurements using Taylor's frozen turbulence hypothesis, compute R_{11} from the spatial series, and then use (12.45) to determine $S_{11}(k_1)$. As described in the next section, the functional dependence of a portion of S_{11} on k_1 and $\overline{\varepsilon}$ can be anticipated from dimensional analysis and insights derived from the progression or cascade of fluctuation kinetic energy through a turbulent flow. Additional relationships for R_{ij} and its associated spectrum tensor may be found (Hinze, 1975).

12.7. TURBULENT ENERGY CASCADE AND SPECTRUM

As mentioned in the introductory section of this chapter, turbulence rapidly dissipates kinetic energy, and an understanding of how this happens is possible via a term-by-term inspection of the equations that govern the kinetic energy in the mean flow and the average kinetic energy of the fluctuations.

An equation for the mean flow's kinetic energy per unit mass, $\overline{E} = (1/2)U_i^2$, can be obtained by multiplying (12.30) by U_i, and averaging (Exercise 12.15). With $\overline{S}_{ij} = 1/2(\partial U_i/\partial x_j + \partial U_j/\partial x_i)$ defining the mean strain-rate tensor, the resulting *energy-balance* or *energy-budget* equation for $\overline{E}$ is

$$\underbrace{\frac{\partial \overline{E}}{\partial t} + U_j \frac{\partial \overline{E}}{\partial x_j}}_{\substack{\text{Time rate of change of } \overline{E} \text{ following the mean flow}}} = \underbrace{\frac{\partial}{\partial x_j}\left(-\frac{U_j P}{\rho_0} + 2\nu U_i \overline{S}_{ij} - \overline{u_i u_j} U_i\right)}_{\text{transport}} - \underbrace{2\nu \overline{S}_{ij}\overline{S}_{ij}}_{\substack{\text{viscous} \\ \text{dissipation}}} + \underbrace{\overline{u_i u_j}\frac{\partial U_i}{\partial x_j}}_{\substack{\text{loss to} \\ \text{turbulence}}} - \underbrace{\frac{g}{\rho_0}\overline{\rho} U_3}_{\substack{\text{loss to} \\ \text{potential} \\ \text{energy}}}. \tag{12.46}$$

The left side is merely the total time derivative of $\overline{E}$ following a mean-flow fluid particle, while the right side represents the various mechanisms that bring about changes in $\overline{E}$.

The first three divergence terms on the right side of (12.46) represent *transport* of mean kinetic energy by pressure, viscous stresses, and Reynolds stresses. If (12.46) is integrated over the volume occupied by the flow to obtain the rate of change of the total (or global) mean-flow kinetic energy, then these transport terms can be transformed into a surface integral by Gauss' theorem. Thus, these terms do not contribute to the total rate of change of $\overline{E}$ if $U_i = 0$ on the boundaries of the flow. Therefore, these three terms only *transport* or redistribute mean-flow kinetic energy from one region to another; they do not generate it or dissipate it.

The fourth term is the product of the mean flow's viscous stress (per unit mass) $2\nu\,\overline{S}_{ij}$ and the mean strain rate $\overline{S}_{ij}$. It represents the *direct viscous dissipation* of mean kinetic energy via its conversion into heat.

The fifth term is analogous to the fourth term. It can be written as $\overline{u_i u_j}\,(\partial U_i/\partial x_j) = \overline{u_i u_j}\,\overline{S}_{ij}$ so that it is a product of the turbulent stress (per unit mass) and the mean strain rate. Here, the doubly contracted product of a symmetric tensor $\overline{u_i u_j}$ and the tensor $\partial U_i/\partial x_j$ is equal to the product of $\overline{u_i u_j}$ and the *symmetric* part of $\partial U_i/\partial x_j$, namely $\overline{S}_{ij}$, as proved in Section 2.10. If the mean flow is given by $U(y)$ alone, then $\overline{u_i u_j}\,(\partial U_i/\partial x_j) = \overline{uv}\,(dU/dy)$. From the preceding section, $\overline{uv}$ is likely to be negative if dU/dy is positive. Thus, the fifth term is likely to be negative in shear flows. So, by analogy with the fourth term, it must represent a mean-flow kinetic energy loss to the fluctuating velocity field. Indeed, this term appears on the right-hand side of the equation for the rate of change of the turbulent kinetic energy, but *with the sign reversed*. Therefore, this term generally results in a loss of mean kinetic energy and a gain of turbulent kinetic energy. It is commonly known as the *shear production* term.

The sixth term represents the work done by gravity on the mean vertical motion. For example, an upward mean motion results in a loss of mean kinetic energy, which is accompanied by an increase in the potential energy of the mean field.

The two viscous terms in (12.46), namely, the viscous transport $2\nu\partial(U_i\,\overline{S}_{ij})/\partial x_j$ and the mean-flow viscous dissipation $-2\nu\overline{S}_{ij}\overline{S}_{ij}$, are small compared to the equivalent turbulence terms in a fully turbulent flow at high Reynolds numbers. Compare, for example, the mean-flow viscous dissipation and the shear-production terms:

$$\frac{2\nu\overline{S}_{ij}\overline{S}_{ij}}{\overline{u_iu_j}\,(\partial U_i/\partial x_j)} \sim \frac{\nu(U/L)^2}{u_{rms}^2(U/L)} \sim \frac{\nu}{UL} = \frac{1}{\mathrm{Re}} \ll 1,$$

where U is the velocity scale for the mean flow, L is a length scale for the mean flow (e.g., the overall thickness of a boundary layer), and u_{rms} is presumed to be of the same order of magnitude as U, a presumption commonly supported by experimental evidence. The direct influence of viscous terms is therefore negligible on the *mean* kinetic energy budget. However, this is *not* true for the *turbulent* kinetic energy budget, in which viscous terms play a major role. What happens is as follows: The mean flow loses energy to the turbulent field by means of the shear production term and the *turbulent* kinetic energy so generated is then dissipated by viscosity.

An equation for the mean kinetic energy $\overline{e} = (1/2)u_i^2$ of the turbulent velocity fluctuations can be obtained by setting $i = j$ (12.35) and dividing by two. With $S'_{ij} = 1/2(\partial u_i/\partial x_j + \partial u_j/\partial x_i)$ defining the fluctuation strain-rate tensor, the resulting energy-budget equation for $\overline{e}$ is:

$$\underbrace{\frac{\partial\overline{e}}{\partial t} + U_j\frac{\partial\overline{e}}{\partial x_j}}_{\substack{\text{Time rate of change of } \overline{e} \text{ following the mean flow}}} = \underbrace{\frac{\partial}{\partial x_j}\left(-\frac{1}{\rho_0}\overline{pu_j} + 2\nu\overline{u_iS'_{ij}} - \frac{1}{2}\overline{u_i^2u_j}\right)}_{\text{transport}} - \underbrace{2\nu\overline{S'_{ij}S'_{ij}}}_{\substack{\text{viscous}\\ \text{dissipation}}} - \underbrace{\overline{u_iu_j}\frac{\partial U_i}{\partial x_j}}_{\substack{\text{gain from}\\ \text{mean flow}}} + \underbrace{g\alpha\overline{u_3T'}}_{\substack{\text{buoyant}\\ \text{production}}}. \tag{12.47}$$

The first three terms on the right side are in divergence form and consequently represent the spatial transport of turbulent kinetic energy via turbulent pressure fluctuations, viscous diffusion, and turbulent stresses.

The fourth term $\overline{\varepsilon} = 2\nu\overline{S'_{ij}S'_{ij}}$ is the *viscous dissipation of turbulent kinetic energy*, and it is *not* negligible in the turbulent kinetic energy budget (12.47), although the analogous term $2\nu\overline{S}_{ij}\overline{S}_{ij}$ is negligible in the mean-flow kinetic energy budget (12.46). In fact, the viscous dissipation $\overline{\varepsilon}$ is always positive and its magnitude is typically similar to that of the turbulence-production terms in most locations.

The fifth term $\overline{u_iu_j}\,(\partial U_i/\partial x_j)$ is the shear-production term and it represents the rate at which kinetic energy is lost by the mean flow and gained by the turbulent fluctuations. It appears in the mean-flow kinetic energy budget with the other sign.

The sixth term $g\alpha\overline{u_3T'}$ can have either sign, depending on the nature of the background temperature distribution $\overline{T}(x_3)$. In a stable situation in which the background temperature increases upward (as found, e.g., in the atmospheric boundary layer at night), rising fluid

elements are likely to be associated with a negative temperature fluctuation, resulting in $\overline{u_3 T'} < 0$, which means a downward turbulent heat flux. In such a stable situation $g\alpha\overline{u_3 T'}$ represents the rate of turbulent energy loss via work against the stable background density gradient. In the opposite case, when the background density profile is unstable, the turbulent heat flux correlation $\overline{u_3 T'}$ is upward, and convective motions cause an increase of turbulent kinetic energy (Figure 12.10). Thus, $g\alpha\overline{u_3 T'}$ is the *buoyant production* of turbulent kinetic energy; it can also be a buoyant *destruction* when the turbulent heat flux is downward. In isotropic turbulence, the upward thermal flux correlation $\overline{u_3 T'}$ is zero because there is no preference between the upward and downward directions.

The buoyant generation of turbulent kinetic energy lowers the potential energy of the mean field. This can be understood from Figure 12.10, where it is seen that the heavier fluid has moved downward in the final state as a result of the heat flux. This can also be demonstrated by deriving an equation for the mean potential energy, in which the term $g\alpha\overline{u_3 T'}$ appears with a *negative* sign on the right-hand side. Therefore, the *buoyant generation* of turbulent kinetic energy by the upward heat flux occurs at the expense of the mean *potential* energy. This is in contrast to the *shear production* of turbulent kinetic energy, which occurs at the expense of the mean *kinetic* energy.

The kinetic energy budgets for constant density flow are recovered from (12.46) and (12.47) by dropping the terms with gravity and re-interpreting the mean pressure as the deviation from hydrostatic (see Section 4.9, "Neglect of Gravity in Constant Density Flows").

The shear-production term represents an essential link between the mean and fluctuating fields. For it to be active (or nonzero), the flow must have mean shear and the turbulence must be anisotropic. When the turbulence is isotropic, the off-diagonal components of the

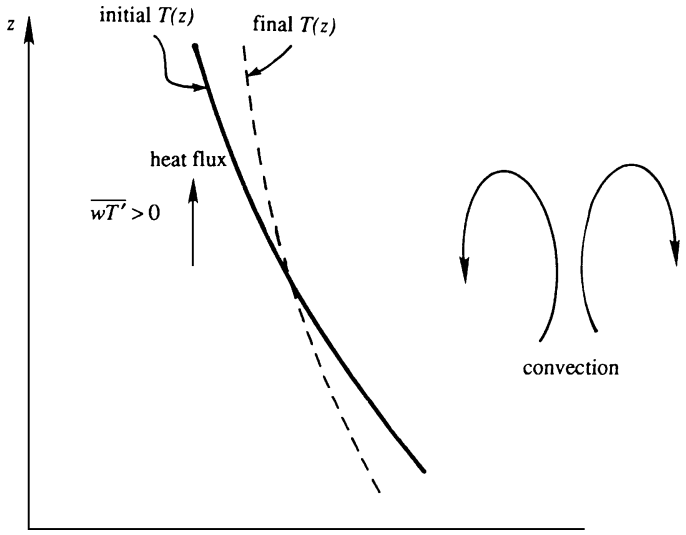

FIGURE 12.10 Heat flux in an unstable environment. Here warm air from below may rise and cool air may sink thereby generating turbulent kinetic energy by lowering the mean potential energy. In the final state, the upper air is warmer and less dense and the lower air is cooler and denser.

Reynolds stress $\overline{u_i u_j}$ are zero (see Section 12.6) and the on-diagonal ones are equal (12.36). Thus the double sum implied by $\overline{u_i u_j}\,(\partial U_i/\partial x_j)$ reduces to:

$$\overline{u_1^2}(\partial U_1/\partial x_1) + \overline{u_2^2}(\partial U_2/\partial x_2) + \overline{u_3^2}(\partial U_3/\partial x_3) \;=\; \overline{u_1^2}(\partial U_i/\partial x_i) \;=\; 0,$$

where the final equality holds from (12.27). Experimental observations suggest the largest eddies in a turbulent shear flow generally span the cross-stream distance L between those locations in a turbulent flow giving the maximum average velocity difference ΔU (Figure 12.11). In a layer with only one sign for the mean shear, L spans the layer as in Figure 12.11a, but for consistency when the shear has both signs, such as in turbulent pipe flow, L is the pipe radius as in Figure 12.11b. These largest eddies feel the mean shear—which must be of order $\Delta U/L$—and are distorted or made anisotropic by it. Energy is provided to these largest eddies by the mean flow as it forces them to deform and turn over. In this situation, turbulent velocity fluctuations are also of order ΔU, so the energy input rate $\dot{W}$ to a region of turbulence by the mean flow (per unit mass of fluid) is

$$\dot{W} \sim \overline{u_i u_j}\,(\partial U_i/\partial x_j) \sim (\Delta U)^2[\Delta U/L] \;=\; (\Delta U)^3/L, \tag{12.48}$$

where L and ΔU are commonly called the *outer* length scale and velocity difference. Of course the details of $\dot{W}$ will vary with flow geometry but its parametric dependence is set by (12.48). In reaching (12.48), it was implicitly assumed that the outer scale Reynolds number $\mathrm{Re}_L = \Delta U L/\nu$ is so large that viscosity plays no role in the interaction between the mean flow and the largest eddies of the turbulent shear flow.

In temporally stationary turbulence, the turbulent kinetic energy $\overline{e}$ cannot build up (or shrink to zero) so the work input at the largest scales from the mean flow must be balanced by the kinetic energy dissipation rate:

$$\dot{W} \;=\; \overline{\varepsilon}\,, \text{ so } \overline{\varepsilon} \sim (\Delta U)^3/L. \tag{12.49}$$

Thus, $\overline{\varepsilon}$ does not depend on ν, but is determined instead by the *inviscid* properties of the largest eddies, which extract energy from the mean flow. Second-tier eddies that are somewhat smaller than the largest ones are distorted and forced to roll over by the strain field

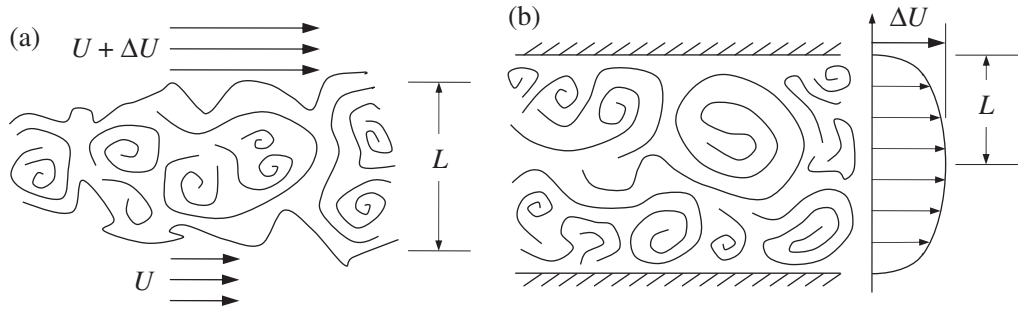

FIGURE 12.11 Schematic drawings of a turbulent flow without boundaries (a), and one with boundaries (b). Here the outer scale of the turbulence L spans the cross-stream distance over which the outer scale velocity difference ΔU develops. Here L may be the half width of the flow when the flow is symmetric as in (b). This choice of L and ΔU ensures that mean-flow velocity gradients will be of order $\Delta U/L$.

of the largest eddies, and these thereby extract energy from the largest eddies by the same mechanism that the largest eddies extract energy from the mean flow. Thus the average turbulent-kinetic-energy cascade pattern is set, and third-tier eddies extract energy from second-tier eddies, fourth-tier eddies extract energy from third-tier eddies, and so on. So, *turbulent kinetic energy is on average cascaded down from large to small eddies by interactions between eddies of neighboring size.* Small eddies are essentially advected in the velocity field of large eddies, since the scales of the strain-rate field of the large eddies are much larger than the size of a small eddy. Therefore, small eddies do not interact directly with the large eddies or the mean field, and are therefore nearly isotropic. The turbulent kinetic-energy cascade process is essentially inviscid with decreasing eddy scale size l' and eddy-velocity u' as long as the eddy Reynolds number $u'l'/\nu$ is much greater than unity. The cascade terminates when the eddy Reynolds number becomes of order unity and viscous effects are important. This average cascade process was first discussed by Richardson (1922), and is a foundational element in the understanding of turbulence.

In 1941, Kolmogorov suggested that the dissipating eddies are essentially homogeneous and isotropic, and that their size depends on those parameters that are relevant to the smallest eddies. These parameters are the rate $\overline{\varepsilon}$, the rate at which kinetic energy is supplied to the smallest eddies, and ν, the kinematic viscosity that smears out the velocity gradients of the smallest eddies. Since the units of $\overline{\varepsilon}$ are $\mathrm{m}^2/\mathrm{s}^3$, dimensional analysis only allows one way to construct a length scale η and a velocity scale u_K from $\overline{\varepsilon}$ and ν:

$$\eta = \left(\nu^3/\overline{\varepsilon}\right)^{1/4} \quad \text{and} \quad u_K = (\nu\overline{\varepsilon})^{1/4}. \tag{12.50}$$

These are called the *Kolmogorov microscale* and *velocity scale*, and the Reynolds number determined from them is

$$\eta u_K/\nu = (\nu\overline{\varepsilon})^{1/4}\left(\nu^3/\overline{\varepsilon}\right)^{1/4}/\nu = 1,$$

which appropriately suggests a balance of inertial and viscous effects for Kolmogorov-scale eddies. The relationship (12.50) and the recognition that ν does not influence $\overline{\varepsilon}$ suggests that a *decrease of ν merely decreases the eddy size at which viscous dissipation takes place*. In particular, the size of η relative to L can be determined by eliminating $\overline{\varepsilon}$ from (12.49) and the first equation of (12.50) to find:

$$\eta/L \sim \mathrm{Re}_L^{-3/4}, \quad \text{where } \mathrm{Re}_L = \Delta U L/\nu. \tag{12.51}$$

Therefore, the sizes of the largest and smallest eddies in high Reynolds number turbulence potentially differ by many orders of magnitude. For flow in a fixed-size device, the length scale L is fixed, so increasing the input velocity that leads to shear (or decreasing ν) leads to an increase in Re_L and a decrease in the size of the Kolmogorov eddies. In the ocean and the atmosphere, the Kolmogorov microscale η is commonly of the order of millimeters. However, in engineering flows η may be much smaller because of the larger power densities and dissipation rates. Landahl and Mollo-Christensen (1986) give a nice illustration of this. Suppose a 100-W household mixer is used to churn 1 kg of water in a cube 0.1 m ($= L$) on a side. Since all the power is used to generate turbulence, the rate of energy dissipation is $\overline{\varepsilon} = 100\ \mathrm{W/kg} = 100\ \mathrm{m}^2/\mathrm{s}^3$. Using $\nu = 10^{-6}\ \mathrm{m}^2/\mathrm{s}$ for water, we obtain $\eta = 10^{-5}$ m from (12.50).

Interestingly, the path that leads to (12.51) can also be used for either of the Taylor microscales (generically labeled λ_T here). Eliminating $\overline{\varepsilon}$ from (12.43) and (12.49) produces:

$$\frac{(\Delta U)^3}{L} \propto \frac{\nu\overline{u^2}}{\lambda_T^2} \rightarrow \frac{\lambda_T^2}{L^2} \propto \frac{\nu\overline{u^2}}{(\Delta U)^3 L} = \frac{\overline{u^2}}{(\Delta U)^2}\left(\frac{\nu}{\Delta U L}\right) \propto \frac{1}{\mathrm{Re}_L}, \text{ or } \frac{\lambda_T}{L} \propto \mathrm{Re}_L^{-1/2}, \tag{12.52}$$

where the final two proportionalities are valid when the fluctuation velocity is proportional to the ΔU. The negative half-power of the outer-scale Reynolds number matches that for laminar boundary-layer thicknesses (see (9.30)). Thus, the Taylor microscale can be interpreted as an internal boundary-layer thickness that develops at the edge of a large eddy during a single rotational movement having a path-length length L. However, it is not a distinguished length scale in the partition of turbulent kinetic energy even though (12.43) associates λ_T with $\overline{\varepsilon}$. The reason for this anonymity is that the velocity fluctuation appearing in (12.43) is not appropriate for eddies that dissipate turbulent kinetic energy. The appropriate dissipation-scale velocity is given by the second equality of (12.50). Thus, in high Reynolds number turbulence, λ_T is larger than η, as is clear from a comparison of (12.51) and (12.52) with $\mathrm{Re} \rightarrow \infty$. In addition, (12.52) implies $\mathrm{Re}_\lambda \sim (\mathrm{Re}_L)^{1/2}$, so a nominal condition for fully turbulent flow is $\mathrm{Re}_L > 10^4$ (Dimotakis, 2000). Above such a Reynolds number, the following ordering of length scales should occur: $\eta < \lambda_T < \Lambda_{(f \text{ or } g)} < L$.

Richardson's cascade, Kolmogorov's insights, the simplicity of homogeneous isotropic turbulence, and dimensional analysis lead to perhaps the most famous and prominent feature of high Reynolds number turbulence: the universal power law form of the energy spectrum in the inertial subrange. Consider the one-dimensional energy spectrum $S_{11}(k_1)$—it is the one most readily determined from experimental measurements—and associate eddy size l with the inverse of the wave number: $l \sim 2\pi/k_1$. For large eddy sizes (small wave numbers), the energy spectrum will not be universal because these eddies are directly influenced by the geometry-dependent mean flow. However, smaller eddies a few tiers down in the cascade may approach isotropy. In this case the mean shear no longer matters, so their spectrum of fluctuations S_{11} can only depend on the kinetic energy cascade rate $\overline{\varepsilon}$, the fluid's kinematic viscosity ν, and the wave number k_1. From (12.45), the units of S_{11} are found to be $\mathrm{m}^3/\mathrm{s}^2$; therefore dimensional analysis using S_{11}, $\overline{\varepsilon}$, ν, and k_1 requires:

$$\frac{S_{11}(k_1)}{\nu^{5/4}\overline{\varepsilon}^{1/4}} = \Phi\left(\frac{k_1\nu^{3/4}}{\overline{\varepsilon}^{1/4}}\right), \text{ or } \frac{S_{11}(k_1)}{u_K^2\eta} = \Phi(k_1\eta) \quad \text{for } k_1 \gg 2\pi/L, \tag{12.53}$$

where Φ is an undetermined function, and both parts of (12.50) have been used to reach the second form of (12.53). Furthermore, for eddy sizes somewhat less than L, but also somewhat greater than η, $2\pi/L \ll k_1 \ll 2\pi/\eta$, the spectrum must be independent of both the mean shear and the kinematic viscosity. This wave number range is known as the *inertial subrange*. Turbulent kinetic energy is transferred through this range of length scales without much loss to viscosity. Thus, the form of the spectrum in the inertial subrange is obtained from dimensional analysis using only S_{11}, $\overline{\varepsilon}$, and k_1:

$$S_{11}(k_1) = const \cdot \overline{\varepsilon}^{2/3} \cdot k_1^{5/3} \quad \text{for } 2\pi/L \ll k_1 \ll 2\pi/\eta. \tag{12.54}$$

The *constant* has been found to be universal for all turbulent flows and is approximately 0.25 for $S_{11}(k_1)$ subject to a *double-sided* normalization:

$$\int_{-\infty}^{+\infty} S_{11}(k_1)dk_1 = \overline{u_1^2} = \int_0^{+\infty} 2S_{11}(k_1)dk_1. \tag{12.55}$$

Equation (12.54) is usually called *Kolmogorov's* $k^{-5/3}$ *law* and it is one of the most important results of turbulence theory. When the spectral form (12.54) is subject to the normalization,

$$\overline{e} = \int_0^{+\infty} S(K)dK,$$

where K is the magnitude of the three-dimensional wave-number vector, the constant in the three-dimensional form of (12.54) is approximately 1.5 (see Pope, 2000). If the Reynolds number of the flow is large, then the dissipating eddies are much smaller than the energy-containing eddies, and the inertial subrange is broad.

Figure 12.12 shows a plot of experimental spectral measurements of $2S_{11}$ from several different types of turbulent flows (Chapman, 1979). The normalizations of the axes follow (12.53), $\overline{\varepsilon}$ is calculated from (12.43), η is calculated from (12.50), and the Taylor-Reynolds numbers (labeled R_λ in the figure) come from the longitudinal autocorrelation $f(r)$. The collapse of the data at high wave numbers to a single curve indicates the universal character of (12.53) at high wave numbers. The spectral form of Pao (1965) adequately fits the data and indicates how the spectral amplitude decreases faster than $k^{-5/3}$ as $k_1\eta$ approaches and then exceeds unity. The scaled wave number at which the data are approximately a factor of two below the $-5/3$ power law is $k_1\eta \approx 0.2$ (dashed vertical line), so the actual eddy size where viscous dissipation is clearly felt is $l_D \approx 30\eta$. The various spectra shown in Figure 12.12 turn horizontal with decreasing $k_1\eta$ where k_1L is of order unity.

Because very large Reynolds numbers are difficult to generate in an ordinary laboratory, the Kolmogorov spectral law (12.54) was not verified for many years. In fact, doubts were raised about its theoretical validity. The first confirmation of the Kolmogorov law came from the oceanic observations of Grant *et al.* (1962), who obtained a velocity spectrum in a tidal flow through a narrow passage between two islands just off the west coast of Canada. The velocity fluctuations were measured by hanging a hot film anemometer from the bottom of a ship. Based on the water depth and the average flow velocity, the outer-scale Reynolds number was of order 10^8. Such large Reynolds numbers are typical of geophysical flows, since the length scales are very large. Thus, the tidal channel data and results from other geophysical flows prominently display the $k^{-5/3}$ spectral form in Figure 12.12.

For the purpose of formulating predictions, the universality of the high wave number portion of the energy spectrum of turbulent fluctuations suggests that a single-closure model might adequately represent the effects of inertial subrange and smaller eddies on the nonuniversal large-scale eddies. This possibility has inspired the development of a wide variety of RANS equation closure models, and it provides justification for the central idea behind large-eddy simulations (LES) of turbulent flow. Such models are described in Pope (2000).

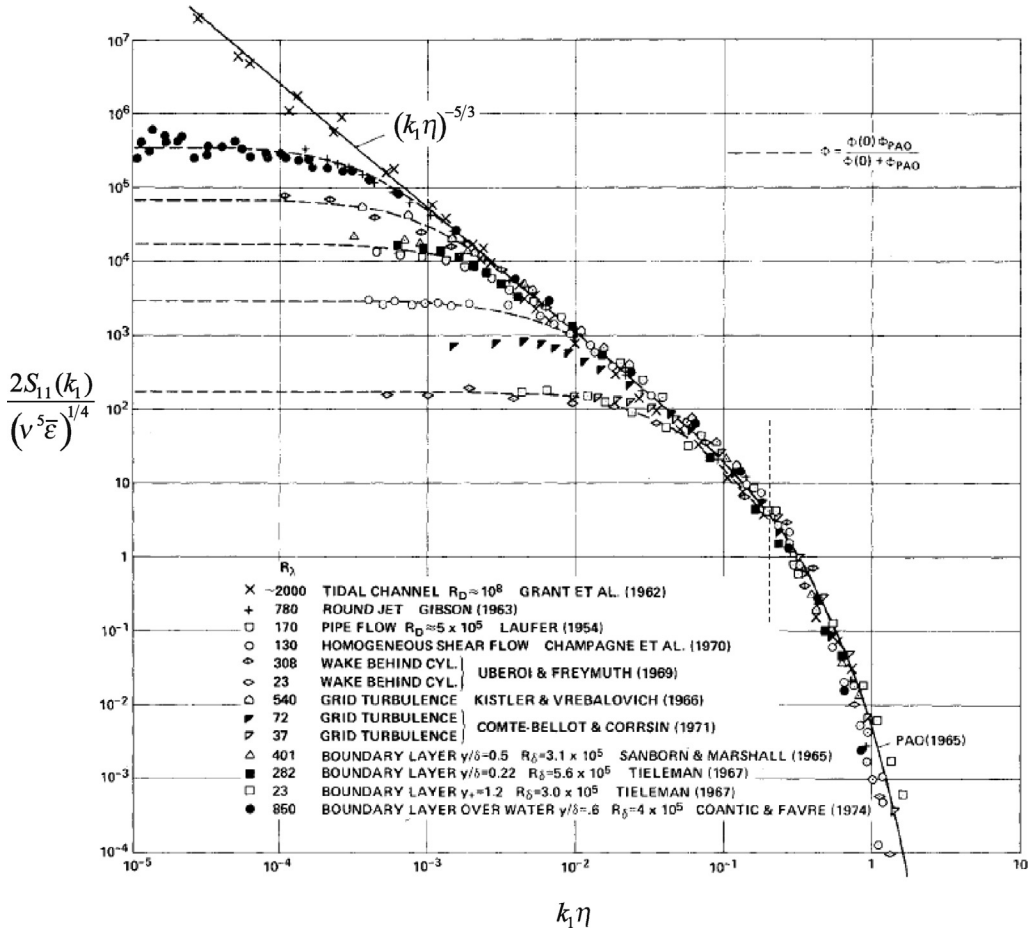

FIGURE 12.12 One-dimensional energy spectra $S_{11}(k_1)$ from a variety of turbulent flows plotted in Kolmogorov normalized form, reproduced from Chapman (1979). Here k_1 is the stream-wise wave number, η is the Kolmogorov scale defined by (12.50), and $\bar{\varepsilon}$ is the average kinetic energy dissipation rate determined from (12.43). Kolmogorov's $-5/3$ power law is indicated by the sloping line. The collapse of the various spectra to this line and to each other as $k_1\eta$ approaches and then exceeds unity strongly suggests that high-wave-number turbulent velocity fluctuations are universal when the Reynolds number is high enough. The dashed vertical line indicates the location where the spectral data are a factor of two below the $-5/3$ line established at lower wave numbers.

12.8. FREE TURBULENT SHEAR FLOWS

Persistent turbulence is maintained by the presence of mean-flow shear. This shear may exist because of a mismatch of fluid momentum within a flow, or because of the presence of one or more solid boundaries near the moving fluid. Turbulent flows in the former category are called *free* turbulent shear flows, and those in the latter are called *wall-bounded* turbulent shear flows. This section covers free turbulent flows that develop away from solid

boundaries. Such flows include jets, wakes, shear layers, and plumes; the first three are depicted in Figure 12.13. A plume is a buoyancy-driven jet that develops vertically so its appearance is similar to that shown in Figure 12.13a when the flow direction is rotated to be vertical. Jets, wakes, and plumes may exist in planar and axisymmetric geometries. Although idealized, such free shear flows are important for mixing reactants and in remote sensing, and are scientifically interesting because their development can sometimes be described by a single length scale and one boundary condition or origin parameter. Such a description commonly results from a similarity analysis in which the mean flow is assumed

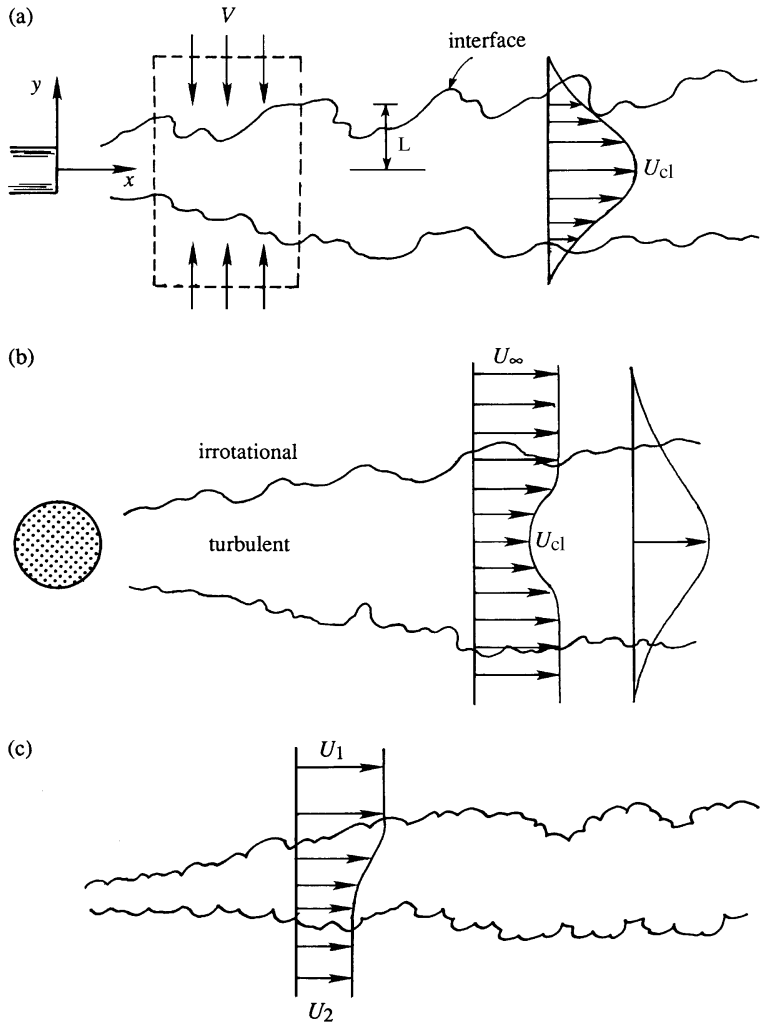

FIGURE 12.13 Three generic free turbulent shear flows: (a) jet, (b) wake, and (c) shear layer. In each case, the region of turbulence coincides with the region of shear in the mean velocity profile, and entrainment causes the cross-stream dimension L or δ of each flow to increase with increasing downstream distance. The fluid outside the region of turbulence is assumed to be irrotational.

to be *self-preserving*. This section presents one such similarity analysis for a single free turbulent shear flow (the planar jet), and then summarizes the similarity characteristics of a variety of planar and axisymmetric free turbulent shear flows. In most circumstances, free turbulent shear flows are simpler than wall-bounded turbulent shear flows. However, the outer portion of a turbulent boundary layer (from $y \sim 0.2\delta$ to its unconstrained edge) is similar to a free shear flow.

In snapshots and laser-pulse images, free shear flows usually appear with an erratic boundary that divides nominally turbulent from irrotational (or nonturbulent) fluid. Locally, the motion of this boundary is determined by the velocity induced by the turbulent vortices inside the region of turbulence. Typically, these vortices induce the surrounding nonturbulent fluid to flow toward the region of turbulence, and this induced flow, commonly called *entrainment*, causes the cross-stream size (L or δ) of the turbulent region to increase with increasing downstream distance. Because of entrainment, a passive scalar in the body of the turbulent flow is diluted with increasing downstream distance. The actual mechanism of entrainment involves both large- and small-eddy motions, and it may be altered within limits in some free shear flows by introducing velocity, pressure, or geometrical perturbations.

When a time-lapse image or an ensemble average of measurements from a free shear flow is examined, the edge of the region of turbulence is diffuse and the average velocity field and average passive scalar fields are found to be smooth functions. Significantly, the shapes of these mean profiles from different downstream locations within the same flow are commonly found to be self-similar when scaled appropriately. When this happens, the flow is in a state of *moving equilibrium*, in which both the mean and the turbulent fields are determined solely by the *local* length and velocity scales, a situation called *self-preservation*.

Some characteristics of the self-preserving state may be determined from a similarity analysis of the mean momentum equation (12.30) for a variety of free turbulent shear flows. The details of such an analysis are provided here for the plane turbulent jet. The scalings for other free turbulent shear flows are listed in Table 12.1, and are covered in this chapter's exercises. A plane turbulent jet is formed by fast-moving fluid that emerges into a quiescent reservoir from a long slot of width d, as shown in Figure 12.13a. Here, the long dimension of the slot is

TABLE 12.1 Self-Similar Far-Field Results for Some Free Turbulent Shear Flows

Flow	Mean Fields	ξ	Profile Widths
Planar Jet	$\frac{U(x,y)}{U_0} = \frac{U_{CL}(x)}{U_0}F(\xi) = 2.4\left(\frac{\rho_s}{\rho}\right)^{1/2}\left(\frac{x}{d}\right)^{-1/2}F(\xi)$	y/x	$(\xi_{1/2})_U = 0.11$
	$\frac{\overline{Y}(x,y)}{Y_0} = \frac{Y_{CL}(x)}{Y_0}H(\xi) = 2.0\left(\frac{\rho_s}{\rho}\right)^{1/2}\left(\frac{x}{d}\right)^{-1/2}H(\xi)$		$(\xi_{1/2})_Y = 0.14$
Planar Plume	$U(x,y) = U_{CL}(x)F(\xi) = 1.9\left(\frac{g(\rho-\rho_s)U_0 d}{\rho}\right)^{1/3}F(\xi)$	y/x	$(\xi_{1/2})_U = 0.12$
	$\frac{\overline{Y}(x,y)}{Y_0} = \frac{Y_{CL}(x)}{Y_0}H(\xi) = 2.4\left(\frac{\rho U_0^2}{g(\rho-\rho_s)d}\right)^{1/3}\left(\frac{x}{d}\right)^{-1}H(\xi)$		$(\xi_{1/2})_Y = 0.13$

(*Continued*)

TABLE 12.1 Self-Similar Far-Field Results for Some Free Turbulent Shear Flows—cont'd

Flow	Mean Fields	ξ	Profile Widths
Round Jet	$\frac{U(x,r)}{U_0} = \frac{U_{CL}(x)}{U_0}F(\xi) = 6.0\left(\frac{\rho_s}{\rho}\right)^{1/2}\left(\frac{x}{d}\right)^{-1}F(\xi)$	r/x	$(\xi_{1/2})_U = 0.090$
	$\frac{\overline{Y}(x,r)}{Y_0} = \frac{Y_{CL}(x)}{Y_0}H(\xi) = 5.0\left(\frac{\rho_s}{\rho}\right)^{1/2}\left(\frac{x}{d}\right)^{-1}H(\xi)$		$(\xi_{1/2})_Y = 0.11$
Round Plume	$U(x,r) = U_{CL}(x)F(\xi) = 3.5\left(\frac{g(\rho-\rho_s)U_0 d}{\rho}\right)^{1/3}\left(\frac{x}{d}\right)^{-1/3}F(\xi)$	r/x	$(\xi_{1/2})_U = 0.11$
	$\frac{\overline{Y}(x,r)}{Y_0} = \frac{Y_{CL}(x)}{Y_0}H(\xi) = 9.4\left(\frac{\rho U_0^2}{g(\rho-\rho_s)d}\right)^{1/3}\left(\frac{x}{d}\right)^{-5/3}H(\xi)$		$(\xi_{1/2})_Y = 0.10$
Shear Layer	$U(x,y) = U_2 + (U_1 - U_2)\frac{\int_{-\infty}^{\xi}F(\xi')d\xi'}{\int_{-\infty}^{+\infty}F(\xi')d\xi'}$	$\frac{y - y_{CL}(x)}{x}$	$(\Delta\xi_{80})_U = 0.085 \times \frac{U_1 - U_2}{\frac{1}{2}(U_1 + U_2)}$
Planar Wake	$U(x,y) = U_\infty - \Delta U_{CL}(x)F(\xi)$ $\frac{\Delta U_{CL}(x)}{U_\infty} = 1.8\,(\frac{x}{\theta_p})^{-1/2};\ \theta_p = \frac{\text{drag force}}{\rho U_\infty^2 \cdot \text{span}}$	$y/\sqrt{\theta_p x}$	$(\xi_{1/2})_U = 0.31$
Round Wake	$U(x,y) = U_\infty - \Delta U_{CL}(x)F(\xi)$ $\frac{\Delta U_{CL}(x)}{U_\infty} = (0.4\ to\ 2.0)\left(\frac{x}{\theta_r}\right)^{-2/3};\quad \theta_r^2 = \frac{\text{drag force}}{\rho U_\infty^2}$	$r/(\theta_r^2 x)^{1/3}$	$(\xi_{1/2})_U = 0.4$ to 0.9

TABLE 12.1 NOMENCLATURE

d = slot- or nozzle-exit width or diameter
U_0 = slot- or nozzle-exit fluid velocity
ρ_s = slot- or nozzle-exit fluid density
ρ = nominally quiescent reservoir fluid density
Y_0 = slot- or nozzle-exit passive scalar mass fraction
x = stream-wise, centerplane, or centerline coordinate
y = distance from the flow's centerplane
r = radial distance from the flow's centerline
$y_{CL}(x)$ = location of the point in the shear layer where $U = (U_1 + U_2)/2$
$(\Delta\xi_{80})_U$ = difference in ξ that spans the central 80% of the velocity difference $U_1 - U_2$
U_∞ = uniform velocity outside the wake
ξ = profile similarity variable
$F(\xi)$, $H(\xi)$ = velocity and mass fraction profiles, approximately = $\exp\{-\ln(2)\xi^2/\xi_{1/2}^2\}$

perpendicular to the page so the mean velocity field has only U and V components. Using the x-y coordinates shown in Figure 12.13a, the self-preserving form for the jet's mean stream-wise velocity and Reynolds shear-stress correlation is:

$$U(x,y) = U_{CL}(x)F(y/\delta(x)),\ \text{and}\ -\overline{uv} = \Psi(x)G(y/\delta(x)), \qquad (12.56, 12.57)$$

where $U_{CL}(x)$ is the mean stream-wise velocity on the centerline of the flow ($y = 0$), $\Psi(x)$ is a function that sets the amplitude of the turbulent shear stress with increasing downstream

distance, F and G are undetermined profile functions, and $\delta(x)$ is a characteristic cross-stream length scale. The profile functions must confine the region of turbulence, so $F, G \to 0$ as $y/\delta \to \pm\infty$, and they must allow the jet to spread equally upward and downward, so F must be even and G must be odd; thus $F(0) = 1$ and $G(0) = 0$. When the self-preserving forms (12.56) and (12.57) are successful, the turbulence is said to have one characteristic length scale. These two equations are the similarity-solution forms (see (8.32)) for the steady mean-flow RANS equations when x and y are the independent variables.

For two-dimensional, constant-density flow with steady boundary conditions, the mean flow equations are:

$$\frac{\partial U}{\partial x}+\frac{\partial V}{\partial y}=0,\ U\frac{\partial U}{\partial x}+V\frac{\partial U}{\partial y}=-\frac{1}{\rho}\frac{\partial P}{\partial x}+\nu\left(\frac{\partial^2 U}{\partial x^2}+\frac{\partial^2 U}{\partial y^2}\right)-\frac{\partial\overline{u^2}}{\partial x}-\frac{\partial\overline{uv}}{\partial y},\ \text{and} \qquad (12.58, 12.59)$$

$$U\frac{\partial V}{\partial x}+V\frac{\partial V}{\partial y}=-\frac{1}{\rho}\frac{\partial P}{\partial y}+\nu\left(\frac{\partial^2 V}{\partial x^2}+\frac{\partial^2 V}{\partial y^2}\right)-\frac{\partial\overline{uv}}{\partial x}-\frac{\partial\overline{v^2}}{\partial y}. \qquad (12.60)$$

For this analysis, the simplest possible form of these equations is adequate. Thus, the jet flow is assumed to be thin, so the boundary-layer approximations are made: $U \gg V$, and $\partial/\partial y \gg \partial/\partial x$. In addition, pressure gradients are presumed small within the nominally quiescent reservoir fluid so that $\partial P/\partial x \approx 0$, and the jet flow's Reynolds number is assumed to be high enough so that viscous stresses can be ignored compared to Reynolds stresses. With these simplifications, the two momentum equations (12.59) and (12.60) become:

$$U\frac{\partial U}{\partial x}+V\frac{\partial U}{\partial y}\cong-\frac{\partial\overline{uv}}{\partial y},\ \text{and}\ 0\cong-\frac{1}{\rho}\frac{\partial}{\partial y}\left(P+\rho\overline{v^2}\right). \qquad (12.61)$$

Because the viscous terms have been dropped, these equations are independent of the Reynolds number and should be valid for all Re that are high enough to justify this approximation. Multiplying (12.58) by U and adding it to the first part of (12.61) produces:

$$\frac{\partial}{\partial x}\left(U^2\right)+\frac{\partial}{\partial y}\left(VU+\overline{uv}\right)\cong 0,$$

which can be integrated in the cross-stream direction between infinite limits to obtain:

$$\frac{\partial}{\partial x}\int_{-\infty}^{+\infty}U^2dy+\left[VU+\overline{uv}\right]_{y=-\infty}^{y=+\infty}\cong 0.$$

When evaluated, the terms in [,]-brackets are zero because U, V, and $\overline{uv}$ are all presumed to go to zero as $y \to \pm\infty$. This equation can be integrated in the stream-wise direction from 0 to x to find:

$$J_s\equiv\rho_s\int_{-\infty}^{+\infty}\left[U^2\right]_{x=0}dy\cong\rho\int_{-\infty}^{+\infty}U^2dy=const. \qquad (12.62)$$

In (12.62), J_s is the momentum injected into the flow per unit span of the slot and the two integrals in (12.62) come from evaluating J_s at $x = 0$ and at a location well downstream in

the jet. Here, ρ_s is the density of the fluid that emerges from the nozzle, and any difference between ρ and ρ_s is presumed to be insignificant downstream in the jet because the fluid that comes from the slot is mixed with and diluted by the nominally quiescent fluid entrained into the jet. The basis for this presumption is provided further on in this section. Overall, (12.62) can be regarded as a constraint that requires the turbulent flow to contain the same amount of stream-wise momentum at all locations downstream of the nozzle.

To determine the form of the similarity solution for the plane jet, first eliminate V from (12.61) using an integrated form of (12.58), $V = -\int_0^y (\partial U/\partial x)d\cancel{y}$, to find

$$U\frac{\partial U}{\partial x} - \left[\int_0^y \left(\frac{\partial U}{\partial x}\right) d\cancel{y}\right] \frac{\partial U}{\partial y} \cong -\frac{\partial \overline{uv}}{\partial y},$$

where $V(0) = 0$ by symmetry and $\cancel{y}$ is an integration variable. Then, substitute (12.56) and (12.57) into this equation to reach a single equation involving the two amplitude functions, U_{CL} and Ψ, and the two profile functions, F and G:

$$U_{CL}F\frac{\partial}{\partial x}(U_{CL}F) - \left[\int_0^y \frac{\partial}{\partial x}(U_{CL}F)d\cancel{y}\right] \frac{\partial}{\partial y}(U_{CL}F) \cong -\frac{\partial}{\partial y}(\Psi G).$$

Although somewhat tedious, the terms of this equation can be expanded and simplified to find:

$$\left\{\frac{\delta U'_{CL}}{U_{CL}}\right\}F^2 - \left\{\frac{\delta U'_{CL}}{U_{CL}} + \delta'\right\}F'\int_0^{\xi} F d\cancel{\xi} = \left\{\frac{\Psi}{U_{CL}^2}\right\}G', \tag{12.63}$$

where a prime indicates differentiation of a function with respect to its is argument, $\xi = y/\delta$, and $\cancel{\xi}$ is an integration variable. For a simple similarity solution to exist, the coefficients inside {,}-braces in (12.63) should not be functions of x. Setting each equal to a constant produces two ordinary differential equations and an algebraic one:

$$\frac{\delta U'_{CL}}{U_{CL}} = C_1,\ \frac{\delta U'_{CL}}{U_{CL}} + \delta' = C_2,\ \text{and}\ \frac{\Psi}{U_{CL}^2} = C_3. \tag{12.64}$$

The first two of these imply $\delta' = C_2 - C_1$, which is readily integrated to find: $\delta(x) = (C_2 - C_1)(x - x_o)$, where x_o is a constant and is known as the virtual origin of the flow. It is traditional to choose $C_2 - C_1 = 1$ and to presume that x_o is small so that $\delta = x$. In experiments, x_o is typically found to be of order d, the width of the slot. With $\delta = x$, the first equation of (12.64) may be integrated to determine: $U_{CL} = C_4 x^{\gamma}$, where C_4 and γ are constants. Substituting this into (12.62) leads to:

$$J_s = \rho\int_{-\infty}^{+\infty} U^2 dy = \rho U_{CL}^2\int_{-\infty}^{+\infty} F^2(\xi)dy = \rho U_{CL}^2\delta\int_{-\infty}^{+\infty} F^2(\xi)d\xi = \rho C_4^2 x^{2\gamma+1}\int_{-\infty}^{+\infty} F^2(\xi)d\xi. \tag{12.65}$$

Here the final definite integral is just a dimensionless number, so the final form of (12.65) can only be independent of x when $2\gamma + 1 = 0$, or $\gamma = -1/2$. Thus, the results of (12.64) imply that (12.56) and (12.57) may be rewritten:

$$\begin{aligned} U(x,y) &= C_5(J_s/\rho)^{1/2}x^{-1/2}F(y/x) \quad \text{and} \\ -\overline{uv} &= C_3U_{CL}^2G(y/x) = C_3C_5^2(J_s/\rho)x^{-1}G(y/x), \end{aligned} \tag{12.66, 12.67}$$

where the constants C_3 and C_4 and the profile functions F and G must be determined from experimental measurements, direct numerical simulations, or an alternate theory. They cannot be determined from this type of simple similarity analysis because (12.63) is one equation for two unknown profile functions, a situation that is a direct legacy of the closure problem. However, the parametric dependencies shown in (12.66) and (12.67) are those found in experiments, and this is the primary reason for seeking self-preserving forms via a similarity analysis.

The result (12.66) may be used to determine the volume flux (per unit span) $\dot{V}$ in the jet via a simple integration,

$$\dot{V}(x) = \int_{-\infty}^{+\infty} U(x,y)dy = C_5(J_s/\rho)^{1/2}x^{+1/2}\int_{-\infty}^{+\infty} F(\xi)d\xi, \tag{12.68}$$

where again the definite integral is just a dimensionless number. Therefore, the volume flux in the jet increases with increasing downstream distance like $x^{1/2}$, so the dilution assumption made about J_s in (12.62) should be valid sufficiently far from the jet nozzle. At such distances, commonly known as the *far field* of the jet, the mean mass fraction $\overline{Y}(x,y)$ of slot fluid (or any other suitably defined passive scalar like a dye concentration) will also follow a similarity form:

$$\overline{Y}(x,y) = Y_{CL}(x)H(y/x), \tag{12.69}$$

where Y_{CL} is the centerline nozzle-fluid mass fraction, and H is another profile function defined so that $H(0) = 1$ and $H \to 0$ as $y/\delta \to \pm\infty$. Conservation of slot fluid requires:

$$\begin{aligned} \dot{M}_s &= \rho_s \int_{-\infty}^{+\infty} [U]_{y=0}dy \cong \rho \int_{-\infty}^{+\infty} \overline{Y}(x,y)U(x,y)dy \\ &= \rho Y_{CL}C_5(J_s/\rho)^{1/2}x^{+1/2}\int_{-\infty}^{+\infty} H(\xi)F(\xi)d\xi, \end{aligned} \tag{12.70}$$

where $\dot{M}_s$ is the slot-fluid mass injection rate per unit span. In (12.70) the stream-wise turbulent scalar transport term $\overline{uY'}$ has been neglected because it tends to be much smaller than the stream-wise mean scalar transport term $\overline{Y}U$. Reducing (12.70) to a single relationship for Y_{CL}, and substituting this into (12.69) produces:

$$\overline{Y}(x,y) = C_6\left(\dot{M}_s/\sqrt{\rho J_s}\right)x^{-1/2}H(y/x), \tag{12.71}$$

where C_6 is another constant. The equations (12.66), (12.67), and (12.71) represent the outcomes from this similarity analysis and can be compared with the $u \propto x^{-1/3}$, $\delta \propto x^{2/3}$ behavior of a planar laminar jet derived in Section 9.10.

Over the years some success has been achieved in determining the various profile shapes and the constants. For example, when the slot exit velocity is uniform and equal to U_0, then $J_s = \rho_s U_0^2 d$ and $\dot{M}_s = \rho_s U_0 d$ so (12.66) and (12.71) reduce to:

$$\begin{aligned} U(x,y) &= C_5 U_0 (\rho_s/\rho)^{1/2} (x/d)^{-1/2} F(y/x), \text{ and} \\ \overline{Y}(x,y) &= C_7 Y_0 (\rho_s/\rho)^{1/2} (x/d)^{-1/2} H(y/x), \end{aligned} \tag{12.72, 12.73}$$

where Y_0 is the mass fraction of a passive scalar in the slot fluid. Here $Y_0 = 1$ if the slot fluid is the passive scalar, but Y_0 may be much less than one if it represents a trace contaminant or a dye concentration. In addition, the profile functions F and H are smooth, bell-shaped curves commonly specified by their one-sided half-widths $(\xi_{1/2})_U$ and $(\xi_{1/2})_Y$, the values of y/δ that produce F and $H = 1/2$, respectively. For example when a Gaussian function is fit to mean profiles of U, the function F becomes:

$$F(y/x) = \exp\left\{ -\ln(2)(y/x)^2/(\xi_{1/2})_U^2 \right\}.$$

Approximate empirical values for C_5, C_6, $(\xi_{1/2})_U$, and $(\xi_{1/2})_Y$ from Chen and Rodi (1980) and Pope (2000) are provided in Table 12.1 for the plane turbulent jet along with results for other free shear flows. The similarity forms shown in this table for the planar and round wakes should also be followed in the far-field of jets in coflowing streams. Unfortunately, variations in the empirical constants between experiments may be ±20% (or even more; see the round-wake results) and these variations are thought to be caused by unintentional experimental artifacts, such as unmeasured vibrations, geometrical imperfections, or fluctuations in one of the input flows.

Interestingly, as pointed out in George (1989), such variation in similarity constants is consistent with the type of similarity analysis presented earlier in this section. The three equations (12.64) determined from the coefficients of the similarity momentum equation specify the simplest possibility leading to self-similarity of the mean flow. A more general version of (12.64) that also leads to self-similarity is:

$$\frac{\delta U'_{CL}}{U_{CL}} = C_8 \left(\frac{\delta U'_{CL}}{U_{CL}} + \delta' \right) = C_9 \frac{\Psi}{U_{CL}^2}, \tag{12.74}$$

which specifies that the x-dependence of the three coefficients must be equal. Here, $\delta \sim x^m$, $U_{CL} \sim x^n$, and $\Psi \sim x^{2n+m-1}$ satisfy (12.74) as do $\delta \sim \exp\{ax\}$, $U_{CL} \sim \exp\{-ax\}$, and $\Psi \sim \exp\{-ax\}$; thus, multiple possibilities are allowed by (12.63) for the plane jet's similarity solution. While the second law of thermodynamics and the constraint (12.62) rule out some of these possibilities, (12.74) or its equivalent for other free shear flows and conditions at the flow's origin ($x = 0$) apparently allow the expected self-similar states for a particular shear flow to vary somewhat from experiment to experiment.

EXAMPLE 12.2

Pure methane gas issues from a round nozzle with diameter $d = 1$ cm at a speed of $U_0 = 20$ m/s into a combustion chamber nominally filled with quiescent air at room temperature and pressure. Assuming the volume fraction of oxygen in air is 0.21, use the round turbulent jet similarity law to estimate the centerline distance from the nozzle exit where the stoichiometric condition is reached, and the centerline speed and nominal width of the jet flow at that point.

Solution

Using subscripts "A" for air and "M" for methane, and molecular weights of 28.96 and 16.04 for air and methane, respectively, the Reynolds number of the flow is:

$$\sqrt{J_s/\rho_A}/\nu \sim (\rho_M/\rho_A)^{1/2} U_0 d/\nu_A = (16.04/28.96)^{1/2}(20\,m/s)(0.01\,m)/\left(1.5\times10^{-5}\,m^2s^{-1}\right) \sim 10^4,$$

which is high enough to form a turbulent jet. Since the relevant chemical reaction is $CH_4 + 2O_2 \rightarrow CO_2 + 2H_2O$, the mole fraction of methane is half that of oxygen at the stoichiometric condition. Thus, at the location of interest x, there are two equations relating mean volume fractions, $\overline{v}_A + \overline{v}_M = 1$ and $\overline{v}_M = 0.5(0.21\overline{v}_A)$, that are readily solved to find: $\overline{v}_A = 1/1.105 = 0.905$, and $\overline{v}_M = 1 - (1/1.105) = 0.095$. With this composition, the mixture density is within 4% or so of the density of air. The requisite mass fraction of methane is:

$$Y_M = (0.095)(16.04)/[(0.905)(28.96) + (0.095)(16.04)] = 0.0549.$$

The location x is found from the entry in Table 12.1 for the mass-fraction field of a round turbulent jet. This means setting $Y_M = 5.0\, Y_0(\rho_s/\rho_A)^{1/2}(x/d)^{-1}$ and solving for x to find:

$$x = 5.0\,(Y_0/Y_M)(\rho_s/\rho_A)^{1/2} d = 5.0(1.0/0.0549)(16.04/28.96)^{1/2}(0.01\,m) \cong 0.68\,m.$$

Using the Table 12.1 entry for the velocity field of a round turbulent jet, the jet centerline velocity at this location is:

$$U_{CL}(x) = 6.0U_o\,(\rho_s/\rho_A)^{1/2}(x/d)^{-1} = 6.0(20\,m/s)(16.04/28.96)^{1/2}(68)^{-1} \cong 1.3\,m/s.$$

The nominal width of the flow will be approximately four times larger than the jet's mean concentration profile half radius $r_{1/2}$. From the round jet profile width entry in Table 12.1, we have:

$$(\xi_{1/2})_Y = 0.11 = (r_{1/2}/x)_Y \quad \text{so } 4r_{1/2} = 4(0.11)(0.68\,m) \cong 0.30\,m.$$

Thus, the width of a jet's cone of turbulence is a little less than half the downstream distance.

When the mean velocity and mass fraction fields of a free turbulent shear flow are self-similar, their corresponding fluctuations are commonly self-similar with the same dependence on the downstream coordinate as that found for the mean fields. However, the profile functions for the various Reynolds stress components or the passive scalar variance are typically not bell-shaped curves. Sample free shear flow measurements for the Reynolds stress components for the plane turbulent jet are shown in Figure 12.14. Results such as these indicate how fluctuation energy varies within a turbulent flow and may be used to develop and

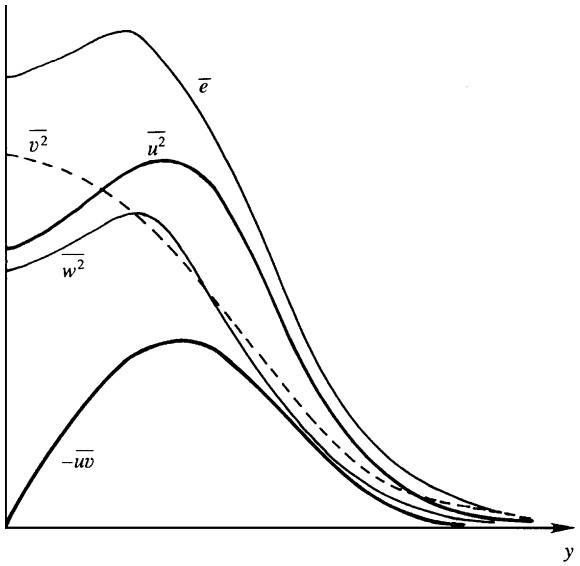

FIGURE 12.14 Sketch of the observed variation of the turbulent kinetic energy $\overline{e}$ and the nonzero Reynolds stress components across a planar jet. Here, $\overline{uv} = 0$ on the jet's centerline ($y = 0$), and $\overline{uw} = \overline{vw} = 0$ throughout the flow because the mean flow is symmetric about $y = 0$, and because the flow is homogeneous in the z-direction.

test closure models for RANS equations. Here $\overline{u^2}$, $\overline{v^2}$, and $\overline{w^2}$ are the velocity component variances (commonly called *turbulent intensities*) in the stream-wise (x), slot-normal (y), and slot-parallel (z) directions, respectively. The Reynolds stresses $\overline{uw}$ and $\overline{vw}$ are zero throughout the planar jet since the flow is homogeneous in the z-direction and there is no reason for w to be mostly of one sign if u or v is either positive or negative. Similarly, the Reynolds stress $\overline{uv}$ is zero on the jet centerline by symmetry. In Figure 12.14, the Reynolds stress reaches a maximum magnitude roughly where $\partial U/\partial y$ is maximum. This is also close to the region where the turbulent kinetic energy $\overline{e}$ reaches a maximum. Such correspondences are commonly exploited in the development of turbulence models.

The terms in the turbulent kinetic energy budget for a two-dimensional jet are shown in Figure 12.15. Under the boundary layer assumption for derivatives, $\partial/\partial y \gg \partial/\partial x$, the budget equation (12.47) becomes

$$0 = -U\frac{\partial \overline{e}}{\partial x} - V\frac{\partial \overline{e}}{\partial y} - \overline{uv}\frac{\partial U}{\partial y} - \frac{\partial}{\partial y}\left(\frac{1}{\rho_0}\overline{pv} + \frac{1}{2}\overline{ev}\right) - \overline{\varepsilon}, \tag{12.75}$$

where the left side represents $\partial\overline{e}/\partial t$. Here, the viscous transport and the term $(\overline{v^2} - \overline{u^2})(\partial U/\partial x)$ arising out of the shear production have been neglected because they are small. The balance of terms shown in this figure is analyzed in Townsend (1976). Here, T denotes turbulent transport represented by the fourth term on the right-hand side of (12.75). The shear production is zero on the jet centerline where both $\partial U/\partial y$ and $\overline{uv}$ are zero, and reaches a maximum close to the position of the maximum Reynolds stress. Near the center of the jet, the dissipation is primarily balanced by the downstream advection

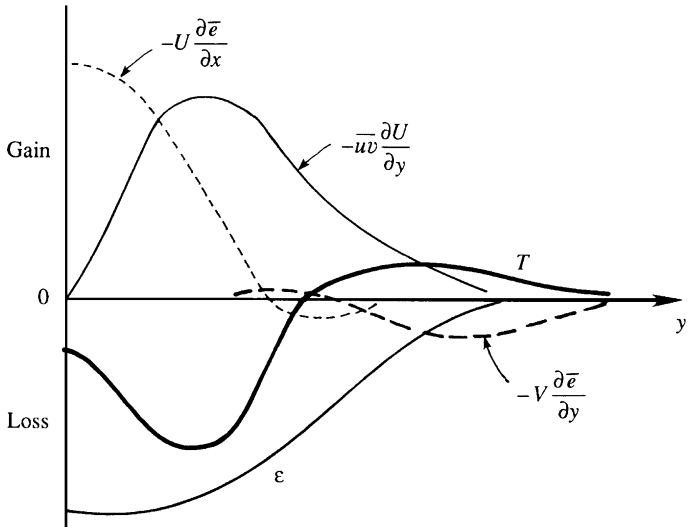

FIGURE 12.15 Sketch of measurements of the terms in the kinetic energy budget of a planar turbulent jet. Here the turbulent transport terms are lumped together and indicated by T. Information of this type is used to build, adjust, and validate closure models for RANS equations.

$-U(\partial\overline{e}/\partial x)$, which is positive because the turbulent kinetic energy $\overline{e}$ decays downstream. Away from the jet's center, but not too close to the jet's outer edge, the production and dissipation terms balance. In the outer parts of the jet, the transport term balances the cross-stream advection. In this region V is negative (i.e., toward the center) due to entrainment of the surrounding fluid, and also $\overline{e}$ decreases with increasing y. Therefore the cross-stream advection $-V(\partial\overline{e}/\partial y)$ is negative, signifying that the entrainment velocity V tends to decrease the turbulent kinetic energy at the outer edge of the jet. A temporally stationary state is therefore maintained by the transport term T carrying $\overline{e}$ away from the jet's center (where $T < 0$) into the outer parts of the jet (where $T > 0$).

12.9. WALL-BOUNDED TURBULENT SHEAR FLOWS

At sufficiently high Reynolds number, the characteristics of free turbulent shear flows discussed in the preceding section are independent of Reynolds number and may be self-similar based on a single length scale. However, neither of these simplifications occurs when the flow is bounded by one or more solid surfaces. The effects of viscosity are always felt near the wall where turbulent fluctuations go to zero, and this gives rise to a second fundamental length scale l_ν that complements the turbulent layer thickness δ. In addition, the persistent effects of viscosity are reflected in the fact that the skin-friction coefficient for a smooth flat plate or smooth round pipe depends on Re, even when $\text{Re} \to \infty$, as seen in Figure 9.11. Therefore, Re independence of the flow as $\text{Re} \to \infty$ does not occur in wall-bounded turbulent shear flows when the wall(s) is(are) smooth.

The importance of wall-bounded turbulence in engineering applications and geophysical situations is hard to overstate since it sets fundamental limits for the efficiency of transportation systems and on the exchange of mass, momentum, and heat at the earth's surface. Thus, the literature on wall-bounded turbulent flows is large and the material provided here merely covers the fundamentals of the mean flow. A more extensive presentation that includes turbulence intensities is provided in Chapter 7 of Pope (2000). Vortical structures in wall-bounded turbulence are discussed in Kline et al. (1967), Cantwell (1981), and Adrian (2007). The review articles by George (2006) and Marusic et al. (2010) are also recommended.

Three generic wall-bounded turbulent shear flows are described in this section: pressure-driven channel flow between smooth stationary parallel plates, pressure-driven flow through a smooth round pipe, and the turbulent boundary-layer flow that develops from nominally uniform flow over a smooth flat plate. The first two are fully confined while the boundary layer has one free edge. The main differences between turbulent and laminar wall-bounded flows are illustrated on Figure 12.16. In general, mean turbulent-flow profiles (solid curves) are blunter, and turbulent-flow wall-shear stresses are higher than those of equivalent steady laminar flows (dashed curves). In addition, a turbulent boundary-layer, mean-velocity profile approaches the free-stream speed very gradually with increasing y so the full thickness of the profile shown in the right panel of Figure 12.16 lies beyond the extent of the figure. Throughout this section, the density of the flow is taken to be constant.

Fully developed channel flow is perhaps the simplest wall-bounded turbulent flow. Here, the modifier *fully developed* implies that the statistics of the flow are independent of the downstream direction. The analysis provided here is readily extended to pipe flow, after a suitable redefinition of coordinates. Further extension of channel flow results to boundary-layer flows is not as direct, but can be made when the boundary-layer approximation replaces the fully

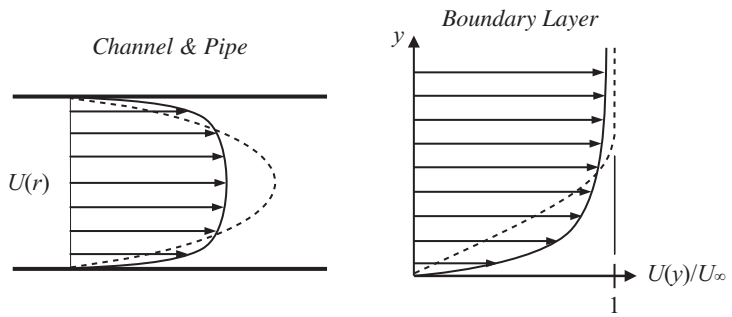

FIGURE 12.16 Sample profiles for wall-bounded turbulent flows (solid curves) compared to equivalent laminar profiles (dashed curves). In general turbulent profiles are blunter with higher skin friction; that is, $\mu(dU/dy)$ evaluated at the wall is greater in turbulent flows than in equivalent laminar ones. In channel and pipe flows, the steady laminar profile is parabolic while a mean turbulent flow profile is more uniform across the central 80% of the channel or pipe. For boundary layers having the same displacement thickness, the steady laminar profile remains linear farther above the wall and converges to the free-stream speed more rapidly than the mean turbulent profile.

developed flow assumption. If we align the x-axis with the flow direction, and chose the y-axis in the cross-stream direction perpendicular to the plates so that $y = 0$ and $y = h$ define the plate surfaces, then fully developed channel flow must have $\partial U/\partial x = 0$. Hence, U can only depend on y, and it is the only mean velocity component because the remainder of (12.27) implies $\partial V/\partial y = 0$, and the boundary conditions $V = 0$ on $y = 0$ and h then require $V = 0$ throughout the channel. Under these circumstances, the mean flow momentum equations are:

$$0 = -\frac{\partial P}{\partial x} + \frac{\partial \overline{\tau}}{\partial y} \quad \text{and} \quad 0 = -\frac{\partial}{\partial y}\left(P + \rho\overline{v^2}\right), \tag{12.76}$$

where $\overline{\tau} = \mu(\partial U/\partial y) - \rho_0\overline{uv}$ is the total average stress and it cannot depend on x. Integrating the second of these equations from the lower wall up to y produces:

$$P(x,y) - P(x,0) = -\rho\overline{v^2} + \rho\left[\overline{v^2}\right]_{y=0} = -\rho\overline{v^2},$$

where the final equality follows because the variance of the vertical velocity fluctuation is zero at the wall ($y = 0$). Differentiating this with respect to x produces:

$$\frac{\partial}{\partial x}P(x,y) - \frac{d}{dx}P(x,0) = -\rho\frac{\partial}{\partial x}\overline{v^2} = 0, \tag{12.77}$$

where $P(x,0)$ is the ensemble-average pressure on $y = 0$ and the final equality follows from the fully developed flow assumption. Thus, the stream-wise pressure gradient is only a function of x; $\partial P(x,y)/\partial x = dP(x,0)/dx$. Therefore, the only way for the first equation of (12.76) to be valid is for $\partial P/\partial x$ and $\partial\overline{\tau}/\partial y$ to each be constant, so the total average stress distribution $\overline{\tau}(y)$ in turbulent channel flow is linear as shown in Figure 12.17a. Away from the wall, $\overline{\tau}$ is due mostly to the Reynolds stress, close to the wall the viscous contribution dominates, and at the wall the stress is entirely viscous.

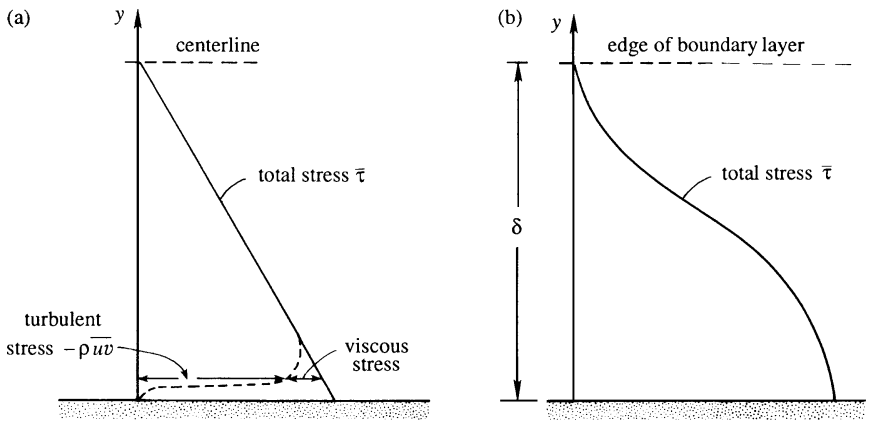

FIGURE 12.17 Variation of total shear stress across a turbulent channel flow (a) and through a zero-pressure-gradient turbulent boundary layer (b). In both cases, the Reynolds shear stress dominates away from the wall but the viscous shear stress takes over close to the wall. The shape of the two stress curves is set by momentum transport between the fast-moving part of the flow and the wall where $U = 0$.

For a boundary layer on a flat plate, the stream-wise mean-flow momentum equation is

$$U\frac{\partial U}{\partial x}+V\frac{\partial U}{\partial y}=-\frac{1}{\rho}\frac{\partial P}{\partial x}+\frac{1}{\rho}\frac{\partial \overline{\tau}}{\partial y}, \tag{12.78}$$

where $\overline{\tau}$ is a function of x and y. The variation of the stress across a boundary layer is sketched in Figure 12.17b for the zero-pressure-gradient (ZPG) condition. Here, a constant stress layer, $\partial\overline{\tau}/\partial y \approx 0$, occurs near the wall since both U and $V \to 0$ as $y \to 0$. When the pressure gradient is not zero, the stress profile approaches the wall with a constant slope. Although it is not shown in the figure, the structure of the near-wall region of the turbulent boundary layer is similar to that depicted for the channel flow in Figure 12.17a with viscous stresses dominating at and near the wall.

The partitioning of the stress based on its viscous and turbulent origins leads to the identification of two different scaling laws for wall-bounded turbulent flows. The first is known as the *law of the wall* and it applies throughout the region of the boundary layer where viscosity matters and the largest relevant length scale is y, the distance from the wall. This region of the flow is typically called the *inner layer*. The second scaling law is known as the *velocity defect law*, and it applies where the flow is largely independent of viscosity and the largest relevant length scale is the overall thickness of the turbulent layer δ. This region of the flow is typically called the *outer layer*. Fortunately, the inner and outer layers of wall-bounded turbulent flow overlap, and in this overlap region the form of the mean stream-wise velocity profile may be deduced from dimensional analysis.

Inner Layer: Law of the Wall

Consider the flow near the wall of a channel, pipe, or boundary layer. Let U_∞ be the centerline velocity in the channel or pipe, or the free-stream velocity outside the boundary layer. Let δ be the thickness of the flow between the wall and the location where $U = U_\infty$. Thus, δ may be the channel half width, the radius of the pipe, or the boundary-layer thickness. Assume that the wall is smooth, so that any surface roughness is too small to affect the flow. Physical considerations suggest that the near-wall velocity profile should depend only on the near-wall parameters and not on U_∞ or the thickness of the flow δ. Thus, very near the smooth surface, we expect

$$U = U(\rho, \tau_0, \nu, y), \tag{12.79}$$

where τ_0 is the shear stress on the smooth surface. This equation may be recast in dimensionless form as:

$$U^+ \equiv \frac{U}{u_*} = f\left(\frac{yu_*}{\nu}\right) = f\left(\frac{y}{l_\nu}\right) = f(y^+) \quad \text{where } u_*^2 \equiv \frac{\tau_0}{\rho}, \tag{12.80, 12.81}$$

f is an undetermined function, u_* is the *friction velocity* or *shear velocity*, and $l_\nu = \nu/u_*$ is the *viscous wall unit*. Equation (12.80) is the *law of the wall* and it states that U/u_* should be a universal function of yu_*/ν near a smooth wall. The superscript plus signs are standard in the literature and indicate a dimensionless law-of-the-wall variable.

The inner part of the wall layer, right next to the wall, is dominated by viscous effects and is called the *viscous sublayer*. In spite of the fact that it contains fluctuations, the Reynolds stresses are small here because the presence of the wall quells wall-normal velocity

fluctuations. At high Reynolds numbers, the viscous sublayer is thin enough so that the stress is uniform within the layer and equal to the wall shear stress τ_0. Therefore the mean velocity gradient in the viscous sublayer is given by

$$\mu(dU/dy) = \tau_0 \rightarrow U = \tau_0 y/\mu \text{ or } U^+ = y^+, \tag{12.82}$$

where the second two equalities follow from integrating the first. Equation (12.82) shows that the velocity distribution is linear in the viscous sublayer, and experiments confirm that this linearity holds up to $yu_*/v \sim 5$, which may be taken to be the limit of the viscous sublayer.

Outer Layer: Velocity Defect Law

Now consider the velocity distribution in the outer part of a turbulent boundary layer. The gross characteristics of the turbulence in the outer region are inviscid and resemble those of a free shear flow. The existence of Reynolds stresses in the outer region results in a drag on the flow and generates a *velocity defect* $\Delta U = U_\infty - U$, just like the planar wake. Therefore, in the outer layer we expect,

$$U = U(\rho, \tau_0, \delta, y), \tag{12.83}$$

and by dimensional analysis can write:

$$\frac{U_\infty - U}{u_*} = F\left(\frac{y}{\delta}\right) = F(\xi) \tag{12.84}$$

so that the deficit velocity, $U_\infty - U$, is proportional to the friction velocity u_* and a profile function. This is called the *velocity defect law*, and this is its traditional form. In the last two decades, it has been the topic of considerable discussion in the research community, and alternative velocity and length scales have been proposed for use in (12.84), especially for turbulent boundary-layer flows.

Overlap Layer: Logarithmic Law

From the preceding discussion, the mean velocity profiles in the inner and outer layers of a wall-bounded turbulent flow are governed by different laws, (12.80) and (12.84), in which the independent coordinate y is scaled differently. Distances in the outer part are scaled by δ, whereas those in the inner part are scaled by the much smaller viscous wall unit $l_\nu = \nu/u_*$. Thus, wall-bounded turbulent flows involve at least two turbulent length scales, and this prevents them from reaching the same type of self-similar form with increasing Reynolds number as that found for simple free turbulent shear flows.

Interestingly, a region of overlap in the two profile forms can be found by taking the limits $y^+ \rightarrow \infty$ and $\xi \rightarrow 0$ simultaneously. Instead of matching the mean velocity directly, in this case it is more convenient to match mean velocity gradients. (The following short derivation closely follows that in Tennekes and Lumley, 1972.) From (12.80) and (12.84), dU/dy in the inner and outer regions is given by

$$\frac{dU}{dy} = \frac{u_*^2}{\nu}\frac{df}{dy^+} \quad \text{and} \quad -\frac{dU}{dy} = \frac{u_*}{\delta}\frac{dF}{d\xi}, \tag{12.85, 12.86}$$

respectively. Equating these and multiplying by y/u_*, produces:

$$-\xi\frac{dF}{d\xi} = y^+\frac{df}{dy^+}, \tag{12.87}$$

an equation that should be valid for large y_+ and small ξ. As the left-hand side can only be a function of ξ and the right-hand side can only be a function of y^+, both sides must be equal to the same universal constant, say $1/\kappa$, where κ is the *von Karman constant* (not the thermal diffusivity). Experiments show that $\kappa \approx 0.4$ with some dependence on flow type and pressure gradient, as is discussed further later on. Setting each side of (12.87) equal to $1/\kappa$, integrating, and using (12.80) gives:

$$U^+ \equiv \frac{U}{u_*} = f(y^+) = \frac{1}{\kappa}\ln(y^+) + B \quad \text{and} \quad F(\xi) = -\frac{1}{\kappa}\ln(\xi) + A, \tag{12.88, 12.89}$$

where B and A are constants with values around 4 or 5, and 1, respectively, again with some dependence on flow type and pressure gradient. Equation (12.88) or (12.89) is the mean velocity profile in the *overlap layer* or the *logarithmic layer*. In addition, the constants in (12.88), κ and B, are known as the logarithmic-law (or log-law) constants. As the derivation shows, (12.88) and (12.89) are only valid for large y^+ and small y/δ, respectively. The foregoing method of justifying the logarithmic velocity distribution near a wall was first given by Clark B. Millikan in 1938. The logarithmic law, however, was known from experiments conducted by the German researchers, and several derivations based on semi-empirical theories were proposed by Prandtl and von Karman. One such derivation using the so-called mixing length theory is presented in the following section.

The logarithmic law (12.88) may be the best-known and most important result for wall-bounded turbulent flows. Experimental confirmation of this law is shown in Figure 12.18 in law-of-the-wall coordinates for the turbulent boundary-layer data reported in Oweis et al. (2010). Nominal specifications for the extent of the viscous sublayer, the buffer layer, the logarithmic layer, and the wake region are shown there as well. On this log-linear plot, the linear viscous sublayer profile appears as a curve for $y^+ < 5$. However, a logarithmic velocity profile will appear as a straight line on a log-linear plot, and such a linear region is evident for approximately two decades in y^+ starting near $y^+ \sim 10^2$. The extent of this logarithmic region increases in these coordinates with increasing Reynolds number. The region $5 < y^+ < 30$, where the velocity distribution is neither linear nor logarithmic, is called the *buffer layer*. Neither the viscous stress nor the Reynolds stresses are negligible here, and this layer is dynamically important because turbulence production reaches a maximum here. Overall, the measured results collapse well to a single curve below $y^+ \sim 10^4$ (or $y/\delta \sim 0.2$) in conformance with the law of the wall. For larger values of y^+, the collapse ends where the overlap region ends and the boundary layer's wake flow begins. Although the wake region appears to be smaller than the log-region on the plot, this is an artifact of the logarithmic horizontal axis. A turbulent boundary layer's wake region typically occupies the outer 80% of the flow's full thickness. These velocity profiles do not collapse in the wake region when plotted with law-of-the-wall normalizations because the wake-flow similarity variable is y/δ (not y/l_ν) and ratio $\delta^+ = \delta/l_\nu$ is different at the three different Reynolds numbers. The fitted curves shown in Figure 12.18 are mildly adjusted versions of

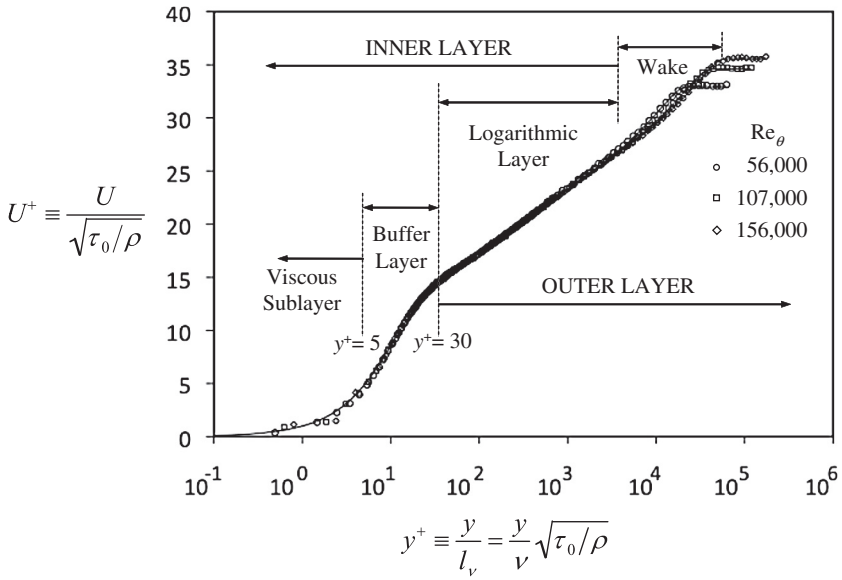

FIGURE 12.18 Mean velocity profile of a smooth-flat-plate turbulent boundary layer plotted in log-linear coordinates with law-of-the-wall normalizations. The data are replotted from Oweis et al. (2010) and represent three Reynolds numbers. The extent of the various layers within a wall-bounded turbulent flow are indicated by vertical dashed lines. The log-layer-to-wake-region boundary is usually assumed to begin at $y/\delta \approx 0.15$ to 0.20 in turbulent boundary layers. Overall the data collapse well for the inner layer region, as expected, and the logarithmic layer extends for approximately two decades. The wake region shows differences between the Reynolds numbers because its similarity variable is y/δ, and δ/l_ν differs between the various Reynolds numbers.

those recommended in Monkewitiz et al. (2007) for smooth-flat-plate ZPG turbulent boundary layers.

For fully developed channel and pipe flows, the mean stream-wise velocity profile does not evolve with increasing downstream distance. However, turbulent boundary layers do thicken. The following parameter results are developed from the systematic fitting and expansion efforts for ZPG turbulent boundary layers described in Monkewitz et al. (2007), and are intended for use when $\mathrm{Re}_x > 10^6$:

$$\text{Momentum thickness} = \theta \approx 0.016 \times \mathrm{Re}_x^{-0.15},$$

$$\text{Displacement thickness} = \delta^* \approx \theta \exp\left\{\frac{7.11\kappa}{\ln(\mathrm{Re}_\theta)}\right\},$$

$$\text{99\% thickness} = \delta_{99} = 0.2\delta^*\left[\kappa^{-1}\ln(\mathrm{Re}_{\delta*}) + 3.30\right], \text{ and}$$

$$\text{Skin friction coefficient} = C_f = \frac{\tau_0}{\frac{1}{2}\rho U_\infty^2} \cong \frac{2.0}{\left[\kappa^{-1}\ln(\mathrm{Re}_{\delta*}) + 3.30\right]^2},$$

where x is the downstream distance, $\mathrm{Re}_x = U_\infty x/\nu$, $\mathrm{Re}_\theta = U_\infty \theta/\nu$, and $\mathrm{Re}_{\delta^*} = U_\infty \delta^*/\nu$. Other common ZPG turbulent boundary-layer skin-friction correlations are those by Schultz-Grunow (1941) and White (2006),

$$C_f \cong 0.370\left(\log_{10}\mathrm{Re}_x\right)^{-2.584} \text{ and } C_f \cong \frac{0.455}{[\ln(0.06\mathrm{Re}_x)]^2},$$

respectively. These formulae should be used cautiously because the influence of a boundary layer's virtual origin has not been explicitly included and it may be substantial (Chauhan et al., 2009; see also Marusic, 2010).

EXAMPLE 12.3

Estimate the boundary layer thicknesses on the underside of the wing of a large commercial airliner on its landing approach. Use the flat-plate results provided above, a chord-length distance of $x = 8$ m, a flow speed of 100 m/s, and a nominal value of $\kappa \approx 0.4$.

Solution

First compute the downstream-distance Reynolds number Re_x using the nominal kinematic viscosity air: $\mathrm{Re}_x = (100\ \mathrm{m/s})(8\ \mathrm{m})/(1.5 \times 10^{-5}\ \mathrm{m^2/s}) = 53 \times 10^6$. This Reynolds number is clearly high enough for turbulent flow, so the estimates are:

$$\theta \approx 0.016 \times \mathrm{Re}_x^{-0.15} = 0.016(8\ \mathrm{m})\left(53 \times 10^6\right)^{-0.15} = 0.0089\ \mathrm{m},$$

$$\delta^* \approx \theta \exp\left\{\frac{7.11\kappa}{\ln(\mathrm{Re}_\theta)}\right\} = (0.0089\ \mathrm{m})\exp\left\{\frac{7.11(0.4)}{\ln\left((0.0089\ \mathrm{m})(100\ \mathrm{m/s})/1.5 \times 10^{-5}\ \mathrm{m^2/s}\right)}\right\} \cong 0.0115\ \mathrm{m}, \text{ and}$$

$$\delta_{99} = 0.2\delta^*\left[\kappa^{-1}\ln(\mathrm{Re}_{\delta*}) + 3.30\right] = 0.2(0.0115\ \mathrm{m})\left[0.4^{-1}\ln\left(\frac{(0.0115\ \mathrm{m})(100\ \mathrm{m/s})}{1.5 \times 10^{-5}\ \mathrm{m^2/s}}\right) + 3.30\right] \cong 0.072\ \mathrm{m}.$$

Here we note that θ and δ^* are almost an order of magnitude smaller than δ_{99}, and that all three boundary-layer thicknesses are miniscule compared to the wing's chord length of 8 m. The latter finding is a primary reason why boundary-layer thicknesses are commonly ignored in aerodynamic analyses.

For the purpose of completeness, the following approximate mean velocity profile functions are offered for wall-bounded turbulent flows:

$$\text{inner profile } y^+ = U^+_{inner} + e^{-\kappa B}\left[\exp\left(\kappa U^+_{inner}\right) - 1 - \kappa U^+_{inner} - \frac{1}{2}\left(\kappa U^+_{inner}\right)^2 - \frac{1}{6}\left(\kappa U^+_{inner}\right)^3\right], \text{ and}$$

$$\text{outer profile } U^+_{outer} = \frac{1}{\kappa}\ln\left(y^+\right) + B + \frac{2\Pi}{\kappa}W(y/\delta),$$

where the inner profile from Spalding (1961) is specified in implicit form, κ and B are the log-law constants from (12.88), and Π and W are the wake strength parameter and a wake function, respectively, both introduced by Coles (1956). The wake function W and the length scale δ in its argument are empirical and are typically determined by fitting curves to experimental profile data.

Of the three generic wall-bounded turbulent flows, the boundary layer's wake is typically the most prominent. For ZPG boundary layers the wake strength is $\Pi = 0.44$ (Chauhan et al., 2009). When the pressure gradient is favorable, Π is lower, and when the pressure gradient is adverse, Π is higher. The wake function is typically chosen to go smoothly from zero to unity as y goes from zero to δ. Among the simplest possibilities for $W(\xi)$ are $3\xi^2 - 2\xi^3$ and $\sin^2(\pi\xi/2)$, however more sophisticated fits are currently in use (see Monkewitz et al., 2007; Chauhan et al., 2009). In the outer profile form given above, δ is interpreted as the 100% boundary-layer thickness where U first equals the local free-stream velocity as y increases. In practice, this requirement cannot be evaluated with finite-precision experimental data so δ is often approximated as being the 99% or the 99.5% thickness, δ_{99} or $\delta_{99.5}$, respectively. Of course, for channel or pipe flows, δ is half the channel height or the pipe radius, respectively.

As of this writing, new and important concepts and results for wall-bounded turbulence continue to emerge. These include the possibility that the overlap layer might instead be of power law form (Barenblatt, 1993; George & Castillo, 1997) and a reinterpretation of the layer structure in terms of stress gradients (Wei et al., 2005; Fife et al., 2005). The comparisons in Monkewitz et al. (2008) suggest that the logarithmic law should be favored over a power law, while the implications of the stress gradient balance approach are still under consideration. These and other topics in the current wall-bounded turbulent flow literature are discussed in Marusic et al. (2010).

The one additional topic raised here concerns the universality of wall-bounded turbulent flow profiles. Are all wall-bounded turbulent flows universal (statistically the same) when scaled appropriately? To answer this question, consider the inner, outer, and overlap layers separately. First of all, the viscous sublayer profile $U^+ = y^+$ (12.82) is universal using law-of-the-wall normalizations. However, geometrical considerations suggest that the wake flow region is not universal. Consider the zone of maximum average fluid velocity at the outer edge of the wake of a wall-bounded flow. This maximum velocity zone occurs on the centerline of a channel flow (a plane), on the centerline of a pipe flow (a line), and at the edge of a boundary layer (a slightly tilted, nearly planar surface). Thus, the ratio of the maximum-velocity area to the bounding-wall surface area is one-half for channel flow, vanishingly small for pipe flow, and slightly greater than unity for boundary-layer flow. On this basis, the three wake flows are distinguished. Additionally, the boundary layer differs from the other two flows because it is bounded on one side only. The boundary layer's wake-flow region entrains irrotational fluid at its free edge and does not collide or interact with turbulent flow arising from an opposing wall, as is the case for channel and pipe flows. Thus, the wake-flow regions of these wall-bounded turbulent flows should all be different and not universal.

Now consider the overlap layer in which the mean velocity profile takes a logarithmic form. Logarithmic profiles have been observed in all three generic wall-bounded turbulent flows. However, in each circumstance, these layers inherit properties from the universal viscous sublayer and from a nonuniversal wake flow. Thus, the log-law (12.88) may imperfectly approach

universality, and this situation is found in experiments. In particular, the current published literature (Nagib & Chauhan, 2008) supports the following values for the logarithmic-law constants at high Reynolds numbers:

Channel flow:	$\kappa = 0.37$	$B = 3.7$
Pipe flow:	$\kappa = 0.41$	$B = 5.0$
ZPG boundary layer:	$\kappa = 0.384$	$B = 4.17$

This observed flow-to-flow variation in log-law constants is not anticipated by the analysis presented earlier in this section because the geometric differences in the wake-flow regions were not accounted for in (12.83). However, the previous analysis remains valid for each outer-layer flow geometry. Thus, the log-law (12.88) does describe the overlap layer of a wall-bounded turbulent flow when the log-law constants are appropriate for that flow's geometry.

Interestingly, there is another issue at play here for turbulent boundary layers. From a flow-parameter perspective, a turbulent boundary layer differs from fully developed channel and pipe flows because the pressure gradient that may exist in a boundary layer flow is not directly linked to the wall shear stress τ_0. In fully developed channel and pipe flow, a stationary control volume calculation (see Exercise 12.31) requires:

$$dP/dx = -2\tau_o/h \text{ or } dP/dx = -4\tau_o/d, \tag{12.90, 12.91}$$

respectively, where h is the channel height and d is the pipe diameter. Thus, the starting points for the dimensional analysis of the inner and outer layers of the mean velocity profile, (12.79) and (12.83), need not include dP/dx for pipe and channel flows because τ_0 is already included. Yet, there is no equivalent to (12.90) or (12.91) for turbulent boundary layers. More general forms of (12.79) and (12.83) that would be applicable to all turbulent boundary layers need to include $\partial P/\partial x$, especially since $\partial P/\partial x$ does not drop from the mean stream-wise momentum equation, (12.78), for any value of y when $\partial P/\partial x$ is nonzero. The apparent outcome of this situation is that the log-law constants in turbulent boundary layers depend on the pressure gradient. Surprisingly, the following empirical correlation, offered by Nagib and Chauhan (2008),

$$\kappa B = 1.6\,[\exp(0.1663B) - 1], \tag{12.92}$$

collapses measured values of κ and B from all three types of wall-bounded shear flows for $0.15 < \kappa < 0.80$, and $-4 < B < 12$. Here, the most extreme values of κ and B arise from turbulent boundary layers in adverse (low values of κ and B) and favorable (high values of κ and B) pressure gradients.

Rough Surfaces

In deriving the logarithmic law (12.88), we assumed that the flow in the inner layer is determined by viscosity. This is true only for *hydrodynamically smooth* surfaces, for which the average height of the surface roughness elements is smaller than the thickness of the

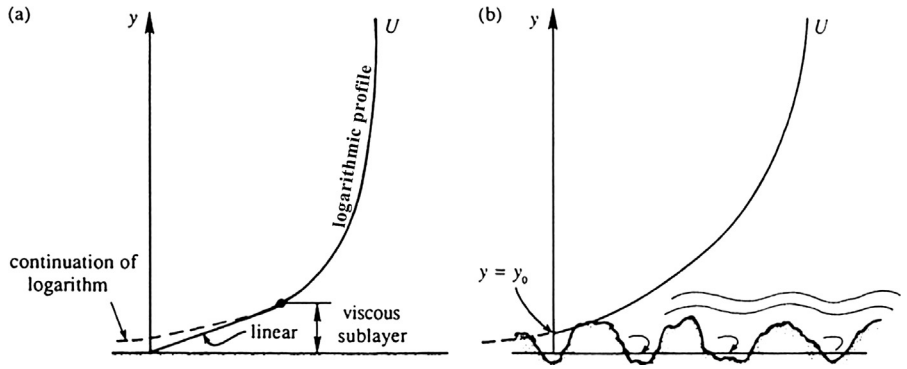

FIGURE 12.19 Logarithmic velocity distributions near smooth (a) and rough (b) surfaces. The presence of roughness may eliminate the viscous sublayer when the roughness elements protrude higher than several l_ν. In this case the log-law may be extended to a virtual wall location y_0 where U appears to go to zero.

viscous sublayer. For a hydrodynamically rough surface, on the other hand, the roughness elements protrude out of the viscous sublayer. An example is the terrestrial boundary layer, where the trees, buildings, etc., act as roughness elements. A wake develops behind each roughness element, and shear stress is transmitted to the wall by the resulting drag on the roughness elements. Viscosity becomes irrelevant for determining either the velocity distribution or the overall drag on the surface. This is why the friction coefficients for a rough pipe and a rough flat surface become constant as $\mathrm{Re} \to \infty$.

The velocity distribution near a rough surface is again logarithmic, but the intercept constant can be set by noting that the mean velocity U is expected to be negligible somewhere within the roughness elements (Figure 12.19b). We can therefore assume that (12.88) applies for $y > y_0$, where y_0 is a measure of the roughness heights and is defined as the value of y at which the logarithmic distribution gives $U = 0$. Appropriately evaluating the constant B in (12.88) then produces:

$$U^+ = \frac{U}{u_*} = \frac{1}{\kappa}\ln\left(\frac{y}{y_0}\right). \tag{12.93}$$

12.10. TURBULENCE MODELING

The closure problem arising from Reynolds-averaging of the equations of fluid motion has lead to the development of approximate models to close systems of RANS equations. Because of the practical importance of such models for weather forecasting and performance prediction for engineered devices, RANS-closure modeling efforts have existed for more than a century and continue to this day. This section presents a truncated overview of the essential elements leading to the so-called k-ε closure model for the RANS mean-flow momentum equation (12.30). Second-order closures, large-eddy simulations, and other RANS closure schemes are described in Part Two of Pope (2000). The review article by Speziale (1991) is also recommended.

The primary purpose of a turbulent-mean-flow closure model is to relate the Reynolds stress correlations $\overline{u_i u_j}$ to the mean velocity field U_i. Prandtl and von Karman developed certain semi-empirical theories that attempted to provide this relationship. These theories are based on drawing an analogy between molecular-motion-based laminar momentum and scalar transport, and eddy-motion-based turbulent momentum and scalar transport. The outcome of such modeling efforts is typically an *eddy viscosity* ν_T (first introduced by Boussinesq in 1877) and *eddy diffusivities* κ_T and κ_{mT} for the closure-model equations:

$$\overline{u_i u_j} = \frac{2}{3}\overline{e}\delta_{ij} - \nu_T\left(\frac{\partial U_i}{\partial x_j} + \frac{\partial U_j}{\partial x_i}\right),\ \overline{u_i T'} = -\kappa_T\frac{\partial \overline{T}}{\partial x_i},\ \text{and}\ \overline{u_i Y'} = -\kappa_{mT}\frac{\partial \overline{Y}}{\partial x_i}. \quad (12.94, 12.95, 12.96)$$

Equation (12.94) is mathematically analogous to the stress-rate-of-strain relationship for a Newtonian fluid (4.37) with the term that includes the turbulent kinetic energy $\overline{e}$ playing the role of a turbulent pressure. It represents the *turbulent viscosity hypothesis*. Similarly, (12.95) and (12.96) are mathematically analogous to Fourier's law and Fick's law for molecular diffusion of heat and species, respectively, and these equations represent the *gradient diffusion hypothesis* for turbulent transport of heat and a passive scalar.

To illustrate the implications of such hypotheses, substitute (12.94) into (12.30) to find:

$$\frac{\partial U_i}{\partial t} + U_j\frac{\partial U_i}{\partial x_j} = -\frac{1}{\rho}\frac{\partial P}{\partial x_j} + \frac{\partial}{\partial x_j}\left([\nu + \nu_T]\left(\frac{\partial U_i}{\partial x_j} + \frac{\partial U_j}{\partial x_i}\right) - \frac{2}{3}\overline{e}\delta_{ij}\right) \quad (12.97)$$

for constant-density flow. The factor in [,]-brackets is commonly known as the *effective viscosity*, and correspondence between this mean-flow equation and its unaveraged counterpart, (4.86) simplified for constant density, is clear and compelling. Mean flow equations for $\overline{T}$ and $\overline{Y}$ similar to (12.97) are readily obtained by substituting (12.95) and (12.96) into (12.32) and (12.34), respectively. Unfortunately, the molecular-dynamics-to-eddy-dynamics analogy is imperfect. Molecular sizes are typically much less than fluid-flow gradient length scales while turbulent eddy sizes are typically comparable to fluid-flow gradient length scales. For ordinary fluid-molecule sizes, averages taken over small volumes include many molecules and these averages converge adequately for macroscopic transport predictions. Equivalent averages over eddies may be unsuccessful because turbulent eddies are so much larger than molecules. Thus, ν_T, κ_T, and κ_{mT} are *not* properties of the fluid or fluid mixture, as ν, κ, and κ_m are. Instead, ν_T, κ_T, and κ_{mT} are properties of the flow, and this transport-flow relationship must be modeled. Hence, (12.97) and its counterparts for $\overline{T}$ and $\overline{Y}$ must be regarded as approximate because (12.94) through (12.96) have inherent limitations. Nevertheless, RANS closure models involving (12.94) through (12.96) are sufficiently accurate for many tasks involving computational fluid dynamics.

From dimensional considerations, ν_T, κ_T, and κ_{mT} should all be proportional to the product of a characteristic turbulent length scale l_T and a characteristic turbulent velocity u_T:

$$\nu_T,\ \kappa_T,\ \text{or}\ \kappa_{mT} \sim l_T u_T. \quad (12.98)$$

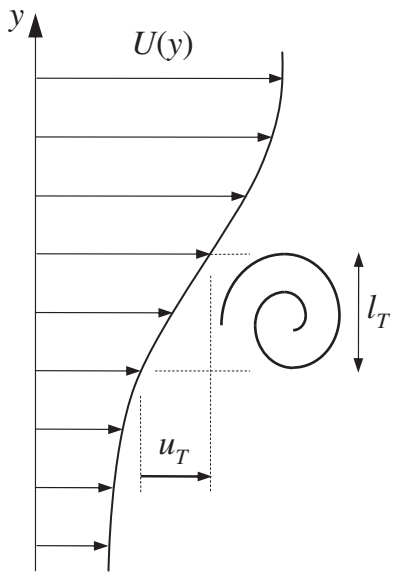

FIGURE 12.20 Schematic drawing of an eddy of size l_T in a shear flow with mean velocity profile $U(y)$. A velocity fluctuation, u or v, that might be produced by this eddy must be of order $l_T(dU/dy)$. Therefore, we expect that the Reynolds shear stress will scale like $\overline{uv} \sim l_T^2(dU/dy)^2$.

For simplicity, consider fully developed, temporally stationary unidirectional shear flow $U(y)$ where y is the cross-stream coordinate (Figure 12.20). The mean-flow momentum equation in this case is:

$$0 = -\frac{1}{\rho}\frac{dP}{dx} + \frac{\partial}{\partial y}\left(\nu\frac{\partial U}{\partial y} - \overline{uv}\right) = -\frac{1}{\rho}\frac{dP}{dx} + \frac{\partial}{\partial y}\left([\nu + \nu_T]\left(\frac{\partial U}{\partial y}\right)\right). \tag{12.99}$$

A Mixing Length Model

An eddy viscosity for this equation can be constructed by interpreting l_T as a *mixing length*, defined as the cross-stream distance traveled by a fluid particle before it gives up its momentum and loses its identity. In this situation, an eddy of size l_T driven by a local shear rate of dU/dy produces a velocity fluctuation of $u_T \sim l_T(dU/dy)$ as it turns over, so

$$-\overline{uv} = \nu_T\frac{dU}{dy} \sim l_T u_T\frac{dU}{dy} \sim l_T\left(l_T\frac{dU}{dy}\right)\frac{dU}{dy} = l_T^2\left(\frac{dU}{dy}\right)^2.$$

The mixing-length concept was first introduced by Taylor (1915), but the approach was fully developed by Prandtl and his coworkers. For a wall-bounded flow it makes sense to assume that l_T is proportional to y when $y = 0$ defines the wall. Thus, setting $l_T = \kappa y$, where κ is

presumed to be constant, completes a simple mixing-length turbulence model, and (12.99) becomes:

$$0 = -\frac{1}{\rho}\frac{dP}{dx} + \frac{\partial}{\partial y}\left(\nu\frac{dU}{dy} + \kappa^2 y^2\left(\frac{dU}{dy}\right)^2\right). \tag{12.100}$$

When the pressure gradient is zero or small enough to be ignored, (12.100) can be integrated once to find:

$$\nu\frac{dU}{dy} + \kappa^2 y^2\left(\frac{dU}{dy}\right)^2 = const. = \frac{\tau_0}{\rho},$$

where the final equality comes from evaluating the expression on the left at $y = 0$. For points outside the viscous sublayer, where the turbulence term dominates, the last equation reduces to a simple ordinary differential equation that is readily integrated to reach:

$$\frac{dU}{dy} \cong \sqrt{\frac{\tau_0}{\rho}}\frac{1}{\kappa y}, \text{ or } \frac{U}{u_*} \cong \frac{1}{\kappa}\ln y + const., \tag{12.101}$$

which replicates the log-law (12.88). This simplest-level turbulence model is known as an *algebraic* or *zero-equation* model. Such mixing length models can be generalized to a certain extent by using a contracted form of the mean strain-rate tensor or the mean rotation-rate tensor in place of $(dU/dy)^2$. However, there is no rational approach for relating l_T to the mean flow field in general.

Since the development of modern computational techniques for solving partial differential equations, the need for simple intuitive approaches like the mixing length theory has essentially vanished, and Prandtl's derivation of the empirically known logarithmic velocity distribution has only historical value. However, the relationship (12.98) remains useful for estimating the order of magnitude of the eddy diffusivity in turbulent flows, and for development of more sophisticated RANS closure models (see below). Consider the estimation task first via the specific example of thermal convection between two horizontal plates in air when the plates are separated by a distance $L = 3$ m, and the lower plate is warmer by $\Delta T = 1°\text{C}$. The equation for the vertical velocity fluctuation gives the vertical acceleration as

$$Dw/Dt \sim g\alpha T' \sim g\Delta T/T, \tag{12.102}$$

since T' is expected to be of order ΔT and $\alpha = 1/T$ for a perfect gas. The time t_r to rise through a height L will be proportional to L/w, so (12.102) gives a characteristic vertical velocity acceleration of

$$w/t_r = w^2/L \sim Dw/Dt \sim g\Delta T/T \rightarrow w \sim \sqrt{gL\Delta T/T} \cong 0.3\ m/s.$$

The largest eddies will scale with the plate separation L, so the thermal eddy diffusivity, κ_T, is

$$\kappa_T \sim wL \sim 0.9\ m^2/s,$$

which is significantly larger than the molecular value of 2×10^{-5} m^2/s.

One-Equation Models

Independently, Kolmogorov and Prandtl suggested that the velocity scale in (12.98) should be determined from the turbulent kinetic energy:

$$u_T = c\sqrt{\overline{e}},$$

where c is a model constant. The turbulent viscosity is then obtained from an algebraic specification of the turbulent length scale l_T, and the solution of a transport equation for $\overline{e}$ that is based on its exact transport equation (12.47). In this case, the dissipation rate $\overline{\varepsilon}$ and the transport terms must be modeled. For high Reynolds number turbulence, the scaling relationship (12.48) and the gradient diffusion hypothesis lead to the following model equations for the dissipation and the transport of turbulent kinetic energy:

$$\overline{\varepsilon} = C_\varepsilon(\overline{e})^{3/2}/l_T \quad \text{and} \quad -\frac{1}{\rho_0}\overline{pu_j} + 2\nu\overline{u_j S'_{ij}} - \frac{1}{2}\overline{u_i^2 u_j} = \frac{\nu_T}{\sigma_e}\frac{\partial \overline{e}}{\partial x_j},$$

where C_ε and σ_e are model constants. So, for constant density, the turbulent kinetic energy model equation is:

$$\frac{\partial \overline{e}}{\partial t} + U_j\frac{\partial \overline{e}}{\partial x_j} = \frac{\partial}{\partial x_j}\left(\frac{\nu_T}{\sigma_e}\frac{\partial \overline{e}}{\partial x_j}\right) - \overline{\varepsilon} - \overline{u_i u_j}\frac{\partial U_i}{\partial x_j}, \tag{12.103}$$

and this represents *one* additional nonlinear second-order partial-differential equation that must be solved, hence the name *one-equation model*. As mentioned in Pope, one-equation models provide a modest accuracy improvement over the simpler algebraic models.

Two-Equation Models

These models eliminate the need for a specified turbulent length scale by generating l_T from the solutions of transport equations for $\overline{e}$ and $\overline{\varepsilon}$. The popular k-ε closure model of Jones and Launder (1972) is described here. A k-ω closure model also exists. (Throughout much of the turbulence modeling literature "k" is used for the turbulent kinetic energy, so the model name "k-ε " is merely a specification of the dependent-field variables in the two extra partial differential equations.) The k-ε model is based on the turbulent viscosity hypothesis (12.94) with ν_T specified by (12.98), $l_T = (\overline{e})^{3/2}/\overline{\varepsilon}$, and $u_T = (\overline{e})^{1/2}$:

$$\nu_T = C_\mu\left[(\overline{e})^{3/2}/\overline{\varepsilon}\right]\sqrt{\overline{e}} = C_\mu(\overline{e})^2/\overline{\varepsilon}, \tag{12.104}$$

where C_μ is one of five model constants. The first additional partial-differential equation is (12.103) for $\overline{e}$. The second additional partial-differential equation is an empirical construction for the dissipation:

$$\frac{\partial \overline{\varepsilon}}{\partial t} + U_j\frac{\partial \overline{\varepsilon}}{\partial x_j} = \frac{\partial}{\partial x_j}\left(\frac{\nu_T}{\sigma_\varepsilon}\frac{\partial \overline{\varepsilon}}{\partial x_j}\right) - C_{\varepsilon 1}\left(\overline{u_i u_j}\frac{\partial U_i}{\partial x_j}\right)\frac{\overline{\varepsilon}}{\overline{e}} - C_{\varepsilon 2}\frac{(\overline{\varepsilon})^2}{\overline{e}}. \tag{12.105}$$

The standard model constants are from Launder and Sharma (1974):

$$C_\mu = 0.09,\ C_{\varepsilon 1} = 1.44,\ C_{\varepsilon 2} = 1.92,\ \sigma_e = 1.0, \text{ and } \sigma_\varepsilon = 1.3,$$

and these have been set so the model's predictions reasonably conform to experimentally determined mean velocity profiles, fluctuation profiles, and energy budgets of the type shown in Figures 12.14 and 12.15 for a variety of simple turbulent flows. More recently renormalization group theory has been used to justify (12.105) with slightly modified constants (Yakhot & Orszag, 1986; Lam, 1992; see also Smith & Reynolds, 1992).

When the density is constant, (12.27), (12.30), (12.94), and (12.103) through (12.105) represent a closed set of equations. Ideally, the usual viscous boundary conditions would be applied to U_i. However, steep near-wall gradients of the dependent field variables pose a significant computational challenge. Thus, boundary conditions on solid surfaces are commonly applied slightly above the surface using empirical *wall functions* intended to mimic the inner layer of a wall-bounded turbulent flow. Wall functions allow the mean-flow momentum equation (12.30) and the turbulence model equations, (12.103) and (12.105), to be efficiently, but approximately, evaluated near a solid surface. Unfortunately, wall functions that perform well with attached turbulent boundary layers are of questionable validity for separating, impinging, and adverse-pressure-gradient flows. Furthermore, the use of wall functions introduces an additional model parameter, the distance above the wall where boundary conditions are applied.

Overall, the k-ε turbulence model is complete and versatile. It is commonly used to rank the performance of fluid dynamic system designs before experimental tests are undertaken. Limitations on its accuracy arise from the turbulent viscosity hypothesis, the $\overline{\varepsilon}$ equation, and wall functions when they are used. In addition, variations in inlet boundary conditions for $\overline{e}$ and $\overline{\varepsilon}$, which may not be known precisely, can produce changes in predicted results. In recent years, two equation turbulence models based on the eddy viscosity hypothesis have begun to be eclipsed by *Reynolds stress models* or *second-order closures* that directly compute the Reynolds stress tensor from a modeled version of its exact transport equation (12.35).

12.11. TURBULENCE IN A STRATIFIED MEDIUM

Effects of stratification become important in such laboratory flows as heat transfer from a heated plate and in geophysical flows such as those in the atmosphere and in the ocean. Some effects of stratification on turbulent flows will be considered in this section. Further discussion can be found in Tennekes and Lumley (1972), Phillips (1977), and Panofsky and Dutton (1984).

As is customary in the geophysical literature, the z-direction points upward opposing gravity so the mean velocity of a horizontally flowing shear flow will be denoted by $U(z)$. For simplicity, U is assumed to be independent of x and y. Turbulence in a stratified medium depends critically on the stability of the vertical density profile. In the neutrally stable state of a compressible environment the density decreases upward, because of the decrease of pressure, at a rate $d\rho_a/dz$ called the *adiabatic density gradient*, as discussed in Section 1.10. A medium is statically stable if the density decreases faster than the adiabatic decrease. The effective density gradient that determines the stability of the environment is then determined by the sign of $d(\rho - \rho_a)/dz$, where $\rho - \rho_a$ is called the *potential density*. In the following discussion, it is assumed that the adiabatic variations of density have been

subtracted out, so that "density" or "temperature" really mean potential density or potential temperature.

The Richardson Numbers

First examine the equation for turbulent kinetic energy (12.47). Omitting the viscous transport and assuming that the flow is independent of x and y, it reduces to

$$\frac{\partial \overline{e}}{\partial t} + U\frac{\partial \overline{e}}{\partial x} = -\frac{\partial}{\partial z}\left(\frac{1}{\rho_0}\overline{p'w'} + \overline{e'w'}\right) - \overline{u'w'}\frac{\partial U}{\partial z} + g\alpha\overline{w'T'} - \overline{\varepsilon}, \tag{12.106}$$

where x increases in the downstream direction. The first term on the right side is the transport of turbulent kinetic energy by vertical velocity fluctuations. The second term is the production of turbulent energy by the interaction of Reynolds stress and the mean shear; this term is almost always positive. The third term is the production of turbulent kinetic energy by the vertical heat flux; it is called the *buoyant production*, and was discussed in Section 12.7. In an unstable environment, in which the mean temperature $\overline{T}$ decreases upward, the heat-flux correlation $\overline{w'T'}$ is positive (upward), signifying that the turbulence is generated convectively by upward heat fluxes. In the opposite case of a stable environment, the turbulence is suppressed by stratification. The ratio of the buoyant destruction of turbulent kinetic energy to the shear production is called the *flux Richardson number*:

$$\mathrm{Rf} = \frac{-g\alpha\overline{w'T'}}{-\overline{u'w'}(dU/dz)} = \frac{\text{buoyant destruction}}{\text{shear production}}. \tag{12.107}$$

As the shear production is positive with the minus sign displayed, the sign of Rf depends on the sign of $\overline{w'T'}$. For an unstable environment in which the heat flux is upward Rf is negative, and for a stable environment it is positive. For $\mathrm{Rf} > 1$, buoyant destruction removes turbulence at a rate larger than the rate at which it is produced by shear production. However, the critical value of Rf at which the turbulence ceases to be self-supporting is less than unity, as dissipation is necessarily a large fraction of the shear production. Observations indicate that the critical value is $\mathrm{Rf_{cr}} \approx 0.25$ (Panofsky & Dutton, 1984, p. 94). If measurements indicate the presence of turbulent fluctuations, but at the same time a value of Rf much larger than 0.25, then a fair conclusion is that the turbulence is decaying. When Rf is negative, a large $-\mathrm{Rf}$ means strong convection and weak mechanical turbulence.

Instead of Rf, it is easier to measure the *gradient Richardson number*, defined as

$$\mathrm{Ri} \equiv \frac{N^2}{(dU/dz)^2} = \frac{\alpha g(d\overline{T}/dz)}{(dU/dz)^2}, \tag{12.108}$$

where N is the buoyancy frequency and the second equality follows for stratification by thermal variations. If we make the turbulent viscosity and gradient diffusion assumptions (12.94) and (12.95), then the two Richardson numbers are related by

$$\mathrm{Ri} = (\nu_T/\kappa_T)\mathrm{Rf}. \tag{12.109}$$

The ratio ν_T/κ_T is the *turbulent Prandtl number*, which determines the relative efficiency of the vertical turbulent exchanges of momentum and heat. The presence of a stable stratification

damps vertical transport of both heat and momentum; however, the momentum flux is reduced less because the internal waves in a stable environment can transfer momentum (by moving vertically from one region to another) but not heat. Therefore, $v_T/\kappa_T > 1$ for a stable environment. Equation (12.109) then shows that turbulence can persist even when $\mathrm{Ri} > 1$, if the critical value of 0.25 applies on the *flux* Richardson number (Turner, 1981; Bradshaw & Woods, 1978). In an unstable environment, on the other hand, v_T/κ_T becomes small. In a neutral environment it is usually found that $v_T \approx \kappa_T$; the idea of equating the eddy coefficients of heat and momentum is called the *Reynolds analogy.*

Monin-Obukhov Length

The Richardson numbers are ratios that compare the relative importance of mechanical and convective turbulence. Another parameter used for the same purpose is not a ratio, but has the unit of length. It is the *Monin-Obukhov length*, defined as

$$L_M \equiv -u_*^3/\kappa\alpha g\overline{wT'}, \tag{12.110}$$

where u_* is the friction velocity, $\overline{wT'}$ is the heat flux correlation, α is the coefficient of thermal expansion, and κ is the von Karman constant introduced for convenience. Although $\overline{wT'}$ is a function of z, the parameter L_M is effectively a constant for the flow, as it is used only in the logarithmic region of the earth's atmospheric boundary layer in which both $\overline{uw}$ and $\overline{wT'}$ are nearly constant. The Monin-Obukhov length then becomes a parameter determined from the boundary conditions of friction and the heat flux at the surface. Like Rf, it is positive for stable conditions and negative for unstable conditions.

The significance of L_M within the atmospheric boundary layer becomes clearer if we write Rf in terms of L_M, using the logarithmic velocity distribution (12.88), from which $dU/dz = u_*/\kappa z$. (Note that z is the distance perpendicular to the surface.) Using $\overline{uw} = u_*^2$ because of the near uniformity of stress in the logarithmic layer, (12.107) becomes

$$\mathrm{Rf} = z/L_M. \tag{12.111}$$

As Rf is the ratio of buoyant destruction to shear production of turbulence, (12.111) shows that L_M is the height at which these two effects are of the same order. For both stable and unstable conditions, the effects of stratification are slight if $z \ll |L_M|$. At these small heights, then, the velocity profile is logarithmic, as in a neutral environment. This is called a *forced convection* region, because the turbulence is mechanically forced. For $z \gg |L_M|$, the effects of stratification dominate. In an unstable environment, it follows that the turbulence is generated mainly by buoyancy at heights $z \gg -L_M$, and the shear production is negligible. The region beyond the forced convecting layer is therefore called a zone of *free convection* (Figure 12.21), containing thermal plumes (columns of hot rising gases) characteristic of free convection from heated plates in the absence of shear flow.

Observations as well as analysis show that the effect of stratification on the velocity distribution in the surface layer is given by the log-linear profile (Turner, 1973):

$$U = \frac{u_*}{\kappa}\left[\ln\frac{z}{z_o} + 5\frac{z}{L_M}\right].$$

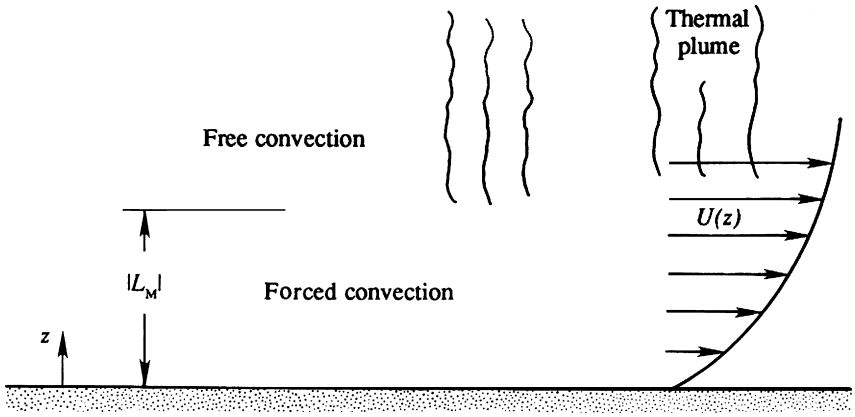

FIGURE 12.21 Forced and free convection zones in an unstable atmosphere. In strongly sheared regions, the turbulence will not include buoyant effects (forced convection). However, where shear is weak, buoyant convection will set the turbulent scales (free convection).

The form of this profile is sketched in Figure 12.22 for stable and unstable conditions. It shows that the velocity is more uniform than $ln(z)$ in the unstable case because of the enhanced vertical mixing due to buoyant convection.

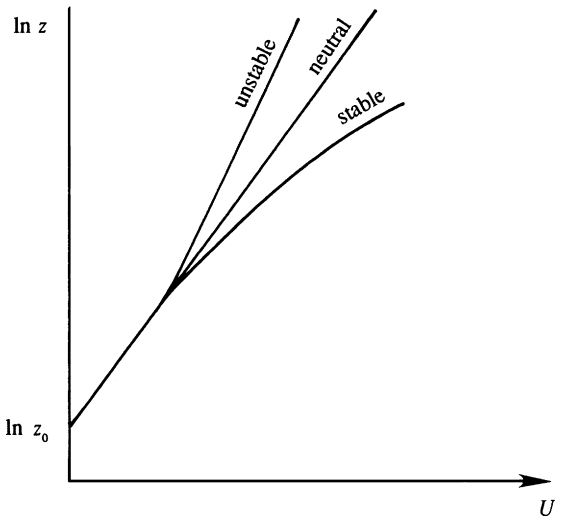

FIGURE 12.22 Effect of stability on velocity profiles in the surface layer. When the atmospheric boundary layer is neutrally stable, the mean velocity profile is logarithmic. When it is stable, vertical turbulent motions are suppressed so higher shear may exist in the mean flow; this is shown as the lower curve labeled *stable*. When the atmospheric boundary layer is unstable, vertical turbulent motions are enhanced, mean flow shear is reduced, and $U(z)$ becomes more nearly uniform; this is shown as the upper curve labeled *unstable*.

Spectrum of Temperature Fluctuations

An equation for the intensity of temperature fluctuations $\overline{T'^2}$ can be obtained in a manner identical to that used for obtaining the turbulent kinetic energy. The procedure is therefore to obtain an equation for DT'/Dt by subtracting those for $D\tilde{T}/Dt$ and $D\overline{T}/Dt$, and then to multiply the resulting equation for DT'/Dt by T' and taking the average. The result is

$$\frac{\partial}{\partial t}\left(\frac{1}{2}\overline{T'^2}\right)+U\frac{\partial}{\partial x}\left(\frac{1}{2}\overline{T'^2}\right)=-\overline{wT'}\frac{d\overline{T}}{dz}-\frac{\partial}{\partial z}\left(\frac{1}{2}\overline{T'^2w}-\kappa\frac{\partial\overline{T'^2}}{\partial z}\right)-\bar{\varepsilon}_{\mathrm{T}}, \tag{12.112}$$

where $\bar{\varepsilon}_{\mathrm{T}}=\kappa\overline{(\partial T'/\partial x_j)^2}$ is the *dissipation rate of temperature fluctuations*, analogous to the dissipation of turbulent kinetic energy $\bar{\varepsilon}$ defined within (12.47) . The first term on the right side is the generation of $\overline{T'^2}$ by the mean temperature gradient, $\overline{wT'}$ being positive if $d\overline{T}/dz$ is negative. The second term on the right side is the turbulent transport of $\overline{T'^2}$.

A wave number spectrum of temperature fluctuations can be defined such that

$$\overline{T'^2}\equiv\int_0^\infty S_T(K)dK,$$

where K is the magnitude of the three-dimensional wave number. As in the case of the kinetic energy spectrum, an inertial range of wave numbers exists in which neither the production by large-scale eddies nor the dissipation by conductive and viscous effects are important. As the temperature fluctuations are intimately associated with velocity fluctuations, $S_T(K)$ in this range must depend not only on ε_T but also on the variables that determine the velocity spectrum, namely ε and K. Therefore

$$S_T=S_T(K,\bar{\varepsilon},\bar{\varepsilon}_T)\ \text{ for }\ 2\pi/L\ll K\ll 2\pi/\eta,$$

where L is the size of the largest eddies. The unit of S_T is $^\circ\mathrm{C}^2$ m, and the unit of ε_{T} is $^\circ\mathrm{C}^2$/s, so dimensional analysis gives

$$S_T\propto\bar{\varepsilon}_T\bar{\varepsilon}^{\,-1/3}K^{-5/3}\quad\text{for }\ 2\pi/L\ll K\ll 2\pi/\eta, \tag{12.113}$$

which was first derived by Obukhov in 1949. Comparing with (12.54), it is apparent that the spectra of both velocity and temperature fluctuations in the inertial subrange have the same $K^{-5/3}$ form.

The spectrum beyond the inertial subrange depends on whether the Prandtl number ν/κ of the fluid is smaller or larger than one. We shall only consider the case of $\nu/\kappa\gg 1$, which applies to water for which the Prandtl number is 7.1. Let η_T be the scale responsible for smearing out the temperature gradients and η be the Kolmogorov microscale at which the velocity gradients are smeared out. For $\nu/\kappa\gg 1$ we expect that $\eta_{\mathrm{T}}\ll\eta$, because then the conductive effects are important at scales smaller than the viscous scales. In fact, Batchelor (1959) showed that $\eta_T=\eta(\kappa/\nu)^{1/2}\ll\eta$. In such a case there exists a range of wave numbers $2\pi/\eta\ll K\ll 2\pi/\eta_T$, in which the scales are not small enough for the thermal diffusivity to smear out the temperature fluctuation. Therefore, $S_T(K)$ continues up to wave numbers of order $2\pi/\eta_T$, although the kinetic energy spectrum has dropped off sharply. This is called the *viscous*

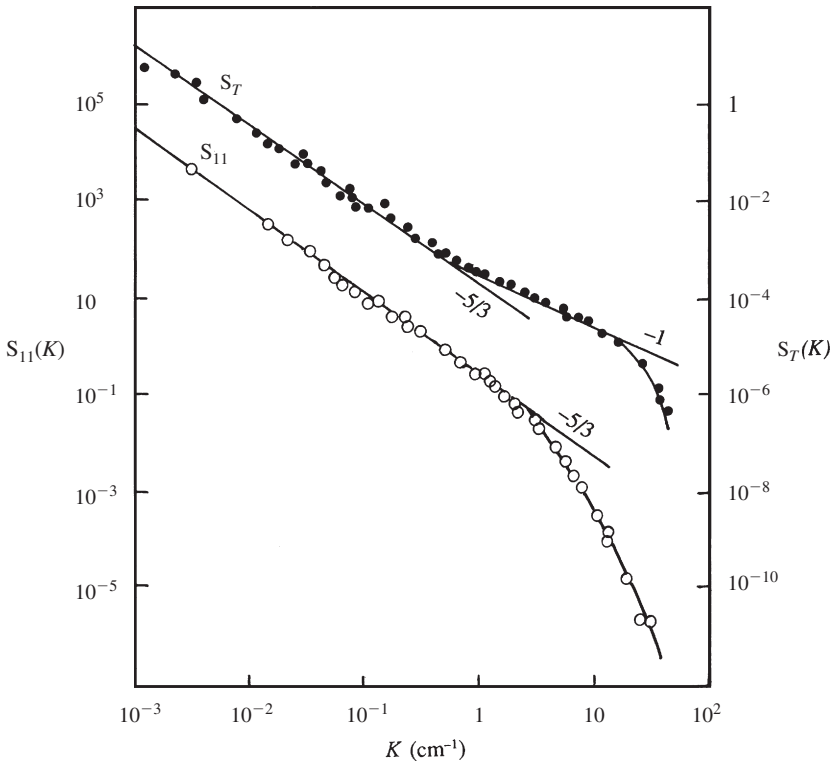

FIGURE 12.23 Temperature and velocity spectra measured by Grant et al. (1968). The measurements were made at a depth of 23 m in a tidal passage through islands near the coast of British Columbia, Canada. The wave number K is in cm^{-1}. Solid points represent S_T in (°C)^2/cm^{-1}, and open points represent S_{11} in (cm/s)^2/cm^{-1}. Powers of K that fit the observation are indicated by straight lines. *O. M. Phillips,* The Dynamics of the Upper Ocean, *1977; reprinted with the permission of Cambridge University Press.*

convective subrange, because the spectrum is dominated by viscosity but is still actively convective. Batchelor (1959) showed that the spectrum in the viscous convective subrange is

$$S_T \propto K^{-1} \text{ for } 2\pi/\eta \ll K \ll 2\pi/\eta_T. \tag{12.114}$$

Figure 12.23 shows a comparison of velocity and temperature spectra, observed in a tidal flow through a narrow channel. The temperature spectrum shows that the spectral slope increases from $-5/3$ in the inertial subrange to -1 in the viscous convective subrange.

12.12. TAYLOR'S THEORY OF TURBULENT DISPERSION

The large mixing rate in a turbulent flow is due to the fact that the fluid particles wander away from their initial location. Taylor (1921) studied this problem and calculated the rate at which a particle disperses (i.e., moves away) from its initial location. The presentation here is

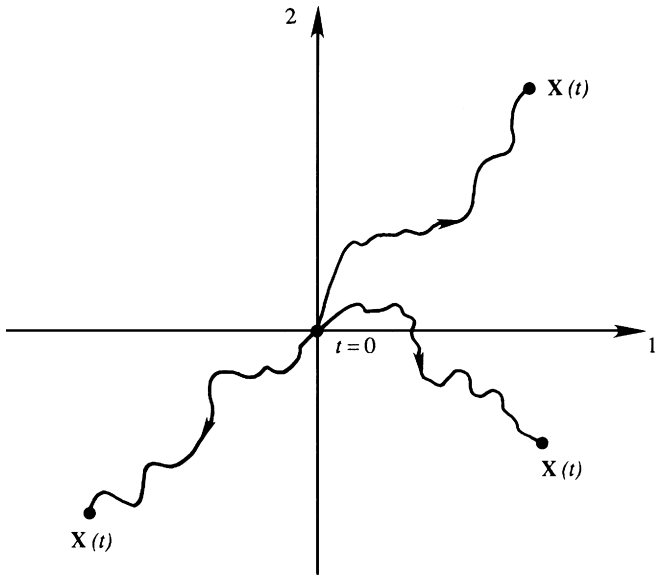

FIGURE 12.24 Three members of an ensemble of particle trajectories, $\mathbf{X}(t)$, at time t for particles released at the origin of coordinates at $t = 0$ in a turbulent flow with zero mean velocity. The distance traveled by the particles indicates how tracer particles disperse in a turbulent flow.

directly adapted from his classic paper. He considered a point source emitting particles, say a chimney emitting smoke. The particles are emitted into a stationary and homogeneous turbulent medium in which the mean velocity is zero. Taylor used Lagrangian coordinates $\mathbf{X}(\mathbf{a}, t)$, which is the present location at time t of a particle that was at location $\boldsymbol{a}$ at time $t = 0$. We shall take the point source to be the origin of coordinates and consider an ensemble of experiments in which we evaluate the location $\mathbf{X}(\mathbf{0}, t)$ at time t of all the particles that started from the origin (Figure 12.24). For notational simplicity the first argument in $\mathbf{X}(\mathbf{0}, t)$ will be dropped from here on so that $\mathbf{X}(\mathbf{0}, t) = \mathbf{X}(t)$.

Rate of Dispersion of a Single Particle

Consider the behavior of a single component of $\mathbf{X}$, say X_α ($\alpha = 1$, 2, or 3). (Recall that a Greek subscript means that the summation convention is *not* followed.) The average rate at which the *magnitude* of X_α increases with time can be found by finding $\overline{d(X_\alpha^2)/dt}$, where the over bar denotes an ensemble average and not a time average. We can write

$$\frac{d}{dt}\left(\overline{X_\alpha^2}\right) = 2\overline{X_\alpha \frac{dX_\alpha}{dt}}, \tag{12.115}$$

where we have used the commutation rule (12.6). Defining $u_\alpha = dX_\alpha/dt$ as the *Lagrangian* velocity component of a fluid particle at time t, (12.115) becomes

$$\begin{aligned}\frac{d}{dt}(\overline{X_\alpha^2}) &= 2\overline{X_\alpha u_\alpha} = 2\overline{\left[\int_0^t u_\alpha(t')\,dt'\right]u_\alpha} \\ &= 2\int_0^t \overline{u_\alpha(t')u_\alpha(t)}\,dt',\end{aligned} \tag{12.116}$$

where we have used the commutation rule (12.7) for averaging and integration. We have also written

$$X_\alpha = \int_0^t u_\alpha(t')\,dt',$$

which is valid when X_α and u_α are associated with the same particle. Because the flow is assumed to be stationary, $\overline{u_\alpha^2}$ is independent of time, and the autocorrelation of $u_\alpha(t)$ and $u_\alpha(t')$ is only a function of the time difference $t - t'$. Defining

$$r_\alpha(\tau) \equiv \frac{\overline{u_\alpha(t)u_\alpha(t+\tau)}}{\overline{u_\alpha^2}}$$

to be the autocorrelation coefficient of the Lagrangian velocity components of a particle, (12.116) becomes

$$\frac{d}{dt}(\overline{X_\alpha^2}) = 2\overline{u_\alpha^2}\int_0^t r_\alpha(t'-t)\,dt' = 2\overline{u_\alpha^2}\int_0^t r_\alpha(\tau)\,d\tau, \tag{12.117}$$

where we have changed the integration variable from t' to $\tau = t - t'$. Integrating, we obtain

$$\overline{X_\alpha^2}(t) = 2\overline{u_\alpha^2}\int_0^t dt'\int_0^{t'} r_\alpha(\tau)\,d\tau, \tag{12.118}$$

which shows how the variance of the particle position changes with time.

Another useful form of equation (12.118) is obtained by integrating it by parts. We have:

$$\begin{aligned}\int_0^t dt'\int_0^{t'} r_\alpha(\tau)\,d\tau &= \left[t'\int_0^{t'} r_\alpha(\tau)\,d\tau\right]_{t'=0}^{t} - \int_0^t t' r_\alpha(t')\,dt' \\ &= t\int_0^t r_\alpha(\tau)\,d\tau - \int_0^t t' r_\alpha(t')\,dt' \\ &= t\int_0^t \left(1-\frac{\tau}{t}\right) r_\alpha(\tau)\,d\tau.\end{aligned}$$

Equation (12.118) then becomes

$$\overline{X_\alpha^2}(t) = 2\overline{u_\alpha^2}t\int_0^t \left(1-\frac{\tau}{t}\right) r_\alpha(\tau)\,d\tau. \tag{12.119}$$

Two limiting cases are examined in what follows.

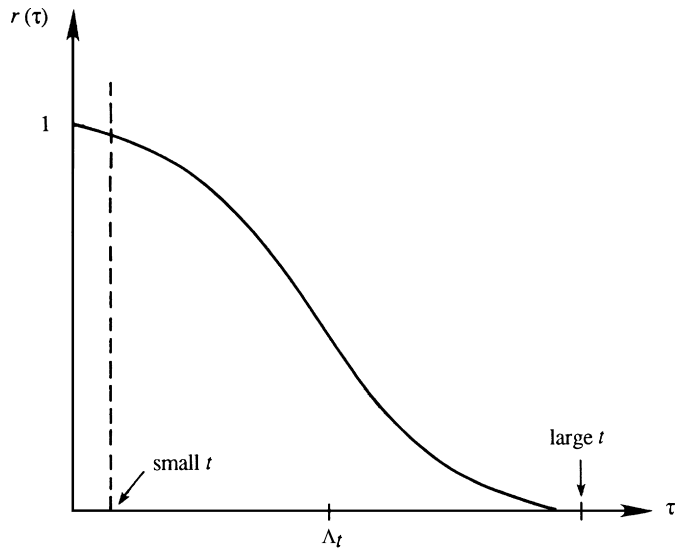

FIGURE 12.25 Small and large values of time on a plot of the correlation function. For small times, $r(\tau)$ is nearly unity, while for large times it is nearly zero.

Behavior for small t

If t is small compared to the correlation scale of $r_\alpha(\tau)$, then $r_\alpha(\tau) \approx 1$ throughout the integral in (12.118) (Figure 12.25). This gives:

$$\overline{X_\alpha^2}(t) \simeq \overline{u_\alpha^2} t^2. \tag{12.120}$$

Taking the square root of both sides, we obtain

$$(X_\alpha)_{rms} = (u_\alpha)_{rms} t \quad \text{for } t \ll \Lambda_t, \tag{12.121}$$

which shows that the *rms* displacement increases linearly with time and is proportional to the standard deviation of the turbulent fluctuations in the medium.

Behavior for large t

If t is large compared with the correlation scale of $r_\alpha(\tau)$, then τ/t in (11.119) is negligible, giving

$$\overline{X_\alpha^2}(t) = 2\overline{u_\alpha^2}\,\Lambda_t\, t, \tag{12.122}$$

where

$$\Lambda_t = \int_0^\infty r_\alpha(\tau) d\tau$$

is the integral time scale determined from the Lagrangian correlation $r_\alpha(\tau)$. Taking the square root of (12.122) gives

$$(X_\alpha)_{rms} = (u_\alpha)_{rms} \sqrt{2\Lambda_t t} \quad \text{for } t \gg \Lambda_t. \tag{12.123}$$

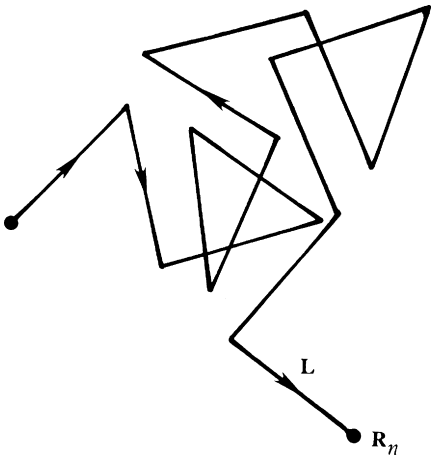

FIGURE 12.26 A sample realization of a random walk where the step length L is a uniform distance, but the step direction is random. After n steps, the vector distance from the starting point is $\mathbf{R}_n$. However, the root-mean-square distance from the starting point is only $L\sqrt{n}$ (not Ln) because many of the n steps lie in nearly opposite directions.

The $t^{1/2}$ behavior of (12.123) at large times is similar to the behavior in a *random walk*, in which the average distance traveled in a series of random (i.e., uncorrelated) steps increases as $t^{1/2}$. This similarity is due to the fact that for large t the fluid particles have *forgotten* their initial behavior at $t = 0$. In contrast, the small time behavior described by (12.121) is due to complete correlation, with *each experiment* giving $X_\alpha \simeq u_\alpha t$. The random walk concept is discussed in what follows.

Random Walk

The description provided here is adapted from Feynman et al. (1963, pp. 5–6, 41–48). Imagine a person walking in a random manner, by which we mean that there is no correlation between the directions of two consecutive steps. Let the vector $\mathbf{R}_n$ represent the distance from the origin after n steps, and the vector $\mathbf{L}$ represent the nth step (Figure 12.26). We assume that each step has the same magnitude L. Then

$$\mathbf{R}_n = \mathbf{R}_{n-1} + \mathbf{L},$$

which gives

$$\begin{aligned} R_n^2 = \mathbf{R}_n \cdot \mathbf{R}_n &= (\mathbf{R}_{n-1} + \mathbf{L}) \cdot (\mathbf{R}_{n-1} + \mathbf{L}) \\ &= R_{n-1}^2 + L^2 + 2\mathbf{R}_{n-1} \cdot \mathbf{L}. \end{aligned}$$

Taking the average, we get

$$\overline{R_n^2} = \overline{R_{n-1}^2} + L^2 + 2\overline{\mathbf{R}_{n-1} \cdot \mathbf{L}}. \tag{12.124}$$

The last term is zero because there is no correlation between the direction of the nth step and the location reached after $n-1$ steps. Using rule (12.124) successively, we get

$$\begin{aligned}\overline{R_n^2} &= \overline{R_{n-1}^2} + L^2 = R_{n-2}^2 + 2L^2 \\ &= \overline{R_1^2} + (n-1)L^2 = nL^2.\end{aligned}$$

The *rms* distance traveled after n uncorrelated steps, each of length L, is therefore

$$(R_n)_{rms} = L\sqrt{n}, \tag{12.125}$$

which is called a *random walk*.

Behavior of a Smoke Plume in the Wind

Taylor's analysis can be easily adapted to account for the presence of a constant mean velocity. Consider the dispersion of smoke into a wind blowing in the x-direction (Figure 12.27). A photograph of the smoke plume, in which the film is exposed for a long time, would outline the average width Z_{rms}. As the x-direction in this problem is similar to time in Taylor's problem, the limiting behavior in (12.121) and (12.123) shows that the smoke plume is parabolic with a *pointed* vertex.

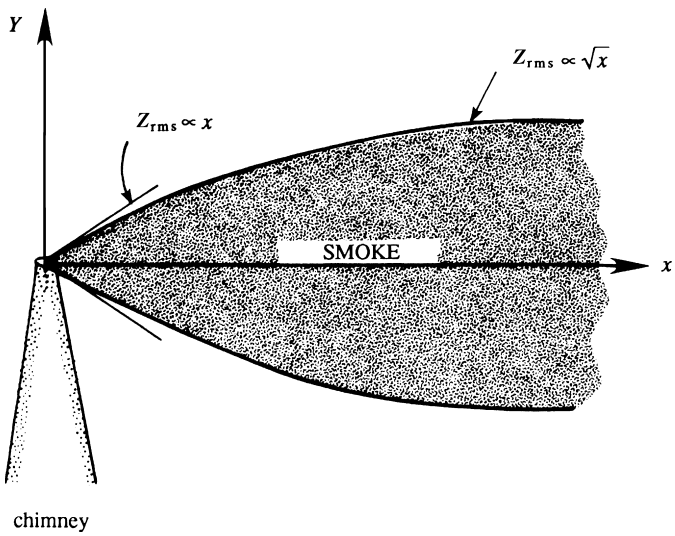

FIGURE 12.27 Average cross-sectional shape of a smoke plume in a turbulent wind blowing uniformly along the x-axis. Close to the chimney outlet, the *rms* width Z_{rms} of the smoke plume is proportional $x^{1/2}$. Far from the chimney, Z_{rms} is proportional to x. *G. I. Taylor,* Proc. London Mathematical Society, 20, *196–211, 1921.*

Turbulent Diffusivity

An equivalent eddy diffusivity can be estimated from Taylor's analysis. The equivalence is based on considering the spreading of a concentrated line source in a fluid of *constant* diffusivity. What should the diffusivity be in order that the spreading rate equals that predicted by (12.117)? The problem of the sudden introduction of a line vortex of strength Γ (Exercise 8.26) is such a problem of diffusion from a concentrated line source. The tangential velocity in this flow is given by

$$u_\theta = \big(\Gamma/2\pi r\big)\exp\big(-r^2/4\nu t\big).$$

The solution is therefore proportional to $\exp(-r^2/4\nu t)$, which has a Gaussian shape in the radial direction r, with a characteristic width of $\sigma = \sqrt{2\nu t}$. It follows that the momentum diffusivity ν in this problem is related to the variance σ^2 as

$$\nu = \frac{1}{2}\frac{d\sigma^2}{dt}, \tag{12.126}$$

which can be calculated if $\sigma^2(t)$ is known. Generalizing (12.126), we can say that the effective diffusivity D_T in a problem of turbulent dispersion of a patch of particles issuing from a point is given by

$$D_T \equiv \frac{1}{2}\frac{d}{dt}\big(\overline{X_\alpha^2}\big) = \overline{u_\alpha^2}\int_0^t r_\alpha(\tau)d\tau, \tag{12.127}$$

where we have used (12.117). From (12.120) and (12.122), the two limiting cases of (12.127) are

$$D_T \cong \overline{u_\alpha^2}\,t \quad \text{for } t \ll \Lambda_t, \quad \text{and} \quad D_T \cong \overline{u_\alpha^2}\,\Lambda_t \quad \text{for } t \ll \Lambda_t. \tag{12.128, 12.129}$$

Equation (12.128) shows the interesting fact that the eddy diffusivity initially increases with time, a behavior different from that in molecular diffusion with constant diffusivity. This can be understood as follows. The dispersion (or separation) of particles in a patch is caused by eddies with scales less than or equal to the scale of the patch, since the larger eddies simply advect the patch and do not cause any separation of the particles. As the patch size becomes larger, an *increasing* range of eddy sizes is able to cause dispersion, giving $D_T \propto t$. This behavior shows that *it is frequently impossible to represent turbulent diffusion by means of a large but constant eddy diffusivity.* Turbulent diffusion does not behave like molecular diffusion. For large times, on the other hand, the patch size becomes larger than the largest eddies present, in which case the diffusive behavior becomes similar to that of molecular diffusion with a constant diffusivity given by (12.129).

12.13. CONCLUDING REMARKS

Turbulence is an area of classical fluid mechanics that is the subject of continuing research. Frequent symposia are held to summarize and communicate new findings and promising approaches and a few are listed in the "Supplementary Reading" section at the end of this chapter.

EXERCISES

12.1. Determine general relationships for the second, third, and fourth central moments (variance $= \sigma^2$, skewness $= S$, and kurtosis $= K$) of the random variable u in terms of its first four ordinary moments: $\overline{u}$, $\overline{u^2}$, $\overline{u^3}$, and $\overline{u^4}$.

12.2. Calculate the mean, mean square, variance, and *rms* value of the periodic time series $u(t) = \overline{U} + U_0 \cos(\omega t)$, where $\overline{U}$, U_0, and ω are positive real constants.

12.3. Show that the autocorrelation function $\overline{u(t)u(t+\tau)}$ of a periodic series $u = U\cos(\omega t)$ is itself periodic.

12.4. Calculate the zero-lag cross-correlation $\overline{u(t)v(t)}$ between two periodic series $u(t) = \cos\ \omega t$ and $v(t) = \cos(\omega t + \phi)$ by performing at time average over one period $= 2\pi/\omega$. For values of $\phi = 0$, $\pi/4$, and $\pi/2$, plot the scatter diagrams of u vs. v at different times, as in Figure 12.8. Note that the plot is a straight line if $\phi = 0$, an ellipse if $\phi = \pi/4$, and a circle if $\phi = \pi/2$; the straight line, as well as the axes of the ellipse, are inclined at 45° to the uv-axes. Argue that the straight line signifies a perfect correlation, the ellipse a partial correlation, and the circle a zero correlation.

12.5. If $u(t)$ is a stationary random signal, show that $u(t)$ and $du(t)/dt$ are uncorrelated.

12.6. Let $R(\tau)$ and $S(\omega)$ be a Fourier transform pair. Show that $S(\omega)$ is real and symmetric if $R(\tau)$ is real and symmetric.

12.7. Compute the power spectrum, integral time scale, and Taylor time scale when $R_{11}(\tau) = \overline{u_1^2}\exp(-\alpha\tau^2)\cos(\omega_o\tau)$, assuming that α and ω_o are real positive constants.

12.8. There are two formulae for the energy spectrum $S_e(\omega)$ of the stationary zero-mean signal $u(t)$:

$$S_e(\omega) = \frac{1}{2\pi}\int_{-\infty}^{+\infty} R_{11}(\tau)\exp\{-i\omega\tau\}\,d\tau \text{ and}$$

$$S_e(\omega) = \lim_{T\to\infty}\frac{1}{2\pi T}\left|\int_{-T/2}^{+T/2} u(t)\exp\{-i\omega t\}dt\right|^2.$$

Prove that these two are identical *without* requiring the existence of the Fourier transformation of $u(t)$.

12.9. Derive the formula for the temporal Taylor microscale λ_t by expanding the definition of the temporal correlation function (12.17) into a two-term Taylor series and determining the time shift, $\tau = \lambda_t$, where this two-term expansion equals zero.

12.10. When x, r, and k_1 all lie in the stream-wise direction, the wave number spectrum $S_{11}(k_1)$ of the stream-wise velocity fluctuation $u_1(x)$ defined by (12.45) can be interpreted as a distribution function for energy across stream-wise wave number k_1.

Show that the energy-weighted mean-square value of the stream-wise wave number is:

$$\overline{k_1^2} \equiv \frac{1}{\overline{u^2}} \int_{-\infty}^{+\infty} k_1^2 S_{11}(k_1) dk_1 \;=\; -\frac{1}{\overline{u^2}} \left[\frac{d^2}{dr^2} R_{11}(r) \right]_{r=0}, \text{ and that } \lambda_f \;=\; \sqrt{2/\overline{k_1^2}}.$$

12.11. In many situations, measurements are only possible of one velocity component at one point in a turbulent flow, but consider a flow that has a nonzero mean velocity and moves past the measurement point. Thus, the experimenter obtains a time history of $u_1(t)$ at a fixed point. In order to estimate spatial velocity gradients, Taylor's frozen-turbulence hypothesis can be invoked to estimate a spatial gradient from a time derivative: $\dfrac{\partial u_1}{\partial x_1} \approx -\dfrac{1}{U_1} \dfrac{\partial u_1}{\partial t}$ where the "1"-axis must be aligned with the direction of the average flow, i.e., $U_i = (U_1, 0, 0)$. Show that this approximate relationship is true when $\sqrt{\overline{u_i u_i}}/U_1 \ll 1$, $p \sim \rho u_1^2$, and Re is high enough to neglect the influence of viscosity.

12.12. **a)** Starting from (12.33), derive (12.34) via an appropriate process of Reynolds decomposition and ensemble averaging.

b) Determine an equation for the scalar fluctuation energy $= \dfrac{1}{2}\overline{T'^2}$, one-half the scalar variance.

c) When the scalar variance goes to zero, the fluid is well mixed. Identify the term in the equation from part b) that dissipates scalar fluctuation energy.

12.13. Measurements in an atmosphere at 20°C show an *rms* vertical velocity of $w_{rms} = 1$ m/s and an *rms* temperature fluctuation of $T_{rms} = 0.1$°C. If the correlation coefficient is 0.5, calculate the heat flux $\rho C_p \overline{wT'}$.

12.14. **a)** Compute the divergence of the constant-density Navier-Stokes momentum equation $\dfrac{\partial u_i}{\partial t} + u_j \dfrac{\partial u_i}{\partial x_j} \;=\; -\dfrac{1}{\rho} \dfrac{\partial p}{\partial x_i} + \nu \dfrac{\partial^2 u_i}{\partial x_j \partial x_j}$ to determine a Poisson equation for the pressure.

b) If the equation $\dfrac{\partial^2 G}{\partial x_j \partial x_j} = \delta(x_j - \tilde{x}_j)$ has solution: $G(x_j, \tilde{x}_j) = \dfrac{-1}{4\pi\sqrt{(x_j - \tilde{x}_j)^2}}$, then use the result from part a) to show that:

$P(x_j) = \dfrac{\rho}{4\pi} \displaystyle\int_{all\ \tilde{x}} \dfrac{1}{\sqrt{(x_j - \tilde{x}_j)^2}} \dfrac{\partial^2}{\partial \tilde{x}_j \partial \tilde{x}_i} \left(U_i U_j + \overline{u_i u_j} \right) d^3\tilde{x}$ in a turbulent flow.

12.15. Starting with the RANS momentum equation (12.30), derive the equation for the kinetic energy of the average flow field (12.46).

12.16. Derive the RANS transport equation for the Reynolds stress correlation (12.35) via the following steps.

a) By subtracting (12.30) from (4.86), show that the instantaneous momentum equation for the fluctuating turbulent velocity u_i is:

$$\frac{\partial u_i}{\partial t} + u_k \frac{\partial U_i}{\partial x_k} + U_k \frac{\partial u_i}{\partial x_k} + u_k \frac{\partial u_i}{\partial x_k} \;=\; -\frac{1}{\rho_0} \frac{\partial p}{\partial x_i} + \nu \frac{\partial^2 u_i}{\partial x_k^2} + g\alpha T' \delta_{i3} + \frac{\partial}{\partial x_k} \overline{u_i u_k}.$$

b) Show that: $\overline{u_i \dfrac{Du_j}{Dt} + u_j \dfrac{Du_i}{Dt}} = \dfrac{\partial}{\partial t}(\overline{u_i u_j}) + U_k \dfrac{\partial}{\partial x_k}(\overline{u_i u_j}) + \dfrac{\partial}{\partial x_k}(\overline{u_i u_j u_k})$

c) Combine and simplify the results of parts a) and b) to reach (12.35).

12.17. Starting from (12.38) and (12.40), set $\mathbf{r} = r\mathbf{e}_1$ and use $R_{11} = \overline{u^2} f(r)$, and $R_{22} = \overline{u^2} g(r)$, to show that $F(r) = \overline{u^2}(f(r) - g(r))r^{-2}$ and $G(r) = \overline{u^2} g(r)$.

12.18. **a)** Starting from R_{ij} from (12.39), compute $\partial R_{ij}/\partial r_j$ for incompressible flow.

b) For homogeneous-isotropic turbulence use the result of part a) to show that the longitudinal, $f(r)$, and transverse, $g(r)$, correlation functions are related by $g(r) = f(r) + (r/2)(df(r)/dr)$.

c) Use part b) and the integral length scale and Taylor microscale definitions to find $2\Lambda_g = \Lambda_f$ and $\sqrt{2}\lambda_g = \lambda_f$.

12.19. In homogeneous turbulence: $R_{ij}(\mathbf{r}_b - \mathbf{r}_a) = \overline{u_i(\mathbf{x} + \mathbf{r}_a) u_j(\mathbf{x} + \mathbf{r}_b)} = R_{ij}(\mathbf{r})$, where $\mathbf{r} = \mathbf{r}_b - \mathbf{r}_a$.

a) Show that $\overline{(\partial u_i(\mathbf{x})/\partial x_k)(\partial u_j(\mathbf{x})/\partial x_l)} = -(\partial^2 R_{ij}/\partial r_k \partial r_l)_{r=0}$.

b) If the flow is incompressible and isotropic, show that

$$-\overline{(\partial u_1(\mathbf{x})/\partial x_1)^2} = -\frac{1}{2}\overline{(\partial u_1(\mathbf{x})/\partial x_2)^2} = +2\overline{(\partial u_1(\mathbf{x})/\partial x_2)(\partial u_2(\mathbf{x})/\partial x_1)}$$
$$= \overline{u^2}\left(d^2 f/dr^2\right)_{r=0}.$$

[*Hint*: Expand $f(r)$ about $r = 0$ *before* taking any derivatives.]

12.20. The turbulent kinetic energy equation contains a pressure-velocity correlation, $K_j = \overline{p(\mathbf{x}) u_j(\mathbf{x} + \mathbf{r})}$. In homogeneous isotropic turbulent flow, the most general form of this correlation is: $K_j = K(r) r_j$. If the flow is also incompressible, show that $K(r)$ must be zero.

12.21. The velocity potential for two-dimensional water waves of small amplitude ξ_o on a deep pool can be written:

$$\phi(x_1, x_2, t) = \frac{\omega \xi_o}{k} e^{+kx_2} \cos(\omega t - k x_1),$$

where x_1 and x_2 are the horizontal and vertical coordinates with $x_2 = 0$ defining the average free surface. Here, ω is the temporal radian frequency of the waves and k is the wave number.

a) Compute the two-dimensional velocity field: $\mathbf{u} = (u_1, u_2) = (\partial\phi/\partial x_1, \partial\phi/\partial x_2)$.

b) Show that this velocity field is a solution of the two-dimensional continuity and Navier-Stokes equations for incompressible fluid flow.

c) Compute the strain-rate tensor $S_{ij} = 1/2(\partial u_i/\partial x_j + \partial u_j/\partial x_i)$.

d) Although this flow is not turbulent, it must still satisfy the turbulent kinetic energy equation that contains an energy dissipation term. Denote the kinematic viscosity by ν, and compute the kinetic energy dissipation rate in this flow: $\varepsilon = 2\nu\overline{S_{ij} S_{ij}}$, where the over bar implies a time average over one wave period is $2\pi/\omega$.

Only time averages of even powers of the trig-functions are nonzero, for example: $\overline{\cos^2(\omega t - kx)} = \overline{\sin^2(\omega t - kx)} = 1/2$ while $\overline{\cos(\omega t - kx)} = \overline{\sin(\omega t - kx)} = 0$.

e) The original potential represents a lossless flow and does not include any viscous effects. Explain how this situation can occur when the kinetic-energy dissipation rate is not zero.

12.22. A mass of 10 kg of water is stirred by a mixer. After one hour of stirring, the temperature of the water rises by 1.0°C. What is the power output of the mixer in watts? What is the size η of the dissipating eddies?

12.23. In locally isotropic turbulence, Kolmogorov determined that the wave number spectrum can be represented by $S_{11}(k)/(\nu^5\overline{\varepsilon})^{1/4} = \Phi(k\nu^{3/4}/\overline{\varepsilon}^{1/4})$ in the inertial subrange and dissipation range of turbulent scales, where Φ is an undetermined function.

a) Determine the equivalent form for the temporal spectrum $S_e(\omega)$ in terms of the average kinetic energy dissipation rate $\overline{\varepsilon}$, the fluid's kinematic viscosity ν, and the temporal frequency ω.

b) Simplify the results of part a) for the inertial range of scales where ν is dropped from the dimensional analysis.

c) To obtain the results for parts a) and b), an implicit assumption has been made that leads to the neglect of an important parameter. Add the missing parameter and redo the dimensional analysis of part a).

d) Use the missing parameter and ω to develop an equivalent wave number. Insist that your result for S_e only depend on this equivalent wave number and $\overline{\varepsilon}$ to recover the minus-five-thirds law.

12.24.[1] Estimates for the importance of anisotropy in a turbulent flow can be developed by assuming that fluid velocities and spatial derivatives of the average-flow (or RANS) equation are scaled by the average velocity difference ΔU that drives the largest eddies in the flow having a size L, and that the fluctuating velocities and spatial derivatives in the turbulent kinetic energy (TKE) equation are scaled by the kinematic viscosity ν and the Kolmogorov scales η and u_K (see (12.50)). Thus, the scaling for a mean velocity gradient is: $\partial U_i/\partial x_j \sim \Delta U/L$, while the mean-square turbulent velocity gradient scales as: $\overline{(\partial u_i/\partial x_j)^2} \sim (u_K/\eta)^2 = \nu^2/\eta^4$, where the "~" sign means "scales as." Use these scaling ideas in parts a) and d):

a) The total energy dissipation rate in a turbulent flow is $2\nu\overline{S}_{ij}\overline{S}_{ij} + 2\nu\overline{S'_{ij}S'_{ij}}$, where $\overline{S}_{ij} = \dfrac{1}{2}\left(\dfrac{\partial U_i}{\partial x_j} + \dfrac{\partial U_j}{\partial x_i}\right)$ and $S'_{ij} = \dfrac{1}{2}\left(\dfrac{\partial u_i}{\partial x_j} + \dfrac{\partial u_j}{\partial x_i}\right)$. Determine how the ratio $\dfrac{\overline{S'_{ij}S'_{ij}}}{\overline{S}_{ij}\overline{S}_{ij}}$ depends on the outer-scale Reynolds number: $Re_L = \Delta U \cdot L/\nu$.

b) Is average-flow or fluctuating-flow energy dissipation more important?

[1]Obtained from Prof. Werner Dahm.

c) Show that the turbulent kinetic energy dissipation rate, $\overline{\varepsilon} = 2\nu\overline{S'_{ij}S'_{ij}}$ can be written:

$$\overline{\varepsilon} = \nu\left[\overline{\frac{\partial u_i}{\partial x_j}\frac{\partial u_i}{\partial x_j}} + \frac{\partial^2}{\partial x_i \partial x_j}\overline{u_i u_j}\right].$$

d) For homogeneous isotropic turbulence, the second term in the result of part c) is zero but it is nonzero in a turbulent shear flow. Therefore, estimate how $\dfrac{\partial^2}{\partial x_i \partial x_j}\overline{u_i u_j} \Big/ \overline{\dfrac{\partial u_i}{\partial x_j}\dfrac{\partial u_i}{\partial x_j}}$ depends on Re_L in turbulent shear flow as means of assessing how much impact anisotropy has on the turbulent kinetic energy dissipation rate.

e) Is an isotropic model for the turbulent dissipation appropriate at high Re_L in a turbulent shear flow?

12.25. Determine the self-preserving form of the average stream-wise velocity $U_x(x,r)$ of a round turbulent jet using cylindrical coordinates where x increases along the jet axis and r is the radial coordinate. Ignore gravity in your work. Denote the density of the nominally quiescent reservoir fluid by ρ.

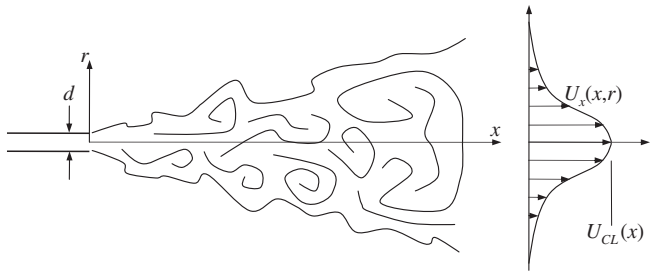

a) Place a stationary cylindrical control volume around the jet's cone of turbulence so that circular control surfaces slice all the way through the jet flow at its origin and at a distance x downstream where the fluid density is ρ. Assuming that the fluid outside the jet is nearly stationary so that pressure does not vary in the axial direction and that the fluid entrained into the volume has negligible x-direction momentum, show

$$J_0 \equiv \int_0^{d/2} \rho_0 U_0^2 2\pi r dr = \int_0^{D/2} \rho U_x^2(x,r) 2\pi r dr,$$

where J_0 is the jet's momentum flux, ρ_0 is the density of the jet fluid, and U_0 is the jet exit velocity.

b) Simplify the exact mean-flow equations

$$\frac{\partial U_x}{\partial x} + \frac{1}{r}\frac{\partial}{\partial r}(rU_r) = 0, \text{ and}$$

$$U_x\frac{\partial U_x}{\partial x} + U_r\frac{\partial U_x}{\partial r} = -\frac{1}{\rho}\frac{\partial P}{\partial x} + \frac{\nu}{r}\frac{\partial}{\partial r}\left(r\frac{\partial U_x}{\partial r}\right) - \frac{1}{r}\frac{\partial}{\partial r}(r\overline{u_x u_r}) - \frac{\partial}{\partial x}(r\overline{u_x^2}),$$

when $\partial P/\partial x \approx 0$, the jet is slender enough for the boundary-layer approximation $\partial/\partial r \gg \partial/\partial x$ to be valid, and the flow is at high Reynolds number so that the viscous terms are negligible.

c) Eliminate the average radial velocity from the simplified equations to find:

$$U_x\frac{\partial U_x}{\partial x} - \left\{\frac{1}{r}\int_0^r \mathscr{r}\frac{\partial U_x}{\partial x}d\mathscr{r}\right\}\frac{\partial U_x}{\partial r} = -\frac{1}{r}\frac{\partial}{\partial r}\left(r\overline{u_x u_r}\right),$$

where $\mathscr{r}$ is just an integration variable.

d) Assume a similarity form: $U_x(x,r) = U_{CL}(x)f(\xi)$, $-\overline{u_x u_r} = \Psi(x)g(\xi)$, where $\xi = r/\delta(x)$ and f and g are undetermined functions, use the results of parts a) and c), and choose constant values appropriately to find $U_x(x,r) = const.(J_0/\rho)^{1/2}x^{-1}F(r/x)$.

e) Determine a formula for the volume flux in the jet. Will the jet fluid be diluted with increasing x?

12.26. Consider the turbulent wake far from a two-dimensional body placed perpendicular to the direction of a uniform flow.

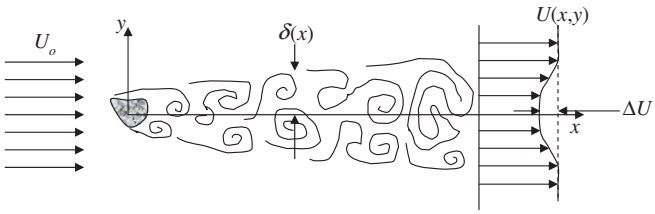

a) Use a large rectangular control volume that encloses the body but only intersects the wake vertically at x somewhere downstream of the body to show that the average fluid-dynamic drag force per unit span, $\overline{F}_D/b$, acting on the body is given by:

$$\frac{\overline{F}_D/b}{\rho U_o^2} = \theta = \int_{-\infty}^{+\infty}\left[\frac{U(x,y)}{U_o}\left(1-\frac{U(x,y)}{U_o}\right) - \frac{\overline{u^2}}{U_o^2}\right]dy,$$

where θ is the momentum thickness of the wake flow (a constant), and $U(x,y)$ is the average horizontal velocity profile a distance x downstream of the body.

b) When $\Delta U \ll U_o$, find the conditions necessary for a self-similar form for the wake's velocity deficit, $U(x,y) = U_o - \Delta U(x)f(\xi)$, to be valid based on the result of part a) and the steady two-dimensional continuity and boundary-layer RANS equations. Here, $\xi = y/\delta(x)$ and δ is the transverse length scale of the wake.

c) Determine how ΔU and δ must depend on x in the self-similar region. State your results in appropriate dimensionless form using θ and U_o as appropriate.

12.27. Consider the two-dimensional shear layer that forms between two steady streams with flow speed U_2 above and U_1 below $y = 0$, that meet at $x = 0$, as shown. Assume a self-similar form for the average horizontal velocity:

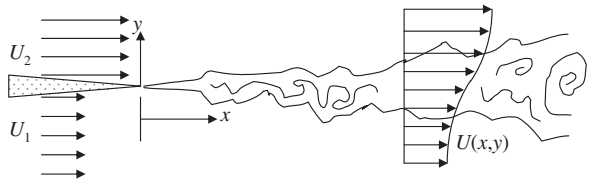

$$U(x,y) = U_1 + (U_2 - U_1)f(\xi) \text{ with } \xi = y/\delta(x).$$

a) What are the boundary conditions on $f(\xi)$ as $y \to \pm\infty$?

b) If the flow is laminar, use $\frac{\partial U}{\partial x} + \frac{\partial V}{\partial y} = 0$ and $U\frac{\partial U}{\partial x} + V\frac{\partial U}{\partial y} = \nu\frac{\partial^2 U}{\partial y^2}$ with $\delta(x) = \sqrt{\nu x/U_1}$ to obtain a single equation for $f(\xi)$. There is no need to solve this equation.

c) If the flow is turbulent, use: $\frac{\partial U}{\partial x} + \frac{\partial V}{\partial y} = 0$ and $U\frac{\partial U}{\partial x} + V\frac{\partial U}{\partial y} = -\frac{\partial}{\partial y}(\overline{uv})$ with $-\overline{uv} = (U_2 - U_1)^2 g(\xi)$ to obtain a single equation involving f and g. Determine how δ must depend on x for the flow to be self-similar.

d) Does the laminar or the turbulent mixing layer grow more quickly as x increases?

12.28. Consider an orifice of diameter d that emits an incompressible fluid of density ρ_o at speed U_o into an infinite half space of fluid with density ρ_∞. With gravity acting and $\rho_\infty > \rho_o$, the orifice fluid rises, mixes with the ambient fluid, and forms a buoyant plume with a diameter $D(z)$ that grows with increasing height above the orifice. Assuming that the plume is turbulent and self-similar in the far-field ($z \gg d$), determine how the plume diameter D, the mean centerline velocity U_{cl}, and the mean centerline mass fraction of orifice fluid Y_{cl} depend on the vertical coordinate z via the steps suggested below. Ignore the initial momentum of the orifice fluid. Use both dimensional and control-volume analysis as necessary. Ignore stream-wise turbulent fluxes to simplify your work. Assume uniform flow from the orifice.

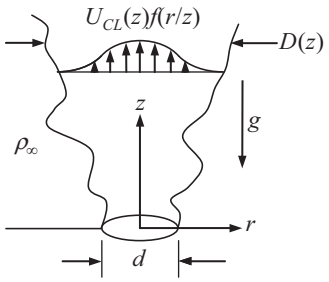

a) Place a stationary cylindrical control volume around the plume with circular control surfaces that slice through the plume at its origin and at height z. Use similarity forms for the average vertical velocity $U_z(z,r) = U_{cl}(z)f(r/z)$ and nozzle fluid mass fraction $\overline{Y}(z,r) = (\rho_\infty - \overline{\rho})/(\rho_\infty - \rho_o) = Y_{cl}(z)h(r/z)$ to conserve the flux of nozzle fluid in the plume, and find: $\dot{m}_o = \int_{source} \rho_o U_o dA = \int_0^{D/2} \rho_o \overline{Y}(z,r) U_z(z,r) 2\pi r dr$.

b) Conserve vertical momentum using the same control volume assuming that all entrained fluid enters with negligible vertical momentum, to determine:

$$-\int_{source} \rho_o U_o^2 dA + \int_0^{D/2} \overline{\rho}(z,r) U_z^2(z,r) 2\pi r dr = \int_{volume} g[\rho_\infty - \overline{\rho}(z,r)] dV,$$

where $\overline{\rho} = \overline{Y}\rho_o + (1-\overline{Y})\rho_\infty$.

c) Ignore the source momentum flux, assume z is large enough so that $Y_{CL} \ll 1$, and use the results of parts a) and b) to find: $U_{cl}(z) = C_1 \cdot \sqrt[3]{B/\rho_\infty z}$ and $\dfrac{\rho_\infty - \rho_o}{\rho_\infty} Y_{cl}(z) = C_2 \sqrt[3]{B^2/g^3\rho_\infty^2 z^5}$ where C_1 and C_2 are dimensionless constants, and $B = \int_{source} (\rho_\infty - \rho_o) g U_o dA$.

12.29. Laminar and turbulent boundary-layer skin friction are very different. Consider skin-friction correlations from zero-pressure-gradient (ZPG) boundary-layer flow over a flat plate placed parallel to the flow.

$$\text{Laminar boundary layer: } C_f = \frac{\tau_0}{(1/2)\rho U^2} = \frac{0.664}{\sqrt{Re_x}} \text{ (Blasius boundary layer).}$$

Turbulent boundary layer: see correlations in Section 12.9.

Create a table of computed results at $Re_x = Ux/\nu = 10^4$, 10^5, 10^6, 10^7, 10^8, and 10^9 for the laminar and turbulent skin-friction coefficients, and the friction force acting on 1.0 m^2 plate surface in sea-level air at 100 m/s and in water at 20 m/s assuming laminar and turbulent flow.

12.30. Derive the following logarithmic velocity profile for a smooth wall: $U^+ = (1/\kappa) \ln y^+ + 5.0$ by starting from $U = (u_*/\kappa)\ln y^+ + const.$ and matching the profile to the edge of the viscous sublayer assuming the viscous sublayer ends at $y = 10.7\, \nu/u_*$.

12.31.[2] Derive the log-law for the mean flow profile in a zero-pressure gradient (ZPG) flat-plate turbulent boundary layer (TBL) through the following mathematical and dimensional arguments.

a) Start with the law of the wall, $U/u^* = f(yu_*/\nu)$ or $U^+ = f(y^+)$, for the near-wall region of the boundary layer, and the defect law for the outer region, $\dfrac{U_e - U}{u_*} = F\left(\dfrac{y}{\delta}\right)$. These formulae must overlap when $y^+ \to +\infty$ and $y/\delta \to 0$. In this matching or overlap region, set U and $\partial U/\partial y$ from both formulas equal to get two equations involving f and F.

b) In the limit as $y^+ \to +\infty$, the kinematic viscosity must drop out of the equation that includes df/dy^+. Use this fact, to show that $U/u_* = A_I \ln(yu_*/\nu) + B_I$ as

[2]Inspired by exercise 7.20 in Pope (2000), p. 311.

$y^+ \to +\infty$ where A_I and B_I are constants for the near-wall or *inner* boundary layer scaling.

c) Use the result of part b) to determine $F(\xi) = -A_I \ln(\xi) - B_O$ where $\xi = y/\delta$, and A_I and B_O are constants for the wake flow or *outer* boundary layer scaling.

d) It is traditional to set $A_I = 1/\kappa$, and to keep B_I but to drop its subscript. Using these new requirements determine the two functions, f_I and F_O, in the matching region. Which function explicitly depends on the Reynolds number of the flow?

12.32. Prove (12.90) and (12.91) by considering a stationary control volume that resides inside the channel or pipe and has stream-normal control surfaces separated by a distance dx and stream-parallel surfaces that coincide with the wall or walls that confine the flow.

12.33. A horizontal smooth pipe 20 cm in diameter carries water at a temperature of 20°C. The drop of pressure is $dp/dx = -8$ N/m^2 per meter. Assuming turbulent flow, verify that the thickness of the viscous sublayer is ≈ 0.25 mm. [*Hint*: Use dp/dx as given by (12.91) to find $\tau_0 = 0.4$ N/m^2, and therefore $u_* = 0.02$ m/s.]

12.34. The cross-section averaged flow speed U_{av} in a round pipe of radius a may be written:

$$U_{av} \equiv \frac{\textit{volume flux}}{\textit{area}} = \frac{1}{\pi a^2}\int_0^a U(y) 2\pi r dr \;\; = \frac{2}{a^2}\int_0^a U(y)(a-y)dy,$$

where r is the radial distance from the pipe's centerline, and $y = a - r$ is the distance inward from the pipe's wall. Turbulent pipe flow has very little wake, and the viscous sublayer is very thin at high Reynolds number; therefore assume the log-law profile, $U(y) = (u_*/\kappa)\ln(yu_*/\nu) + u_* B$, holds throughout the pipe to find

$$U_{av} \cong u_*[(1/\kappa)\ln(au_*/\nu) + B - 3/2\kappa].$$

Now use the definitions $C_f = \tau_0/(1/2)\rho U_{av}^2$, $\mathrm{Re}_d = 2U_{av}a/\nu$, $\overline{f} = 4C_f =$ Darcy friction factor, $\kappa = 0.41$, and $B = 5.0$, and switch to base-10 logarithms to reach Prandtl's 1935 correlation for turbulent pipe flow friction: $\overline{f}^{-1/2} = 2.0\log_{10}(\mathrm{Re}_d \overline{f}^{1/2}) - 1.0$. When the second constant is adjusted from -1.0 to -0.8, this correlation is valid for $\mathrm{Re}_d \geq 4000$ (White, 2006) and yields $\overline{f}$-values substantially larger than the laminar pipe flow result $\overline{f} = 64/\mathrm{Re}_d$.

12.35. Perhaps the simplest way to model turbulent flow is to develop an eddy viscosity from dimensional analysis and physical reasoning. Consider turbulent Couette flow with wall spacing h. Assume that eddies of size l produce velocity fluctuations of size $l(\partial U/\partial y)$ so that the turbulent shear stress correlation can be modeled as: $-\overline{uv} \propto l^2(\partial U/\partial y)^2$. Unfortunately, l cannot be a constant because it must disappear near the walls. Thus, more educated guessing is needed, so for this problem assume $\partial U/\partial y$ will have some symmetry about the channel centerline (as shown) and

try: $l = Cy$ for $0 \le y \le h/2$ where C is a positive dimensionless constant and y is the vertical distance measured from the lower wall. With this turbulence model, the RANS equation for $0 \le y \le h/2$ becomes:

$$U\frac{\partial U}{\partial x} + V\frac{\partial U}{\partial y} = -\frac{1}{\rho}\frac{d\overline{p}}{dx} + \frac{1}{\rho}\frac{\partial \tau_{xy}}{\partial y} \quad \text{where } \tau_{xy} = \mu\frac{\partial U}{\partial y} + \rho C^2 y^2 \left(\frac{\partial U}{\partial y}\right)^2.$$

Determine an analytic form for $U(y)$ after making appropriate simplifications of the RANS equation for fully developed flow assuming the pressure gradient is zero. Check to see that your final answer recovers the appropriate forms as $y \to 0$ and $C \to 0$. Use the fact that $U(y = h/2) = U_o/2$ in your work if necessary.

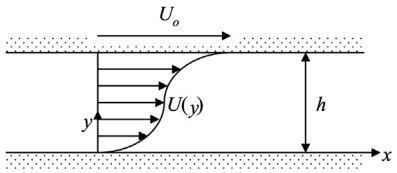

12.36. Turbulence largely governs the mixing and transport of water vapor (and other gases) in the atmosphere. Such processes can sometimes be assessed by considering the conservation law (12.34) for a passive scalar.

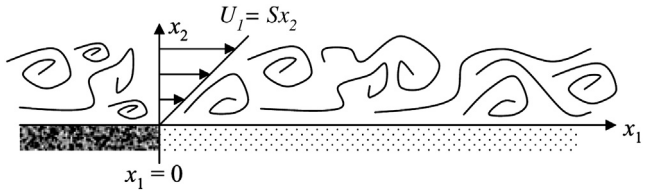

a) Appropriately simplify (12.34) for turbulence at high Reynolds number that is characterized by: an outer length scale of L, a large-eddy turnover time of T, and a mass-fraction magnitude of Y_o. In addition, assume that the molecular diffusivity κ_m is at most as large as $\nu = \mu/\rho =$ the fluid's kinematic viscosity.

b) Now consider a simple model of how a dry turbulent wind collects moisture as it blows over a nominally flat water surface ($x_1 > 0$) from a dry surface ($x_1 < 0$). Assume the mean velocity is steady and has a single component with a linear gradient, $U_j = (Sx_2, 0, 0)$, and use a simple gradient diffusion model: $-\overline{u_j Y'} = \Delta U L(0, \partial\overline{Y}/\partial x_2, 0)$, where ΔU and L are (constant) velocity and length scales that characterize the turbulent diffusion in this case. This turbulence model allows the turbulent mean flow to be treated like a laminar flow with a large diffusivity $= \Delta UL$ (a turbulent diffusivity). For the simple boundary conditions: $\overline{Y}(x_j) = 0$ for $x_1 < 0$, $\overline{Y}(x_j) = 1$ at $x_2 = 0$ for $x_1 > 0$, and $\overline{Y}(x_j) \to 0$ as $x_2 \to \infty$, show that

$$\overline{Y}(x_1, x_2, x_3) = \int_{\xi}^{\infty} \exp\left(-\frac{1}{9}\zeta^3\right) d\zeta \Bigg/ \int_{0}^{\infty} \exp\left(-\frac{1}{9}\zeta^3\right) d\zeta$$

$$\text{where } \xi = x_2 \left(\frac{S}{\Delta U L x_1}\right)^{1/3} \quad \text{for } x_1, x_2 > 0.$$

12.37. Estimate the Monin-Obukhov length in the atmospheric boundary layer if the surface stress is 0.1 N/m^2 and the upward heat flux is 200 W/m^2.

12.38. Consider one-dimensional turbulent diffusion of particles issuing from a point source. Assume a Gaussian-Lagrangian correlation function of particle velocity:

$$r(\tau) = e^{-\tau^2/t_c^2},$$

where t_c is a constant. By integrating the correlation function from $\tau = 0$ to ∞, find the integral time scale Λ_t in terms of t_c. Using the Taylor theory, estimate the eddy diffusivity at large times $t/\Lambda_t \gg 1$, given that the *rms* fluctuating velocity is 1 m/s and $t_c = 1$ s.

Literature Cited

Adrian, R. J. (2007). Hairpin vortex organization in wall turbulence. *Physics of Fluids, 19*, 041301.

Barenblatt, G. I. (1993). Scaling laws for fully developed shear flows. Part I. Basic hypotheses and analysis. *Journal of Fluid Mechanics, 248*, 513–520.

Batchelor, G. K. (1953). *The Theory of Homogeneous Turbulence*. New York: Cambridge University Press.

Batchelor, G. K. (1959). Small scale variation of convected quantities like temperature in turbulent fluid. Part I: General discussion and the case of small conductivity. *Journal of Fluid Mechanics, 5*, 113–133.

Bird, R. B., Stewart, W. E., & Lightfoot, E. N. (1960). *Transport Phenomena*. New York: John Wiley and Sons.

Bradshaw, P., & Woods, J. D. (1978). Geophysical turbulence and buoyant flows. In P. Bradshaw (Ed.), *Turbulence*. New York: Springer-Verlag.

Cantwell, B. J. (1981). Organized motion in turbulent flow. *Annual Review of Fluid Mechanics, 13*, 457–515.

Chapman, D. R. (1979). Computational aerodynamics development and outlook. *AIAA Journal, 17*, 1293–1313.

Chauhan, K. A., Monkewitz, P. A., & Nagib, H. M. (2009). Criteria for assessing experiments in zero pressure gradient boundary layers. *Fluid Dynamics Research, 41*, 021404.

Chen, C. J., & Rodi, W. (1980). *Vertical Turbulent Buoyant Jets—A Review of Experimental Data*. Oxford: Pergamon Press.

Coles, D. E. (1956). The law of the wake in the turbulent boundary layer. *Journal of Fluid Mechanics, 1*, 191–226.

Dimotakis, P. E. (2000). The mixing transition in turbulent flows. *Journal of Fluid Mechanics, 409*, 69–98.

Feynman, R. P., Leighton, R. B., & Sands, M. (1963). *The Feynman Lectures on Physics*. New York: Addison-Wesley.

Fife, P., Wei, T., Klewicki, J., & McMurtry, P. (2005). Stress gradient balance layers and scale hierarchies in wall-bounded turbulent flows. *Journal of Fluid Mechanics, 532*, 165–189.

George, W. K. (1989). The self-preservation of turbulent flows and its relation to initial conditions and coherent structures. In W. K. George, & R. Arndt (Eds.), *Advances in Turbulence* (pp. 39–73). New York: Hemisphere Publishing Corp.

George, W. K. (2006). Recent advancements toward the understanding of turbulent boundary layers. *AIAA Journal, 44*, 2435–2449.

George, W. K., & Castillo, L. (1997). Zero-pressure-gradient turbulent boundary layer. *Applied Mechanics Reviews, 50*, 689–729.

Grant, H. L., Hughes, B. A., Vogel, W. M., & Moilliet, A. (1968). The spectrum of temperature fluctuation in turbulent flow. *Journal of Fluid Mechanics, 34*, 423–442.

Grant, H. L., Stewart, R. W., & Moilliet, A. (1962). The spectrum of a cross-stream component of turbulence in a tidal stream. *Journal of Fluid Mechanics, 13*, 237–240.

Hinze, J. O. (1975). *Turbulence* (2nd ed.). New York: McGraw-Hill.

Jones, W. P., & Launder, B. E. (1972). The prediction of laminarization with a two-equation model of turbulence. *International Journal of Heat and Mass Transfer, 15*, 301–314.

Kline, S. J., Reynolds, W. C., Schraub, F. A., & Runstadler, P. W. (1967). The structure of turbulent boundary layers. *Journal of Fluid Mechanics, 30*, 741–773.

Kolmogorov, A. N. (1941a). Dissipation of energy in locally isotropic turbulence. *Doklady Akademii Nauk SSSR, 32*, 19–21.

Kolmogorov, A. N. (1941b). The local structure of turbulence in incompressible viscous fluid for very large Reynolds numbers. *Doklady Akademii Nauk SSSR, 30*, 299–303.

Kuo, K. K. (1986). *Principles of Combustion*. New York: John Wiley and Sons.

Lam, S. H. (1992). On the RNG theory of turbulence. *The Physics of Fluids A, 4*, 1007–1017.

Landahl, M. T., & Mollo-Christensen, E. (1986). *Turbulence and Random Processes in Fluid Mechanics*. London: Cambridge University Press.

Launder, B. E., & Sharma, B. I. (1974). Application of the energy dissipation model of turbulence to the calculation of flow near a spinning disk. *Letters in Heat and Mass Transfer, 1*, 131–137.

Lesieur, M. (1987). *Turbulence in Fluids*. Dordrecht, Netherlands: Martinus Nijhoff Publishers.

Marusic, I., Mckeon, B. J., Monkewitz, P. A., Nagib, H. M., Smits, A. J., & Sreenivasan, K. R. (2010). Wall bounded turbulent flows at high Reynolds numbers: Recent advances and key issues. *Physics of Fluids, 22*, 065103.

Monin, A. S., & Yaglom, A. M. (1971, 1975). In J. L. Lumley (Ed.), *Statistical Fluid Mechanics, Vol. I and II*. Cambridge, MA: MIT Press.

Monkewitz, P. A., Chauhan, K. A., & Nagib, H. M. (2007). Self-consistent high-Reynolds-number asymptotics for zero-pressure-gradient turbulent boundary layers. *Physics of Fluids, 19*, 115101.

Monkewitz, P. A., Chauhan, K. A., & Nagib, H. M. (2008). Comparison of mean flow similarity laws in zero pressure gradient turbulent boundary layers. *Physics of Fluids, 20*, 105102.

Nagib, H. M., & Chauhan, K. A. (2008). Variations of von Kármán coefficient in canonical flows. *Physics of Fluids, 20*, 101518.

Obukhov, A. M. (1949). Structure of the temperature field in turbulent flow. *Izvestiya Akademii Nauk SSSR, Georgr. and Geophys. Ser., 13*(1), 58–69.

Oweis, G. F., Winkel, E. S., Cutbirth, J. M., Ceccio, S. L., Perlin, M., & Dowling, D. R. (2010). The mean velocity profile of a smooth-flat-plate turbulent boundary layer at high Reynolds number. *Journal of Fluid Mechanics, 665*, 357–381.

Panofsky, H. A., & Dutton, J. A. (1984). *Atmospheric Turbulence*. New York: Wiley.

Pao, Y. H. (1965). Structure of turbulent velocity and scalar fields at large wave numbers. *The Physics of Fluids, 8*, 1063–1075.

Phillips, O. M. (1977). *The Dynamics of the Upper Ocean*. London: Cambridge University Press.

Pope, S. B. (2000). *Turbulent Flows*. London: Cambridge University Press.

Richardson, L. F. (1922). *Weather Prediction by Numerical Process*. Cambridge: Cambridge University Press.

Schultz-Grunow, F. (1941). New frictional resistance law for smooth plates. *NACA Technical Memorandum, 17*(8), 1–24.

Smith, L. M., & Reynolds, W. C. (1992). On the Yakhot-Orszag renormalization group method for deriving turbulence statistics and models. *The Physics of Fluids A, 4*, 364–390.

Spalding, D. B. (1961). A single formula for the law of the wall. *Journal of Applied Mechanics, 28*, 455–457.

Speziale, C. G. (1991). Analytical methods for the development of Reynolds-stress closures in turbulence. *Annual Review of Fluid Mechanics, 23*, 107–157.

Taylor, G. I. (1915). Eddy motion in the atmosphere. *Philosophical Transactions of the Royal Society of London, A215*, 1–26.

Taylor, G. I. (1921). Diffusion by continuous movements. *Proceedings of the London Mathematical Society, 20*, 196–211.

Tennekes, H., & Lumley, J. L. (1972). *A First Course in Turbulence*. Cambridge, MA: MIT Press.

Townsend, A. A. (1976). *The Structure of Turbulent Shear Flow*. London: Cambridge University Press.

Turner, J. S. (1973). *Buoyancy Effects in Fluids*. London: Cambridge University Press.

Turner, J. S. (1981). Small-scale mixing processes. In B. A. Warren, & C. Wunch (Eds.), *Evolution of Physical Oceanography*. Cambridge, MA: MIT Press.

Wei, T., Fife, P., Klewicki, J., & McMurtry, P. (2005). Properties of the mean momentum balance in turbulent boundary layer, pipe and channel flows. *Journal of Fluid Mechanics, 522*, 303–327.

White, F. M. (2006). *Viscous Fluid Flow.* Boston: McGraw-Hill.

Yakhot, V., & Orszag, S. A. (1986). Renormalization group analysis of turbulence. I. Basic theory. *Journal of Scientific Computing, 1*, 3–51.

Supplemental Reading

George, W. K., & Arndt, R. (Eds.). (1989). *Advances in Turbulence*. New York: Hemisphere Publishing Corp.

Hunt, J. C. R., Sandham, N. D., Vassilicos, J. C., Launder, B. E., Monkewitz, P. A., & Hewitt, G. F. (2001). Developments in turbulence research: are view based on the 1999 Programme of the Isaac Newton Institute, Cambridge. Published in *Journal of Fluid Mechanics, 436*, 353–391.

Proceedings of the Boeing Symposium on Turbulence. (1970). Published in *Journal of Fluid Mechanics, 41*, Parts 1 (March) and 2 (April).

Symposium on Fluid Mechanics of Stirring and Mixing, IUTAM. (1991). Published in *Physics of Fluids, A*(5), 3, May, Part 2.

The Turbulent Years. (2002). John Lumley at 70, A Symposium in Honor of John L. Lumley on his 70th Birthday. Published in *Physics of Fluids, 14*, 2424–2557.